

ELASTIC AND PLASTIC BUCKLING OF SPHERICAL SHELLS UNDER VARIOUS
LOADING CONDITIONS

by

SHAHIN NAYYERI AMIRI

B.Sc., University of Tabriz, 2000

M.Sc., University of Tabriz, 2003

M.Phil., University of Tabriz, 2006

M.Sc., Kansas State University, 2010

AN ABSTRACT OF A DISSERTATION

submitted in partial fulfillment of the requirements for the degree

DOCTOR OF PHILOSOPHY

Department of Civil Engineering

College of Engineering

KANSAS STATE UNIVERSITY

Manhattan, Kansas

2011

Abstract

[Spherical shells are widely used in aerospace, mechanical, marine, and other industrial applications. Accordingly, the accurate determination of their behavior becomes more and more important. One of the most important problems in spherical shell behavior is the determination of buckling loads either experimentally or theoretically. Therefore, in this study some elastic and plastic buckling problems associated with spherical shells are investigated.

The first part of this research study presents the analytical, numerical, and experimental results of moderately thick and thin hemispherical metal shells into the plastic buckling range illustrating the importance of geometry changes on the buckling load. The hemispherical shell is rigidly supported around the base circumference against horizontal translation and the load is vertically applied by a rigid cylindrical boss (Loading actuator) at the apex. Kinematics stages of initial buckling and subsequent propagation of plastic deformation for a rigid-perfectly plastic shell models are formulated on the basis of Drucker- Shield's limited interaction yield condition. The effect of the radius of the boss used to apply the loading, on the initial and subsequent collapse load is studied. In the numerical model, the material is assumed to be isotropic and linear elastic perfectly plastic without strain hardening obeying the Tresca or Von Mises yield criterion. Finally, the results of the analytical solution are compared and verified with the numerical results using ABAQUS software and experimental findings. Good agreement is observed between the load-deflection curves obtained using three different fundamental approaches.

In the second part, the Southwell's nondestructive method for columns is analytically extended to spherical shells subjected to uniform external pressure acting radially. Subsequently finite element simulation and experimental work shown that the theory is applicable to spherical shells with an arbitrary axi-symmetrical loading too. The results showed that the technique provides a useful estimate of the elastic buckling load provided care is taken in interpreting the results. The usefulness of the method lies in its generality, simplicity and in the fact that, it is non-destructive. Moreover, it does not make any assumption regarding the number of buckling waves or the exact localization of buckling.]

ELASTIC AND PLASTIC BUCKLING OF SPHERICAL SHELLS UNDER VARIOUS
LOADING CONDITIONS

by

SHAHIN NAYYERI AMIRI

B.Sc., University of Tabriz, 2000

M.Sc., University of Tabriz, 2003

M.Phil., University of Tabriz, 2006

M.Sc., Kansas State University, 2010

A DISSERTATION

submitted in partial fulfillment of the requirements for the degree

DOCTOR OF PHILOSOPHY

Department of Civil Engineering

College of Engineering

KANSAS STATE UNIVERSITY

Manhattan, Kansas

2011

Approved by:

Major Professor

Dr. Hayder A Rasheed

Copyright

SHAHIN NAYYERI AMIRI

2011

Abstract

[Spherical shells are widely used in aerospace, mechanical, marine, and other industrial applications. Accordingly, the accurate determination of their behavior becomes more and more important. One of the most important problems in spherical shell behavior is the determination of buckling loads either experimentally or theoretically. Therefore, in this study some elastic and plastic buckling problems associated with spherical shells are investigated.

The first part of this research study presents the analytical, numerical, and experimental results of moderately thick and thin hemispherical metal shells into the plastic buckling range illustrating the importance of geometry changes on the buckling load. The hemispherical shell is rigidly supported around the base circumference against horizontal translation and the load is vertically applied by a rigid cylindrical boss (Loading actuator) at the apex. Kinematics stages of initial buckling and subsequent propagation of plastic deformation for a rigid-perfectly plastic shell models are formulated on the basis of Drucker- Shield's limited interaction yield condition. The effect of the radius of the boss used to apply the loading, on the initial and subsequent collapse load is studied. In the numerical model, the material is assumed to be isotropic and linear elastic perfectly plastic without strain hardening obeying the Tresca or Von Mises yield criterion. Finally, the results of the analytical solution are compared and verified with the numerical results using ABAQUS software and experimental findings. Good agreement is observed between the load-deflection curves obtained using three different fundamental approaches.

In the second part, the Southwell's nondestructive method for columns is analytically extended to spherical shells subjected to uniform external pressure acting radially. Subsequently finite element simulation and experimental work shown that the theory is applicable to spherical shells with an arbitrary axi-symmetrical loading too. The results showed that the technique provides a useful estimate of the elastic buckling load provided care is taken in interpreting the results. The usefulness of the method lies in its generality, simplicity and in the fact that, it is non-destructive. Moreover, it does not make any assumption regarding the number of buckling waves or the exact localization of buckling.]

Table of Contents

List of Tables	ix
List of Figures	x
Acknowledgements.....	xv
Dedication.....	xvi
Preface.....	xvii
A Review of Literature	xxi
I. Historical Background of the Spherical Shell Buckling.....	xxi
II. A Brief History of Yield Line Theory.....	xxxii
III. Historical Background of the Southwell Method	xxxiii
CHAPTER 1 - Plastic Buckling of Hemispherical Shell Subjected to Concentrated Load at the Apex	1
1.1 Introduction and Purpose of this Chapter	1
1.2 Preliminary Considerations.....	3
1.3 Analytical Formulation.....	4
1.3.1. Kinematics Assumptions	4
1.3. 2. The Initial Collapse Load and Reversal of Curvature.....	7
1.3.3. Propagation of the Dimple	12
1.3.4. Solution of the Complete Problem.....	17
1.4. Nonlinear Finite Element Analysis (FEA).....	22
1.4.1 Elements and Modeling	22
1.4.2 Numerical Results	26
1.5. Experimental Program	30
1.5.1 Parameters and test setup	30
1.5.2 Experimental Results:	35
1.6 Results and Discussion	44
1.7 Conclusions.....	52
Notation used in this chapter.....	54
CHAPTER 2 - Nondestructive Method to Predict the Buckling Load in Elastic Spherical Shells	55

2.1 Introduction and Purpose of this chapter	55
2.2 Southwell Method in Columns	56
2.3 Agreement of Test Results in Columns	64
2.4 An Extension of the Southwell Method for columns in a Frame structure	71
2.4.1 Formulation of the Governing Equations	71
2.4.2 Member Formulations and Solutions.....	75
2.4.3 Southwell Plot.....	76
2.4.4 Case Study	77
2.4.5 Discussion Results and Conclusion	79
2.5 The Southwell Method Applied to Shells.....	83
2.5.1 Deformation of an Element of a Shell of Revolution	84
2.5.2 Equations of Equilibrium of a Spherical shell	88
2.5.3 Equations of Equilibrium for the Case of Buckled Surface of the Shell	90
2.5.4 Buckling of Uniformly Compressed Spherical Shells.....	93
2.5.5 Southwell Procedure Applied to Shells	100
2.6. Nonlinear Finite Element Analysis (FEA).....	106
2.7. Experimental Program	124
2.8. Results and Discussion	134
2.8.1 Experimental work findings.....	135
2.8.2 Numerical Study results.....	140
2.8.2.1. For uniform radial pressure case with hinge support:.....	140
2.8.2.2. For uniform downward pressure case with hinge support:.....	142
2.8.2.3. For uniform radial pressure case with roller support :.....	143
2.8.2.4. For Ring load case with hinge support:	144
2.9. Conclusion	146
Notation that used in this chapter.....	148
References.....	149
Appendix A - Collapse load of circular plate	158
Solution for Tresca Plate.....	160
Appendix B - Axisymmetrically Loaded Circular Plates	162

Appendix C - Effect of Axial Force on the Stiffness of the Frame Member

..... 165

List of Tables

Table 2. 1: Nos. 1, 2, 3a, 3b, 4a, 4b, 5 and 6. Mild steel: Modulus of Elasticity = $2170000 \frac{kgf}{cm^2}$	66
Table 2. 2: T. Von Karman's tests	69
Table 2. 3: Robertson's Strut No:5. Mild steel: Effective length- 22.25 inches.....	69
Table 2. 4: Characteristics of Wood's Frame	78
Table 2. 5: Results for Member 8 of Wood's Frame subjected to the given loading pattern <i>Pkips</i> , <i>inches</i>	79

List of Figures

Figure 1. 1: Sample construction procedure for the experimental study	2
Figure 1. 2: Geometry and post buckling of hemispherical shells subjected to a concentrated load	3
Figure 1. 3: Initial buckling under concentrated load.....	4
Figure 1. 4: Post buckling deformation at initial collapse load P_0	5
Figure 1. 5: Plastic buckling deformation extends outward under an increasing load P	6
Figure 1. 6: n-sided regular polygon plate carrying a single concentrated load at its center.....	8
Figure 1. 7: Profile of deformation during initial buckling and post buckling behavior	10
Figure 1. 8: Equilibrium of an axisymmetric shell element.....	13
Figure 1. 9: Deformed part of hemispherical shell shape before the secondary bifurcation point	19
Figure 1. 10: Effect of axial force on plastic moment capacity	19
Figure 1. 11: Deformation pattern of the hemispherical shell using 8 node axisymmetric rectangular shell element.	23
Figure 1. 12: Different cuts of the deformed moderately thick shell $R/t_0 \leq 100$	24
Figure 1. 13: Deformation pattern of the moderately thick shell $R/t_0 \leq 100$ using six node triangular shell element.	25
Figure 1. 14: Buckling initiation of thin shell $R/t_0 > 100$ using six node triangular shell elements.	26
Figure 1. 15: Subsequent deformation of thin shell $R/t_0 > 100$ showing the secondary bifurcation phenomenon.	27
Figure 1. 16: Different cuts of the deformed thin shell $R/t_0 > 100$	28
Figure 1. 17: Deformation pattern of the thin shell $R/t_0 > 100$ showing the secondary bifurcation phenomenon.	29
Figure 1. 18: Different hemispherical shell samples were made for experimental study.....	31
Figure 1. 19: Three different boss size used for loading ($b = 1.25, 2.5, 5.0 \text{ mm}$).....	31
Figure 1. 20: Grooved base plate as a support for two sizes of hemispherical shells.....	32

Figure 1. 21: Riehle Universal testing machine for displacement control mesurments	33
Figure 1. 22: Stress strain diagram for copper alloy.....	34
Figure 1. 23: Stress strain diagram for Bronze.....	34
Figure 1. 24: Stress strain diagram for Stainless Steel.....	35
Figure 1. 25: Deformation of the moderately thick shell (Copper alloy $R/t_0 \approx 75$)	36
Figure 1. 26: Initial buckling and post buckling of the thin shell (Stainless Steel $R/t_0 \approx 166$)..	36
Figure 1. 27: Degeneration of axisymmetric deformation of the thin shell (Stainless Steel $R/t_0 \approx 166$).....	37
Figure 1. 28: Secondary bifurcation deformation of the thin shell (stainless steel $R/t_0 \approx 166$) .	38
Figure 1. 29: Initial buckling and axisymmetric post buckling of the thin shell (Bronze $R/t_0 \approx 250$)	39
Figure 1. 30: Degeneration of the axisymmetric deformation of the thin shell (Bronze $R/t_0 \approx 250$)	40
Figure 1. 31: Secondary bifurcation deformation of the thin shell (Bronze $R/t_0 \approx 250$)	41
Figure 1. 32: Different stages of the triangular with secondary bifurcation (Bronze $R/t_0 \approx 250$)	42
Figure 1. 33: Final deformation of the thin shell (Bronze $R/t_0 \approx 250$)	43
Figure 1. 34: Dimensionless Load deflection curve for copper alloy shell ($R/t_0 \approx 75$)	45
Figure 1. 35: Comparison of initial collapse response for copper alloy shell ($R/t_0 \approx 75$).....	45
Figure 1. 36: Dimensionless initial collapse load vs boss size for copper alloy shell ($R/t_0 \approx 75$)	46
Figure 1. 37: Dimensionless initial collapse load vs initial collapse angle for copper alloy ($R/t_0 \approx 75$).....	46
Figure 1. 38: Initial collapse angle vs boss size for copper alloy ($R/t_0 \approx 75$)	47
Figure 1. 39: Dimensionless Load vs knuckle meridional angle in rad for copper alloy shell ($R/t_0 \approx 75$).....	47
Figure 1. 40: Dimensionless Load deflection curve for Bronze shell ($R/t_0 \approx 250$).....	48
Figure 1. 41: Comparison of initial collapse response for Bronze shell ($R/t_0 \approx 250$).....	48

Figure 1. 42: Dimensionless initial collapse load vs boss size for Bronze shell ($R/t_0 \approx 250$) ...	49
Figure 1. 43: Dimensionless Load deflection curve for Stainless Steel shell ($R/t_0 \approx 166$)	49
Figure 1. 44: Comparison of initial collapse response for Stainless Steel shell ($R/t_0 \approx 166$).....	50
Figure 1. 45: Dimensionless initial collapse load vs boss size for Stainless Steel shell ($R/t_0 \approx 166$).....	50
Figure 1. 46: Numerical bifurcation point for Bronze, Stainless Steel, and Copper alloy versus (R/t_0).....	51
Figure 2. 1: Column under compression force.....	57
Figure 2. 2: Load Deflection curve in Southwell Method	61
Figure 2. 3: Notation for member and structure	72
Figure 2. 4: Wood's frame	81
Figure 2. 5: Loading of frame, Soutwell plot for member 8.....	82
Figure 2. 6: Element taken from a shell by two pairs of adjacent plans normal to the middle surface	85
Figure 2. 7: Spherical shell element and corresponding forces	89
Figure 2. 8: Meridian of a spherical shell before and after buckling.....	92
Figure 2. 9: Deformation pattern for hemispherical shell with hinge support under radially uniform pressure	107
Figure 2. 10: Subsequent deformation of hemispherical shell with hinge support under radially uniform pressure	108
Figure 2. 11: Deformation of hemispherical shell with hinge support under maximum radially uniform pressure	109
Figure 2. 12: Different cuts of the deformed hemispherical shell with hinge support under radially uniform pressure	110
Figure 2. 13: Subsequent deformations in the cuts of the deformed hemispherical shell with hinge support under radially uniform pressure	111
Figure 2. 14: Buckling initiation of the hemispherical shell with roller support under radially uniform pressure	112

Figure 2. 15: Subsequent deformation of the hemispherical shell with roller support under radially uniform pressure	113
Figure 2. 16: Second mode of the deformation in hemispherical shell with roller support under radially uniform pressure	114
Figure 2. 17: Buckling initiation of the hemispherical shell with hinge support under ring load in $R/2$	115
Figure 2. 18: Buckling of the hemispherical shell with hinge support under ring load at $R/2$..	116
Figure 2. 19: Subsequent deformation of the hemispherical shell with hinge support under ring load at $R/2$	117
Figure 2. 20: Large deformation of the hemispherical shell with hinge support under ring load distributed at $R/2$	118
Figure 2. 21: Buckling initiation of the hemispherical shell with hinge support under ring load in $R/3$	119
Figure 2. 22: Buckling of the hemispherical shell with hinge support under ring load at $R/2$..	120
Figure 2. 23: Large deformation of the hemispherical shell with hinge support under ring load distributed at $R/3$	121
Figure 2. 24: Buckling initiations of the hemispherical shell with hinge support under gravity loading.....	122
Figure 2. 25: Subsequent deformation of the hemispherical shell with hinge support under gravity loading	123
Figure 2. 26: Hemispherical shells samples made of polyethylene	125
Figure 2. 27: A test made of R=75 mm shell using suction pressure and three displacement gages at various points.....	126
Figure 2. 28: Deformation measurement with three gages at different locations in hemispherical shells under uniform suction pressure (R= 75mm).....	127
Figure 2. 29: Tests made of R=50 mm shells with suction pressure and three displacement gages at different locations hemispherical shells under uniform suction pressure (R= 50 mm). .	128

Figure 2. 30: Deformation measurement with three gages in different locations at hemispherical shells under uniform suction pressure (R= 50 mm).....	129
Figure 2. 31: Initial buckling of hemispherical shells under uniform suction pressure (R= 50 mm).....	130
Figure 2. 32: Initial buckling of hemispherical shells under uniform suction pressure (R= 50 mm).....	131
Figure 2. 33: Initial buckling of hemispherical shells under uniform suction pressure (R= 75 mm).....	132
Figure 2. 34: Several tests made on different samples using suction pressure with three and five gages at different locations.	133
Figure 2. 35: Plot of w/p against w ($R = 50mm, t_0 = 0.5mm$).....	135
Figure 2. 36: Plot of w/p against w ($R = 50mm, t_0 = 0.5mm$).....	136
Figure 2. 37: Plot of w/p against w ($R = 50mm, t_0 = 0.5mm$).....	137
Figure 2. 38: Plot of w/p against w ($R = 75mm, t_0 = 0.5mm$).....	138
Figure 2. 39 : Plot of w/p against w ($R = 75mm, t_0 = 0.5mm$).....	139
Figure 2. 40: Plot of w/p against w ($R = 50mm, t_0 = 0.5mm$).....	140
Figure 2. 41: Plot of p against w ($R = 75mm, t_0 = 0.5mm$).....	141
Figure 2. 42: Plot of w/p against w ($R = 50mm, t_0 = 0.5mm$).....	142
Figure 2. 43: Plot of w/p against w ($R = 50mm, t_0 = 0.5mm$).....	143
Figure 2. 44: Plot of w/p against w ($R = 50mm, t_0 = 0.5mm$).....	144
Figure 2. 45: Comparison of Southwell experimental prediction to theoretical buckling pressures.	145

Acknowledgements

First and most, all praises be to source of all goodness who is the Lord of the universe, the most gracious, and the most merciful.

I would like to express my deepest gratitude to my advisor, Prof. Hayder Rasheed, for the immeasurable amount of support, guidance and valuable advice throughout the research, and also for his outstanding performance in teaching Advanced Structural Analysis I, Advanced Structural Analysis II, and Theory of Structural Stability courses. His continued support led me to the realization of this work.

I would also like to extend my appreciation to my committee members: Dr. Asad Esmaily, Dr. Hani Melhem, and Dr. Jones Byron for their advice during my research.

I extend my sincere thanks to Mr. Saeid Kalami for helping me to draw the figures and for his friendship.

I am also indebted to the entire staff of the Khak Kavan test Laboratory, which has performed the experiments that are related to this study with patience, care and perseverance. Special sincere thanks are due to Mr. Amirali Mahouti the manager of this lab, for his cooperative guidance, careful supervision and very helpful suggestions

Finally, very special thanks are for all the faculty members of the Civil Engineering Department at Kansas State University, for their contributions to my education at the graduate level.

Dedication

This dissertation is dedicated to *my mother*, who has always given me the encouragement to complete all tasks that I undertake and continuously supports me whenever I face any difficulty in my life as well as for her love and sacrifice. To *my sister, Yasaman*, who has always inspired and helped me.

Preface

A shell can be defined as a body that is bounded by two closely spaced parallel curved surfaces. A shell is identified by its three features: its reference surface that is the locus of points which are equidistant from the bounding surfaces, its thickness, and its edges. Of these, the reference surface is the most significant because it defines the shape of the shell where its behavior is governed by the behavior of its reference surface. The thickness of a point of a shell is the length of the normal bounded by the bounding surfaces at that point. Edges of the shell are designed by appropriate values of the coordinates that are established on the reference surface. Shells may have no edges at all, in which case they are referred to as closed or complete shells. A spherical shell is a generalization of an annulus to three dimensions. A spherical shell is therefore the region between two concentric spheres of differing radii.

A shell is called “thin” if the ratio of its thickness to its minimum principle radius of curvature is small compared to unity. A shell is said to be “shallow” if the ratio of its maximum rise to the base diameter is small.

The analysis of shells of revolution considering nonlinearities is of importance in various engineering areas. When analyzing a shell structure subjected to a given loading one could make use of the general equations of the three dimensional theory of elasticity to come up with the state at stress at any given point. However, these equations are quite complicated and in only a few idealized cases can a solution be achieved. For this reason, three dimensional incident is approximated by making use of two dimensional theory of elasticity. The following assumptions are the basis for the classical linear shell theory.

1. Shell thickness is small

2. The displacements and rotations are small
3. The normals to the shell surface before loading remain normal after loading
4. The transverse normal stress is negligible

The most common shell theories are based on linear elasticity concepts. Linear shell theories adequately predict stresses and deformations for shells exhibiting small elastic deformations, that is, deformations for which it is assumed that the equilibrium equation conditions for deformed elements are the same as if they were not deformed and Hook's law applies.

The nonlinear theory of elasticity forms the basis for the finite deflection and stability theories of shells. Large deflection theories are often required when dealing with shallow shells, highly elastic membranes and buckling problems. The nonlinear shell equations are considerably more difficult to solve and for this reason are more limited in use.

Shells play an important part in all branches of engineering applications, especially in aerospace, nuclear, marine and petrochemical industries. The sophisticated use of shells in components are being made, such as missiles, space vehicles, submarines, nuclear reactor vessels, and refinery equipment is very common. As the shells are subjected to various loading conditions such as external pressure, seismic and/or thermal loads, compressive membrane forces are developed which may cause the shells to fail due to buckling or compressive instability. Among shell structures, the spherical shell is used frequently in the form of a spherical cap or a hemisphere and recently, the problem of the buckling of spherical shells has received considerable attention. Accordingly, in the present study, a treatise of two independent parts elastic and plastic buckling of spherical shells under various loading conditions are investigated.

Objectives and Research Methodology

Spherical shell structures are widely used in several branches of engineering. The class of shells covered here in are thin, and moderately thick so failure by buckling is often the controlling design criterion. It is therefore essential that the buckling behavior of these shells is properly understood and then suitable mathematical models can be established. The objectives of this study are stated below:

The first chapter of this study presents the analytical, numerical, and experimental results of moderately thick and thin hemispherical metal shells into the plastic buckling range illustrating the importance of geometry changes on the buckling load. The hemispherical shell is rigidly supported around the base circumference against vertical horizontal translation and the load is vertically applied by a rigid cylindrical boss actuator at the apex. Kinematic stages of initial buckling and subsequent propagation of plastic deformation for rigid-perfectly plastic shells are formulated on the basis of Drucker- Shield's limited interaction yield condition. The effect of the radius of the boss, used to apply the loading, on the initial and subsequent collapse load is studied. In the numerical model, the material is assumed to be isotropic and linear elastic perfectly plastic without strain hardening obeying the Tresca or Von Mises yield criterion. Both axisymmetric and 3D models are implemented in the numerical work to verify the absence of non-symmetric deformation modes in the case of moderately thick shells. In the end, the results of the analytical solution are compared and verified with the numerical results using ABAQUS software and experimental findings. Good agreement is observed between the load-deflection curves obtained using three different approaches.

In the second chapter, Southwell's nondestructive method for columns is extended to spherical shells subjected to uniform external pressure acting radially. Subsequently by means of finite element simulation and experimental work, it is shown that the theory is applicable to spherical shells with an arbitrary axi-symmetrical loading. For this technique any measurable deformation may be used. The results showed that the technique provides a useful estimate of the critical load provided care is taken in interpreting the results. The usefulness of the method lies in its generality, simplicity and in the fact that, it is non-destructive. Moreover, it does not need any assumption regarding the number of buckling waves or the exact locality of buckling.

A Review of Literature

I. Historical Background of the Spherical Shell Buckling

The first problems of instability, concerning lateral buckling of compressed members were solved about 200 years ago by L. Euler. At that time the principle structural materials were wood and stone. The relatively low strength of these materials necessitated stout structural members for which the question of elastic stability is not of primary importance. Thus Euler's theoretical solution, developed for slender bars, remained for a long time without application. Only with the beginning of extensive construction of steel railway bridges did the question of buckling of compression members become of practical importance.

At the beginning of the twentieth century, the construction of thin reinforced concrete shell concrete roofs was widespread in Europe. This roof is of the type where a cylindrical shell with a span between 3.00 and 5.00 m is built between arch beams that give the shape of the roof. These arches have a tie beam to resist thrusts and there is therefore only a vertical reaction on the piers. Arches are placed at the bottom side of the shell. At this period concrete was considered to be an elastic and linear material that obeyed Hooke's law and the arches were therefore analyzed in these terms.

In Germany, Walter Bauersfeld and Mergler, engineers at Dyckerhoff and Widmann, built the first spherical dome of concrete in 1922. In order to build the dome, they proposed installing a spherical net of steel bars and Mergler suggested projecting concrete against formwork. The spherical shape of the dome allowed the use of the same pieces of formwork again and again. The dome was analyzed like a continuous surface.

The construction of the dome at Jena city was made possible by Prof. Spangenberg's report. Construction began in the winter of 1923-1924. The bars close to the edge started to buckle and some stabilization bars were needed. In this construction, Bauersfeld analyzed the bending moment and deformation. In the first dome (Jena, 16.00 m span), not only were the in plane tension and compression in the plan of the dome taken into account, but bending moments and deformation were also studied.

The theory of the rigid of dome rotation was published by Föppl, Drang and Zwang. Second order differential equations were needed to solve the problem. Bauersfeld found an approach which yielded a solution, in which the Zoelly formula was used to analyze the problem of buckling, which gives a safety factor of 13.

Bauersfeld asked Dr. Geckeler to undertake some experiments. He did many tests and found that in the loads close to the Zoelly formula buckling start.

In the autumn of 1933 Torroja began several projects with shell structures. The first project he undertook was the roof of Algeciras Market. This was a dome of 46.22 m span, supported by 8 piers. The shell consisted of a spherical concrete construction. The shell was built using wooden formwork on a scaffold. With this method there was no problem with bars buckling as had happened to Bauersfeld with the construction of his first dome in Jena.

In 1934 Flügge proposed a value for the critical buckling load of spherical shells. However the expression was given for a full sphere.

Von Karman and Tsien (1939) showed that the state of stability of some structures, usually shell like structures, is weak. In other words, a small disturbance might cause them to snap into a badly deformed configuration. They also attempted to explain the discrepancy between the classical and experimental buckling pressures for clamped shallow spherical shells

under a uniform pressure. After the studies of Von Karman and Tsien (1939), the buckling problem of spherical shell has been examined both theoretically and experimentally by many investigators under various types of loading. Tsien (1942) showed that a small disturbance in a test would cause the shell to jump to a new configuration with large displacements as soon as the buckling load was exceeded.

Kaplan and Fung (1954) and Simons (1955) studied the buckling behavior of spherical caps from pressure deflection curve. Their analysis was based on integration of nonlinear finite deflection equations. Kaplan and Fung (1954) made some experiments for very shallow clamped spherical caps under a uniform pressure. They compared these results with the ones obtained by a perturbation solution of the governing nonlinear equations and observed that the agreement was satisfactory.

Buckling of clamped shallow spherical shells under external pressure has been studied extensively both experimentally and theoretically. In 1954, Kaplan and Fung performed an analytical and experimental investigation of clamped shallow spherical shells. Thurston (1961) obtained a numerical solution for the nonlinear equations for clamped shallow spherical shells under external pressure and presented the results in the post buckling range not previously computed. Then he compared the upper buckling and lower post buckling pressures with the experimental data of Kaplan and Fung (1954).

Huang (1964) worked on the problem of clamped shallow spherical shells for symmetric and unsymmetric buckling as well. Huang compared his numerical finding with the experimental results.

Famili and Archer (1965) investigated the buckling behavior of shallow shells by using the nonlinear equations, considering the asymmetric deformations at the beginning of the

buckling to be finite. The nonlinear eigenvalue problem was solved numerically. Their results were in agreement with those of Huang (1965).

Thurston and Penning (1966) conducted an extensive experimental and analytical investigation of the buckling of clamped shells with axisymmetric imperfections. They basically compared the pressure strain and pressure deflection results obtained both experimentally and theoretically. They found out that the effect of axisymmetric imperfections is not large enough to give good agreement between theory and experiments for very thin shells.

Hutchinson (1967) studied the initial post buckling behavior of a shallow section of a spherical shell subjected to external pressure. He found out that imperfection in the shell geometry have the same severe effect on the buckling strengths of spherical shells as demonstrated for axially compressed cylindrical shells.

Budiansky (1969) and Weinitschke (1970) also determined the axisymmetric buckling pressures of shallow spherical shells numerically. There is a good agreement among all the results obtained.

Fitch (1968) studied the elastic buckling and initial post buckling behavior of clamped shallow spherical shells under concentrated loading. He determined that bifurcation into an asymmetric pattern will occur before axisymmetric snap-buckling unless the ratio of the shell rise to the thickness lies within a narrow range corresponding to moderately thick shells. Fitch (1970) also investigated the elastic buckling and initial post buckling behavior of clamped shallow spherical shells under axisymmetric load. He found out that as the area of the loaded region increase, the buckling behavior changes from asymmetric bifurcation to axisymmetric snap-through, and then back to asymmetric bifurcation.

Stricklin and Martinez (1969) studied nonlinear analysis of shells of revolution by the matrix displacement method. The nonlinear strain energy expression was evaluated using linear functions for all displacements. Five different procedures were examined for solving the equations of equilibrium, with Houbolt's method to be the most suitable. Solutions were presented for the symmetric and asymmetric buckling of shallow caps under step pressure loadings and a wide variety of other problems including some highly nonlinear ones. The difficulty of repeated solutions of a large number of equations has been circumvented by placing the nonlinear terms on the right hand side of the equations of equilibrium and treating them as additional loads. The solutions of the governing equations were obtained by iterations and found to yield accurate results for some practical problems. For highly nonlinear problems, the equations were solved by the Newton-Raphson procedure, with the coupling between harmonics being ignored when the nonlinear terms were treated as pseudo loads and taken to the right hand side of the equations.

Huang (1969) studied the behavior of axisymmetric dynamic snap-through of elastic clamped shallow spherical shells under impulsive and step loading with infinite duration. It was observed that the dynamic snap-through buckling was not possible under impulsive loads but it was achieved under step loading conditions. The results obtained for static uniform pressure and dynamic loading formed a benchmark for many investigators in the verification of their results.

Axisymmetric and dynamic buckling of spherical caps due to centrally distributed pressure was studied by Stephens and Fulton (1969). Sanders' axisymmetric nonlinear elastic shell theory was approximated by finite difference equations including the Houbolt backward difference formulation in time. The equations were linearized using an iterative Newton-Raphson procedure. Axisymmetric buckling loads were given for a spherical cap subjected to a constant

static pressure or step pulse of infinite duration distributed axisymmetrically over a portion over the center of the shell. The influence of the size of the loaded area and of moment and inplane boundary conditions on both static and dynamic buckling was studied, as well as various buckling criteria to define dynamic buckling were used.

Grossman et al. (1969) investigated the axisymmetric vibrations of spherical caps with various edge conditions by carrying out a consistent sequence of approximations with respect to space and time. Numerical results were obtained for both free and forced oscillations involving finite deflections. The effect of curvature was examined with particular emphasis on the transition from a flat plate to a curved shell. In such a transition, the nonlinearity of the hardening type gradually reversed into one of softening.

Tillman (1970) presented the results of a theoretical and experimental investigation into elastic buckling of clamped shallow spherical shells under a uniform pressure, focusing mainly on low values of the geometric parameter, for which the symmetrical and first two asymmetrical deformations are valid.

Archer (1981) studied the behavior of shallow spherical shells subjected to dynamic loads of sufficient magnitude to result in finite nonlinear axisymmetric deformations. Marguerre's equations for the small finite deflections of shallow shells with the inclusion of inertia terms were taken as the governing equations. Results for the quasi statically loaded shell before and after snap through and snap back were studied and compared with known results. The dynamic response of the shell to rectangular pulse loading and buckling loads were obtained.

Dynamic buckling of orthotropic shallow spherical shells by Ganapathi and Varadan (1982) and axisymmetric static and dynamic buckling of orthotropic shallow spherical cap with circular hole by Dumir (1983) were investigated.

Geometric nonlinear 3D dynamic analysis of shells based on a total Lagrangian formulation and the direct time integration of the equation of motion was derived by Wouters (1982).

Dumir et al. (1984) investigated axisymmetric buckling of orthotropic shallow spherical cap with circular hole. Analysis has been carried out for uniformly distributed load and a ring load at the hole.

Zheng and Zhou (1989) developed semi-analytical computer method to solve a set of geometrically nonlinear equations of plates and shells. By this method, analytical solutions such as exact expansion in series, perturbations and iterations of the equations can be obtained.

Hsiao and Chen (1989) used a degenerated isoparametric shell element for the nonlinear analysis of shell structures. Six types of rotation variables and rotation strategies were employed to describe the rotation of the shell normal. In particular, a finite rotation method was proposed and tested. Both the rotation variations between two successive increments and the rotation corrections between two successive iterations were used as the incremental rotation (rotation variables) to update the orientation of the shell normal.

Chan and Chung (1989) used higher order finite elements for the geometrically nonlinear analysis of shallow shells. Based on K. Marguerre's shell theory, a family of higher order finite elements was developed. A step iteration Newton-Raphson scheme was adopted in solving the final system of nonlinear equations.

Bhimaraddi and Moss (1989) developed a shear deformable finite element for the analysis of general shells of revolution.

Xie, Chen and Ho (1990) studied the nonlinear axisymmetric behavior of truncated shallow spherical shells under transverse loading. Load-deflection relation were obtained

through iteration and numerical integration. Shells subjected to uniform pressure and combined uniform pressure and concentrated ring loading were investigated.

Eller (1990) derived finite element procedures for the stability analysis of nonlinear periodically excited shell structures. Starting from a geometrically nonlinear shell theory and applying Ljapunow's first method as well as Floquet's theory, a numerical stability criterion was deduced.

Luo et al. (1991) investigated the influence of pre buckling deformations and stresses on the buckling of the spherical shell. They obtained from Von Karman's large deflection equation of the plate and by assuming that a plate has an initial deflection in the form of a spherical cap, the equilibrium equations of a spherical cap subjected to hydrostatic pressure were written.

Chang (1991) developed a non-linear shear-deformation theory for the axisymmetric deformations of a shallow spherical cap comprising laminated curved-orthotropic layers. He expressed the governing equations in terms of the transverse displacement, stress function and rotation. Numerical results on the buckling and post-buckling behavior of spherical caps under uniformly-distributed loads were presented for various boundary conditions, cap rises, base radius-to-thickness ratios, numbers of layers and material properties.

Delpak and peshkm (1991) developed a variational approach to the geometrically nonlinear analysis of asymmetrically loaded shells revolution. The formulation was based on taking the second variation of the total potential energy equation. The analysis commenced by taking the first and second variation of the total potential energy of the elastic system by ensuring that load increments were applied infinitely slowly. After separating the load and the stiffness terms and factorizing the nodal variables, a distinct demarcation in the contribution of linear and

second order terms was observed which provided a clear methodology in calculating nonlinear and geometric matrices that lead to the generation of the tangent matrix.

A large deformation elastic plastic dynamic analysis of square plate and spherical shell subjected to shock loading was studied by Liang, Liao and Ma (1991). A transient dynamic finite element method was proposed for shock loading dynamic analysis. An incremental updated Lagrangian finite element procedure was driven. A 16-node isoparametric shell element was chosen for the study of the square plate and 8-node two dimensional axisymmetric element for the spherical shell.

Goncalves (1992) investigated the axisymmetric buckling behavior of clamped spherical shells under uniform pressure. He examined the buckling characteristics of the spherical shells using a fully nonlinear Galerkin solution procedure, a classical bifurcation analysis and a reduced stiffness bifurcation analysis.

Polassopoulos (1992) presented a new analytical method for the determination of the strength of structures subjected to bifurcation buckling affected by small structural imperfections.

Chaotic dynamic analysis of viscoelastic shallow spherical shells was performed by Karaesmen (1992).

The nonlinear dynamic buckling strength of clamped spherical caps under uniform step loading was investigated by Lee, Lie and Liou (1993). The geometric coordinates were updated at every time step. Thus, linearized finite element incremental equations based on the principle of virtual work could be derived. A three dimensional shell element with arbitrary geometry was used in the finite element formulation.

Terndrup et al. (1995) studied the buckling behavior of imperfect spherical shells subjected to different loading conditions. They analyzed the bifurcation and initial post-buckling behaviour of highly imperfection-sensitive large spherical shells, such as cargo tanks for ship transportation of liquefied natural gas and large spherical containment shells for nuclear power plants.

Zhang (1999) studied the torsional buckling of spherical shells under circumferential shear loads. He used Galerkin variational method, for studying the general stability of the hinged spherical shells with the circumferential shear loads.

Uchiyama et al. (2003) studied nonlinear buckling of elastic imperfect shallow spherical shells by mixed finite elements. They used nine-node-shell element and mixed formulation for stress resultant vectors then they compared finite element results with fifty-two experiments on the elastic buckling of clamped thin-walled shallow spherical shells under external pressure.

Grünitz (2003) examined the buckling strength of clamped and hinged spherical caps under uniform pressure with a circumferential weld depression by using the finite element method. The results obtained show a significant decrease in the buckling strength due to these imperfections depending on the location of the weld.

Dumir et al. (2005) presented axisymmetric buckling analysis for moderately thick laminated shallow annular spherical cap under transverse load. In their study, buckling was considered under uniformly distributed transverse load, applied statically. Annular spherical caps have been analyzed for clamped and simple supports with movable and immovable in-plane edge conditions and typical numerical loads and have been compared with the classical lamination theory.

Jones et al. (2007) investigated the problem of a thin spherical linearly-elastic shell, perfectly bonded to an infinite linearly-elastic medium. A constant axisymmetric stress field is applied at infinity in the elastic medium, and the displacement and stress fields in the shell and elastic medium are evaluated by means of harmonic potential functions.

Nie et al. (2009) derived an asymptotic solution for nonlinear buckling of orthotropic shell on elastic foundation. They performed an extensive parametric study for deformation and buckling of such structures.

The foregoing literature review is by no means exhaustive. However, the references cited and surveyed cover some of the important studies that have been contributed in this area.

II. A Brief History of Yield Line Theory

As early as 1922, the Russian, A. Ingerslev presented a paper to the institution of Structural Engineers in London on the collapse modes of rectangular slabs. Later on yield Line theory as it is known today was pioneered in the 1940s by the Danish engineer and researcher KW Johansen.

Authors such as R. H. Wood, L. L. Jones, A. Sawczuk and T. Jaeger, R. Park, K. O. Kemp, C.T. Morley, M. Kwiecinski and many others, consolidated and extended Johansen's original work so that now the validity of the theory is well established. In the 1960s, 1970s, and 1980s a significant amount of theoretical work on the application of yield line theory was carried out around the world and was widely reported. To support this method, extensive testing was undertaken to prove the validity of the theory. Excellent agreement was obtained between the theoretical and experimental yield line patterns and the ultimate loads. The differences between the theory and tests were small and mainly on the conservative side.

III. Historical Background of the Southwell Method

Sir Richard Vynne Southwell (1888– 1970) was a British mathematician who specialized in applied mechanics as an engineering science academic. Richard Southwell was educated at the University of Cambridge, where in 1912 he achieved first class degree results in both the mathematical and mechanical science tripos. In 1914, he became a Fellow of Trinity College, Cambridge, and a lecturer in Mechanical Sciences. Southwell was in the Royal Naval Air Service during World War I. After World War I, he was head of the Aerodynamics and Structures Divisions at the Royal Aircraft Establishment, Farnborough. In 1920, he moved to the National Physical Laboratory. He then returned to Trinity College in 1925 as Fellow and Mathematics Lecturer. Next, in 1929, he moved to Oxford University as Professor of Engineering Science and Fellow of Brasenose College. There, he developed a research group, including Derman Christopherson, with whom he worked on his relaxation method. He became a member of a number of UK governmental technical committees, including the Air Ministry, at the time when the R100 and R101 airships were being conceived.

Southwell was rector at Imperial College, London from 1942 until his retirement in 1948. He continued his research at Imperial College. He was also involved in the opening of a new student residence, Selkirk Hall.

As a scientist, in 1932, Southwell presented his analysis for the special case of a pin ended strut of constant flexural rigidity of EI . Southwell method for determining the minimum buckling load is a nondestructive test for pinned-end, initially imperfect struts. Southwell showed that the load deflection curve of such a member is a hyperbolic in the neighborhood of the smallest critical load, while the asymptote is a horizontal line, $P = P_{cr}$. By suitable

transformation of variables this hyperbolic portion of load deflection curve may be converted into a straight line for which the inverted slope is the minimum critical load.

CHAPTER 1 - Plastic Buckling of Hemispherical Shell Subjected to Concentrated Load at the Apex

1.1 Introduction and Purpose of this Chapter

Due to the increasing use of shell type structures in space vehicles, submarines, buildings and storage tanks, interest in the stability of shells has accordingly increased by researchers and practicing engineers. Because a hemispherical shell is able to resist higher pure internal pressure loading than any other geometrical vessel with the same wall thickness and radius, the hemispherical shell is one of the important structural elements in engineering applications. It is also a major component of pressure vessel construction. In practice, most pressure vessels are subjected to external loading due to hydrostatic pressure, or external impact in addition to internal pressure. Consequently, they should be designed to resist the worst combination of loading without failure. The load transmitted by a cylindrical rigid actuator applied at the summit of the sphere is considered a common external load. Thus, it is important to study its effect on the initial buckling and plastic buckling propagation of this type of shells. This study presents the analytical, numerical, and experimental results of moderately thick hemispherical metal shells into the plastic buckling range illustrating the importance of geometry changes on the buckling load. The hemispherical shell is rigidly supported around the base circumference against vertical and horizontal translation and the load is vertically applied by a rigid cylindrical boss at the apex. Kinematic stages of initial buckling and subsequent propagation of plastic deformation for rigid-perfectly plastic shells are formulated on the basis of Drucker-Shield's limited interaction yield condition. The effect of the radius of the boss, used to apply the loading, on the initial and subsequent collapse load is studied. In the numerical

model, the material is assumed to be isotropic and linear elastic perfectly plastic without strain hardening obeying the Tresca or Von Mises yield criterion. Both axisymmetric and 3D models are implemented in the numerical work to verify the absence of non-symmetric deformation modes in the case of moderately thick shells. In the end, the results of the analytical solution are compared and verified with the numerical results using ABAQUS software and experimental findings. Good agreement is observed between the load-deflection curves obtained using the three different approaches. The preparations to conduct experimental verifications are also shown in Fig. 1.1.



Figure 1. 1: Sample construction procedure for the experimental study

1.2 Preliminary Considerations

This study is focused on the following physical phenomenon. A hemispherical shell is compressed by a concentrated load at the summit. At the load below a certain critical value, called the initial buckling load, the shell remains spherical or unbuckled but when the increasing applied load reaches the critical initial buckling value, the shell snaps into a non-spherical buckled state which is characterized by a round dimple around the apex of the hemispherical shell. Therefore, it creates a deformation state which extends or propagates over the surface of the shell leaving undetermined the amplitude of deformation at various levels of load (Fig. 1.2).

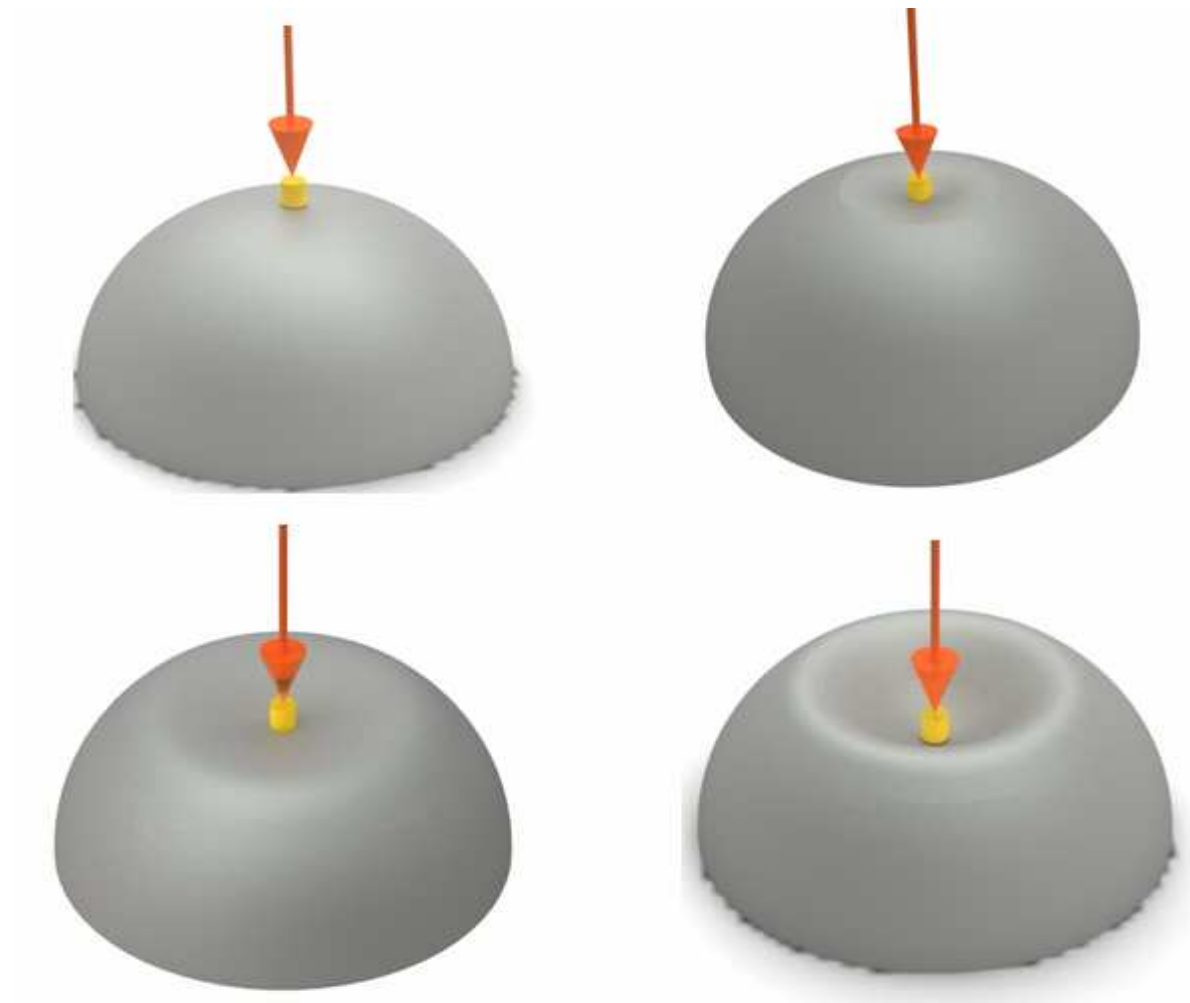


Figure 1. 2: Geometry and post buckling of hemispherical shells subjected to a concentrated load

1.3 Analytical Formulation

1.3.1. Kinematics Assumptions

The behavior of a moderately thick metal hemispherical shell under a concentrated load at the summit may be analyzed as follows:

- a) The perfectly-rigid state culminating at the attainment of the initial collapse load P_0 .

For a concentrated load acting on a hemispherical shell the initial collapse takes place only in a vanishingly small region of the shell, Fig. 1.3. The collapse load P_0 depends on the plastic moment M_0 of the shell material. If a rigid cylindrical boss is used for loading purposes, the size of this boss influences the region of collapse and hence the collapse load P_0 .

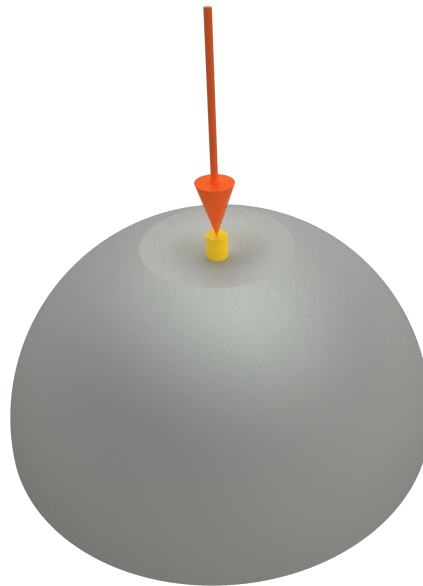


Figure 1. 3: Initial buckling under concentrated load

b) Deformation under the collapse load P_0 .

At the load P_0 , the shell snaps to reverse its curvature and continues to deform under the same load, resulting in the formation of a dimple. The dimple is taken to be conical in shape and the apex of the cone is the point where the load is acting. This assumption is not at variance with the observed behavior. The extent of the dimple depends again on the plastic moment M_0 of the shell material and on the radius of the loading boss or actuator. A section of the shell through a meridional plane, immediately after the deformation under the initial collapse load P_0 , is shown in Fig.1.4.

The outer undeformed portion of the shell (of radius R and constant thickness t_0) and the conical dimple are connected by an annular zone to which the cone is tangent, and which shares a common tangent with the undeformed part of the shell. Both the conical dimple, and the annular zone which looks in section like a knuckle of radius ρ symmetrical about the axis of revolution, are plastic.

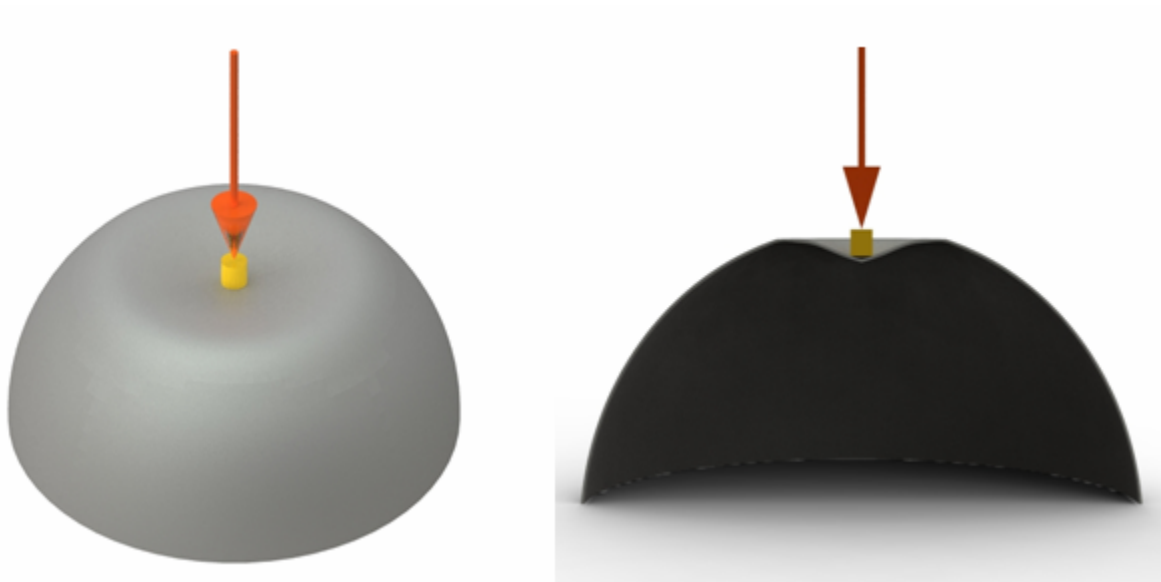


Figure 1. 4: Post buckling deformation at initial collapse load P_0

c) Propagation of the annular zone.

This is the third stage of deformation. It takes place only after the deformation under the constant load P_0 is complete. The dimple extends outward with an axisymmetric deformation under an increasing load P to render a greater portion of the shell plastic Fig.1.5. The deformation involves a conical shape and an annular zone.

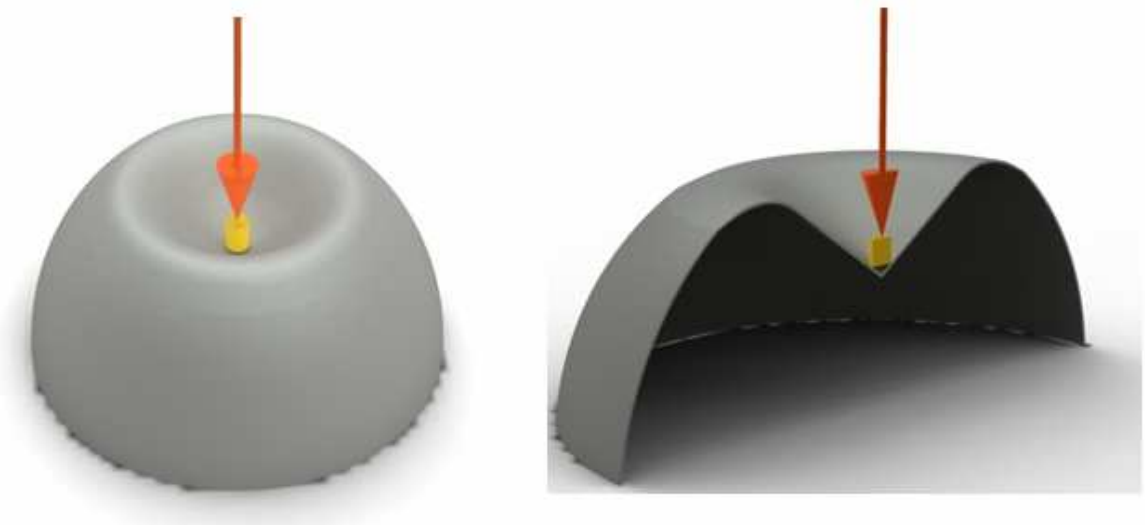


Figure 1. 5: Plastic buckling deformation extends outward under an increasing load P

d) Degeneration of the shape of deformation.

After the annular zone (which is circular in plan) has propagated to an extent depending for a given material on the R/t_0 ratio, the axisymmetric deformation described above begins to change. The annular zone becomes triangular and then polygonal in plan. A new mechanism which involves the folding of the shell material about the edges of a pyramid-like surface takes over and replaces the conical part of the deformation. This phenomenon could be associated with some sort of a secondary instability. This stage of deformation will not be addressed in part of this study, because it is unlikely to take place in moderately thick shells.

1.3. 2. *The Initial Collapse Load and Reversal of Curvature*

Shells are commonly subjected to transverse loads, i.e. loads that act in the direction perpendicular to the surface of the shell. Such shells may fail locally by so called fan mechanism, with positive yield lines radiating from the point load. Consequently, at sufficiently high load, the shells may experience extensive plastic deformation locally and eventually lose all its structural function and changes its curvature direction this phenomenon known as local plastic collapse.

Unlike elastic analysis, exact solutions for the plastic collapse load are not available in most cases. Even for the idealized rigid perfectly plastic constitutive relation, the collapse load can only be approximated over a range of values. The technique used to define the boundary of the collapse load is known as limit load and the theorem associated with it known as limit analysis.

Consider an n-sided regular polygon plate carrying a single concentrated load at its center and rigidly supported along the n sides, Fig.1.6. If a small virtual displacement δ is imposed under the load, the external work done is $W_e = P_0 \delta$ and the internal work exerted during the assigned virtual displacement is found by summing the products of plastic moment M_0 per unit length of yield lines times the plastic rotation θ at the respective yield lines, consistent with the virtual displacement. If the resisting moment M_0 is constant along a yield line of length a_i and if a rotation θ is experienced, the internal work is $W_i = M_0 a_i \theta$ for each yield line. Because there are n yield lines, the total internal work is $W_{Ti} = \sum_{i=1}^n M_0 a_i \theta$. The rotation at the plastic hinge can be calculated in terms of the deflection thus, $\theta = \left(\frac{\delta}{OH} + \frac{\delta}{OK} \right)$. In view of the fact

that $OK = a_i \tan \alpha'_i$ and $OH = a_i \tan \alpha_i$, Fig.1.6 By equating W_{Ti} and W_e one obtains $P_0 = M_0 \sum_{i=1}^n (\cot \alpha_i + \cot \alpha'_i)$. Because in an n-sided regular polygon $\alpha_i = \alpha'_i = \left(\frac{\pi}{2} - \frac{\pi}{n}\right)$ and accordingly, $P_0 = 2nM_0 \cot\left(\frac{\pi}{2} - \frac{\pi}{n}\right) = 2nM_0 \tan \frac{\pi}{n}$. If n tends to infinity, n-sided regular polygon converts to a circle and $P_0 = \lim_{n \rightarrow \infty} \left(2nM_0 \tan \frac{\pi}{n}\right)$. Using LHopital once $P_0 = 2\pi M_0$. Thus, for a circular plate, the value of the concentrated load necessary to initiate collapse is given by $P_0 = 2\pi M_0$ and as it can be seen, the collapse load is independent of the size of the plate. This formula can be proven using another method too (See appendix A)

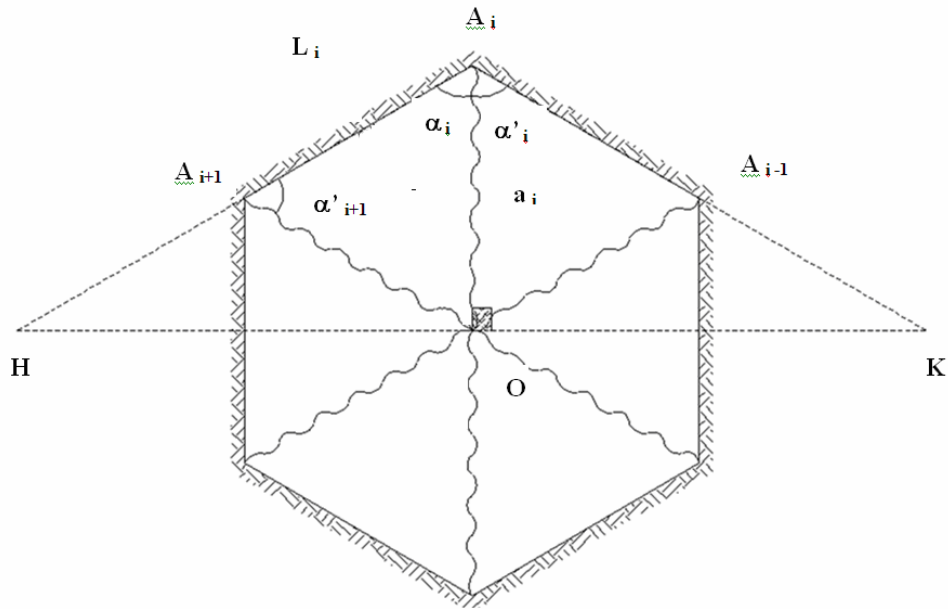


Figure 1. 6: n-sided regular polygon plate carrying a single concentrated load at its center

Following the same procedure, it can be easily proven that the load applied through a rigid boss of radius b , to a circular plate of radius a produces a collapse load level given by:

$$P_0 = \frac{2\pi M_0}{1 - \frac{2b}{3a}} \quad (1.1)$$

The region of a hemisphere subjected to downward concentrated load at the apex that initially collapses with a reversal of curvature is quite small and can be easily considered to be a very shallow spherical cap. If the boss size is ignored, $2\pi M_0$ is known to be the exact collapse load for any circular plate and therefore it can serve as a lower bound on the initial collapse load of a shallow spherical cap. The initial collapse load of a hemispherical shell under a concentrated load should thus approach the value $2\pi M_0$ because the local nature of the collapse may mean that the collapse load is less dependent on the shell curvature. When the shell is loaded by means of a finite rigid boss of radius b , the collapse load P_0 has a value which is observed to be greater than $2\pi M_0$ while it is dependent on the size. As mentioned earlier, this is also true of a plate loaded with a boss, and so the same modification of the collapse load formula referred to above can be made. The difference is that while the flat plate radius a is known, the dimple radius at initial collapse in the case of a hemispherical shell is not readily available but has to be calculated. The value of this dimple radius for the shell is found by equating the initial collapse load P_0 with the load predicted by the mechanism of dimple propagation at the start of the third stage of deformation, as shown below. The initial collapse and subsequent deformation mechanism can be seen in Fig. 1.7.

The shell initially collapses at a load value of P_0 which is equal to or greater than $2\pi M_0$ to an extent depending on the boss radius b . A portion of the shell shown as a dotted line at its initial position as part of a hemisphere of radius R takes up the buckled position shown by the bold line, comprising a cone and an annular zone, Fig.1.7 The extent of the deformation is measured by θ_0 the meridional angle corresponding to the boundary of the

plastic region. During this deformation, the load P_0 remains constant. It is between these initial and final positions that the toroidal annular zone with the knuckle radius ρ and the cone come into being. It is only after this stage is complete that the third stage of deformation with a different type of mechanism takes over. This comprises the propagation of the dimple and the outward movement of the annular zone.

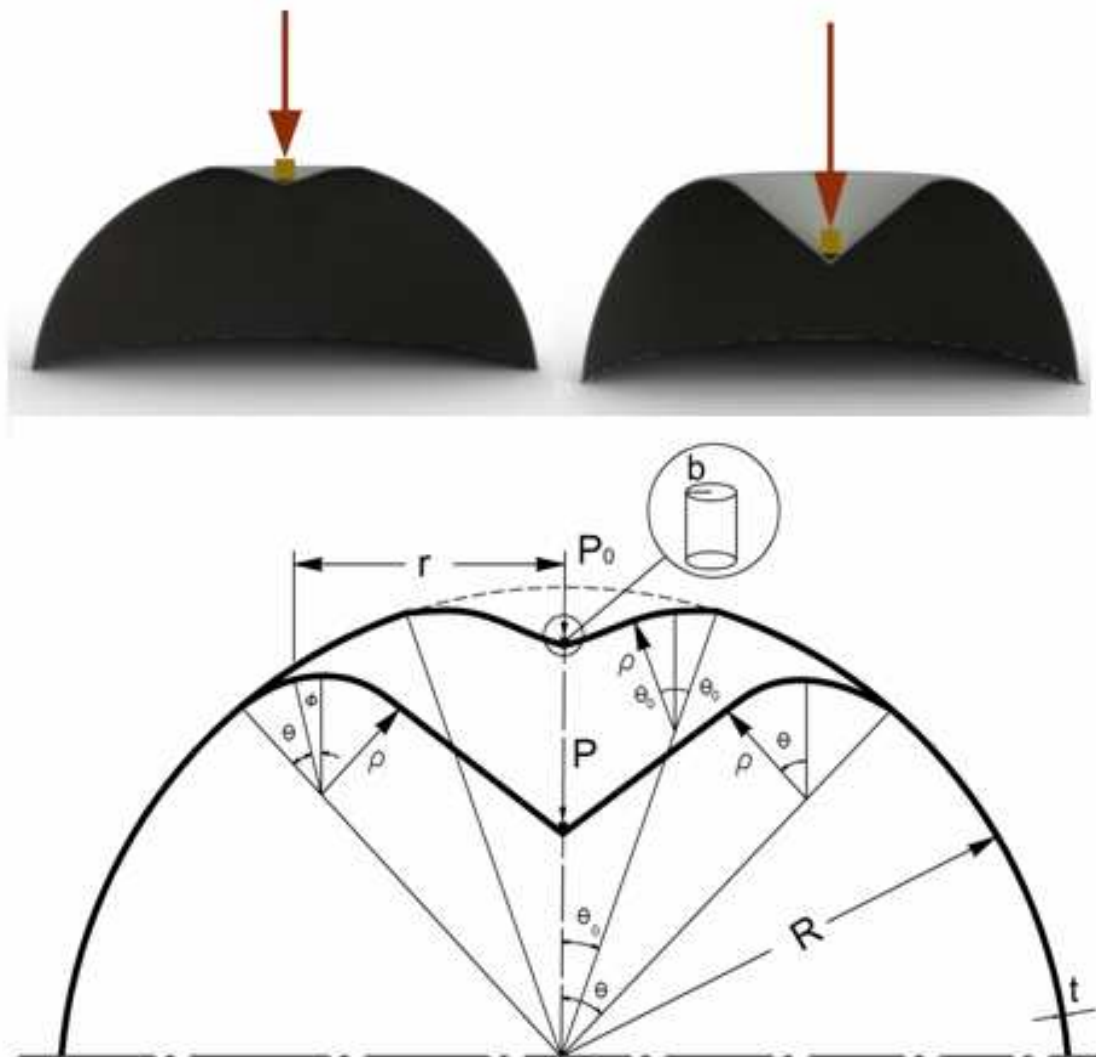


Figure 1. 7: Profile of deformation during initial buckling and post buckling behavior

In the ideal case of a concentrated load acting at the shell apex, it is natural to expect that the second step of deformation should begin almost immediately after the shell load reaches the value $2\pi M_0$. The following geometrical relations in which the boss will not play a significant part can be derived for the initial collapse using the incompressibility condition, and assuming no difference between the thickness of the shell in the dimple region before and after collapse:

The surface area of the spherical cap which reverses curvature is:

$$\text{Surface Area initial} = 2\pi R^2(1 - \cos \theta_0). \quad (1.2)$$

This must be equated to the sum of the surface areas of the cone and the annular zone, which are equal to:

Surface Area Buckled = Surface area of annular part + Surface area on conical part =

$$2\pi(R - \rho)\sin \theta_0 \cdot 2\rho\theta_0 + \frac{\pi(R - 2\rho)^2 \sin^2 \theta_0}{\cos \theta_0} \quad (1.3)$$

Equating eqs. (1.2) and (1.3) then simplifying, the following equation is obtained:

$$1 - \cos \theta_0 = \frac{2\rho}{R}(1 - \rho/R)\theta_0 \sin \theta_0 + \frac{1}{2}(1 - 2\rho/R)^2 \frac{\sin^2 \theta_0}{\cos \theta_0} \quad (1.4)$$

As θ_0 is small, $1 - \cos \theta_0 = \theta_0^2/2 - \theta_0^4/24$, and $\sin \theta_0 = \theta_0 - \theta_0^3/6$. Neglecting the second terms on the right hand side of the cosine and sine series expansions and ignoring the fourth power of θ_0 would make equation (1.4) trivially satisfied. Substituting these values into equation (1.4) and neglecting powers of θ_0 higher than the fourth, the equation reduces to:

$$\theta_0^4 \left[\frac{\rho^2}{R^2} - \frac{\rho}{R} + 3/16 \right] = 0 \quad (1.5)$$

For any non-zero value of θ_0 , the solution gives $\rho/R = 0.25$ and/ or 0.75 . For the larger value of $\rho/R = 0.75$, $R - 2\rho$ becomes negative, which means that the conical part of the dimple cannot exist. Thus the relevant value of ρ is $R/4$. Although θ_0 has a small value, it can be assumed that ρ is equal to $R/4$ throughout the subsequent deformation for which θ is greater than θ_0 roughly until $\theta \cong 1rad = 57.296^\circ$ since all assumptions are satisfied.

1.3.3. Propagation of the Dimple

During the formation of the initial dimple, the deformation is small and the buckling happens under a constant load P_0 . As the deflection increases, the effect of geometry change starts to become significant and the load increases with continuing deformation. When the non-plastic material surrounding the deforming region cannot support a load higher than P_0 , the plastic region must grow in size with increasing load. It is assumed here that the deforming surface maintains a geometrical similarity during the propagation of the dimple as evidenced by the the numerical results. The deformation stage being identified by a single parameter θ , which is the angular position of the surface at the boundary of the plastic region (Fig.1.7). It is assumed that the radius of curvature of the toroidal knuckle remains constant while its crown moves away from the axis of revolution by continuous rotation and translation of the rigid material entering into the plastic region.

The middle surface of the deforming shell forms a surface of revolution and the state of stress is completely specified by the direct forces, resultant moments and transverse shear. If N_ϕ and N_β denote the meridional and circumferential forces per unit length, M_ϕ and M_β the cor-

responding bending moments, and Q the transverse shear force (Fig. 1.8), the meridional equations of equilibrium for a shell of revolution can be written as

$$\frac{\partial}{\partial \phi}(rN_\phi) - r_1 N_\beta \cos \phi - rQ = 0 \quad (1.6)$$

$$\frac{\partial}{\partial \phi}(rM_\phi) - r_1 M_\beta \cos \phi - r r_1 Q = 0 \quad (1.7)$$

where r is the distance of the element from the axis of revolution and r_1 its mean meridional radius of curvature, which is equal to ρ at the annular zone.

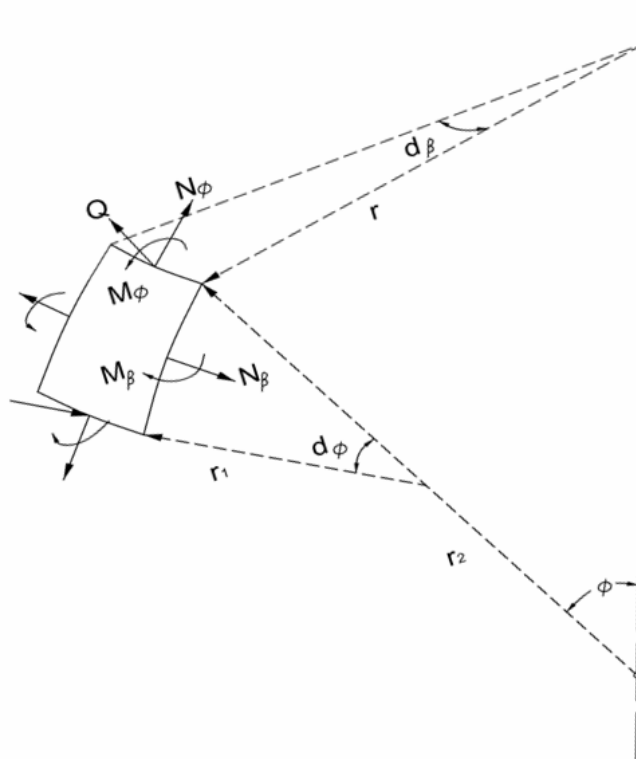


Figure 1. 8: Equilibrium of an axisymmetric shell element

In our assumed deformation model, the annular zone has a constant radius of curvature ρ , It is easily visualized that N_ϕ changes sign from positive (tension) to negative (compression) as we move from the inner to the outer part of the toroidal knuckle.

N_ϕ at the boundary of the cone annular zone is tension and at the boundary of the annular zone- undeformed shell is compression to resist the downward P such that $\sum F_y = 0$. In other words, under increasing load the shell material from the outer undeformed region is pushed into the annular zone and material from the annular zone is pulled into the conical dimple. Thus N_ϕ may be assumed to vanish at the crown of the toroid. Considering the outer part of the knuckle defined by $0 \leq \phi \leq \theta$ and noting that N_ϕ is compressive in this region, it is evident that N_β should also be compressive. This is due to the fact that compressive N_ϕ causes expansion in the hoop direction while the rigid shell restrains the knuckle from expansion thus inducing compressive stress:

$$N_\beta = -\sigma_0 t, \quad (1.8)$$

where σ_0 is the (constant) yield stress of the material and t is the current thickness. The first equation of equilibrium, equation (1.6), therefore reduces to

$$\frac{\partial}{\partial \phi} (r N_\phi) = -\rho \sigma_0 t \cos \phi + r Q \quad (1.9)$$

This equation must be supplemented with the equation of vertical equilibrium, namely

$$2\pi (N_\phi \sin \phi + Q \cos \phi) = -P \quad (1.10)$$

where P is the total vertical downward load at the conical apex. Eliminating Q between (1.9) and (1.10),

$$\frac{\partial}{\partial \phi} (r N_\phi \sec \phi) = -\rho \sigma_0 t - \frac{P}{2\pi} \sec^2 \phi \quad (1.11)$$

Assuming that the thickness variation may be neglected in the equilibrium equations and noting that $t = t_0$ (the initial thickness) at $\phi = \theta$, equation (1.11) can be integrated to obtain

$$r N_\phi = -\left(\rho \sigma_0 t_0 \phi \cos \phi + \frac{P}{2\pi} \sin \phi \right), \quad (1.12)$$

where $N_\phi = 0$ at $\phi = 0$ is used as a boundary condition.

Considering the moment equation of equilibrium, it is observed that the second term of equation (1.7) is of the order of t/r times that of the last term, as proven by Drucker & Shield (1959), and hence the second term may be neglected when the region of interest is not close to the axis of revolution. Equation (1.7) then reduces to

$$\frac{\partial}{\partial \phi} (r M_\phi) = \rho r Q \quad (1.13)$$

From eqs. (1.10) and (1.12),

$$r Q = \rho \sigma_0 t_0 \phi \sin \phi - \frac{P}{2\pi} \cos \phi \quad (1.14)$$

and eq. (1.13) becomes

$$\frac{\partial}{\partial \phi} (r M_\phi) = \rho \left\{ \rho \sigma_0 t_0 \phi \sin \phi - \frac{P}{2\pi} \cos \phi \right\} \quad (1.15)$$

Since the crown of the toroidal knuckle suffers the most severe bending, it is natural to assume that M_ϕ at the crown is equal to the yield moment M_0 . It may also be

assumed that at the boundary of the rigid region, M_ϕ attains the value of the yield moment. Neglecting again the thickness variation, the boundary conditions can be written $M_\phi = -M_0$ at $\phi = 0$ and $\phi = \theta$. Integration of eq. (1.15) between the limits of 0 and θ gives:

$$\begin{aligned} rM_\phi &= \int \rho^2 \sigma_0 t_0 \phi \sin \phi d\phi - \frac{P}{2\pi} \int \rho \cos \phi d\phi = -\phi \cos \phi \rho^2 \sigma_0 t_0 + \int \rho^2 \sigma_0 t_0 \cos \phi d\phi - \frac{\rho P}{2\pi} \sin \phi + C \\ &= \rho^2 \sigma_0 t_0 (\sin \phi - \phi \cos \phi) - \frac{\rho P}{2\pi} \sin \phi + C \end{aligned}$$

$$\phi = 0 \rightarrow M_\phi = -M_0 \rightarrow C = -R \sin \theta M_0 + \rho M_0 \sin \theta$$

$$\phi = \theta \rightarrow M_\phi = -M_0$$

$$-R \sin \theta M_0 = \rho^2 \sigma_0 t_0 (\sin \theta - \theta \cos \theta) - \frac{\rho P}{2\pi} \sin \theta - R \sin \theta M_0 + \rho M_0 \sin \theta$$

This will then lead to:

$$-M_0 \sin \theta = \rho \sigma_0 t_0 (\sin \theta - \theta \cos \theta) - \frac{P}{2\pi} \sin \theta \quad (1.16)$$

Inserting the values $M_0 = \frac{\sigma_0 t_0^2}{4}$ and $\rho = \frac{R}{4}$, equation (1.16) reduces to

$$\frac{P}{2\pi M_0} = 1 + R/t_0 \left(1 - \frac{\theta}{\tan \theta} \right) \quad (1.17)$$

This formula directly relates the downward vertical load to the angular position of the dimple denoted by $\theta \geq \theta_0$. It is independent of the size of the boss, provided the diameter of the boss is small in comparison with the diameter of the shell. For a truly concentrated load θ_0 is vanishingly small and the solution reduces to the well known result $P_0 = 2\pi M_0$.

1.3.4. Solution of the Complete Problem

If the shell is loaded by a concentrated load at the apex, the formula (1.17) provides the complete load- deformation characteristic of the shell. However, a fully concentrated load is only a mathematical convenience which cannot be realized in practice. In fact the initial collapse load is very sensitive to the size of the boss and a small boss can considerably increase the collapse load from the value $P_0 = 2\pi M_0$. It is therefore essential to include the boss size in developing a realistic theory.

The initial angle for the propagating dimple θ_0 is also a measure of the plastic region corresponding to the initial collapse. Assuming that this small portion of the shell behaves like a plate during collapse even when the load is applied by a finite boss in the form of a rigid punch of a small base radius b , equation (1.1) can be rewritten as:

$$\frac{P_0}{2\pi M_0} = \frac{1}{1 - \frac{2b}{3R\theta_0}} \quad (1.18)$$

Since the load corresponding to the beginning of the dimple propagation is also P_0 , eq. (1.17) gives

$$\frac{P_0}{2\pi M_0} = 1 + \frac{R}{t_0} \left(1 - \frac{\theta_0}{\tan \theta_0} \right) \quad (1.19)$$

Since θ_0 is small, therefore;

$$\left(1 - \frac{\theta_0}{\tan \theta_0} \right) = 1 - \left(\frac{\theta_0}{\theta_0 + \frac{\theta_0^3}{3} + \frac{2\theta_0^5}{15} + \dots} \right)$$

If the power greater than three is neglected so,

$$\left. \begin{aligned} \left(1 - \frac{\theta_0}{\tan \theta_0}\right) &= 1 - \frac{1}{1 + \frac{\theta_0^2}{3}} \\ \frac{1}{1 + \frac{\theta_0^2}{3}} &= 1 - \frac{\theta_0^2}{3} \end{aligned} \right\} \Rightarrow 1 - \frac{\theta_0}{\tan \theta_0} = 1 - \left(1 - \frac{\theta_0^2}{3}\right) = \frac{\theta_0^2}{3}$$

Thus,

$$\frac{P_0}{2\pi M_0} = 1 + \frac{R \theta_0^2}{t_0^3} \quad (1.20)$$

Equations (1.18) and (1.20) furnish the following equation for θ_0 :

$$\theta_0^2 \left(\frac{R}{b} \theta_0 - \frac{2}{3} \right) = \frac{2t_0}{R}, \quad (1.21)$$

which can be solved numerically for each particular case. An immediate conclusion from (1.21) is that θ_0 is always greater than b/R . It is easily seen from the geometry in Fig.1.7 that the punch penetration corresponding to the position of the dimple given by θ is

$$h = R(1 - \cos \theta) + (R - 2\rho) \sin \theta \tan \theta \quad (1.22)$$

and

$$\frac{h}{R} = \frac{1}{2}(1 - \cos \theta)(3 + \sec \theta) \quad (1.23)$$

by using the result $\rho = R/4$.

Eqs. (1.17) and (1.23) give the load-deflection relationship parametrically through θ when $\theta \geq \theta_0$.

When $R/t < 100$, this solution is found to correct for large amplitudes of deflection, however for $R/t > 100$ the deformation follows the same axisymmetric pattern in the beginning. Then, the annular zone degenerates into various n-sided polygon deformation modes and bifurcation in deformation pattern is observed. In order to determine the bifurcation point during deformation, assume the deformed part behaves similar to a clamped circular plate of radius c with large deformation before bifurcation point (Fig. 1.9). For thin circular clamped plate the radial and tangential moments are (see Appendix B):

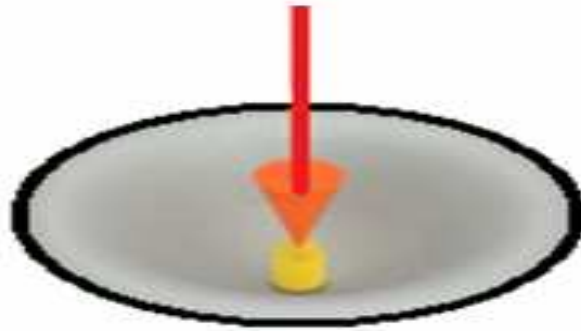


Figure 1. 9: Deformed part of hemispherical shell shape before the secondary bifurcation point

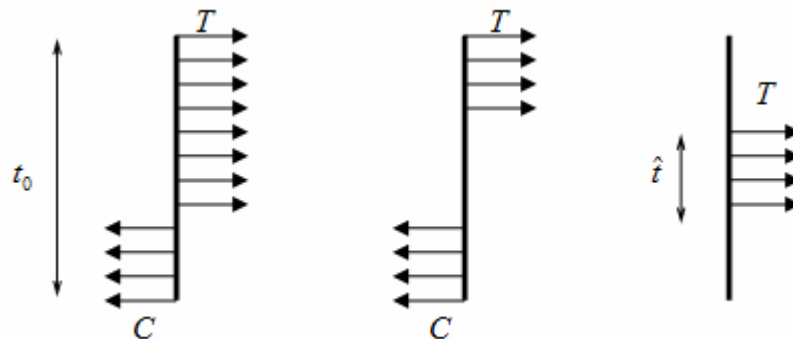


Figure 1. 10: Effect of axial force on plastic moment capacity

$$M_r = \frac{P}{4\pi} \left[(1+\nu) \ln \frac{c}{r} - 1 \right] \quad (1.24)$$

$$M_t = \frac{P}{4\pi} \left[(1+\nu) \ln \frac{c}{r} - \nu \right] \quad (1.25)$$

In the bifurcation point $c = R \sin \theta - \rho \sin \theta \xrightarrow{\rho=R/4} c = 3R/4 \sin \theta$

Assuming that at the bifurcation point, M_t reaches to the plastic moment

at $r = c - \rho \sin \theta = R/2 \sin \theta$ (as evidenced by the numerical and experimental findings). By

combining equations (1.17) and (1.25) and inserting the value $P = 2\pi M_0 \left[1 + R/t_0 \left(1 - \frac{\theta}{\tan \theta} \right) \right]$ it

can be written:

$$M_t = M_{plastic} = \frac{2\pi M_0 \left[1 + R/t_0 \left(1 - \frac{\theta}{\tan \theta} \right) \right]}{4\pi} \left[(1+\nu) \ln \frac{3R/4 \sin \theta}{R/2 \sin \theta} - \nu \right] \rightarrow$$

Because of the membrane effect, shell plastic moment is not $M_0 = \frac{\sigma_0 t^2}{4}$ anymore and it will be

almost equal to $M_p \approx M_0 - \frac{\sigma_0 \hat{t}^2}{4}$. In this equation, $\hat{t} = \frac{P\nu}{2\pi r \sin \theta \sigma_0}$ and consequently:

$$M_p = \frac{M_0 \left[1 + R/t_0 \left(1 - \frac{\theta}{\tan \theta} \right) \right]}{2} [(1+\nu) \ln 1.5 - \nu] \rightarrow$$

Hence:

$$M_0 - \frac{\sigma_0 \hat{t}^2}{4} = \frac{\frac{\sigma_0 t_0^2}{4} \left[1 + R/t_0 \left(1 - \frac{\theta}{\tan \theta} \right) \right]}{2} [(1+\nu) \ln 1.5 - \nu] \quad (1.26)$$

In the last stage of deformation, hemispherical shell will be punched under the point load.

Subsequently; the ultimate bearing capacity is roughly equal to:

$$P_U \approx 2\pi \left(b + \frac{t_0}{2} \right) t_0 \sigma_0 \quad (1.27)$$

1.4. Nonlinear Finite Element Analysis (FEA)

1.4.1 Elements and Modeling

Finite element analysis (FEA) is capable of modeling elastic-perfectly plastic material behavior with nonlinear geometry where the analysis is based on the initial geometrical shape. This should give a limit load and load-deformation response almost equal to the rigid-plastic limit load and overall response since the elastic deformations are negligible compared to the plastic deformations. This makes it possible to compare the results using the finite element method with those of the analytical solution. All FEA for this investigation was performed using the general purpose program ABAQUS Version 6.7. The boss used to load the spherical shell was modeled as a rigid element. Both eight node axisymmetric rectangular and six node triangular shell elements were used to model the hemispherical shell Figs.1.11-1.13. In the present numerical analyses, the hybrid element was chosen for all finite element models in order to avoid the problem of mesh locking and to get correct element stiffness and accurate results. The shell is pinned at the base and the material behavior after yielding is assumed to obey the Tresca or Von Mises yield criterion.

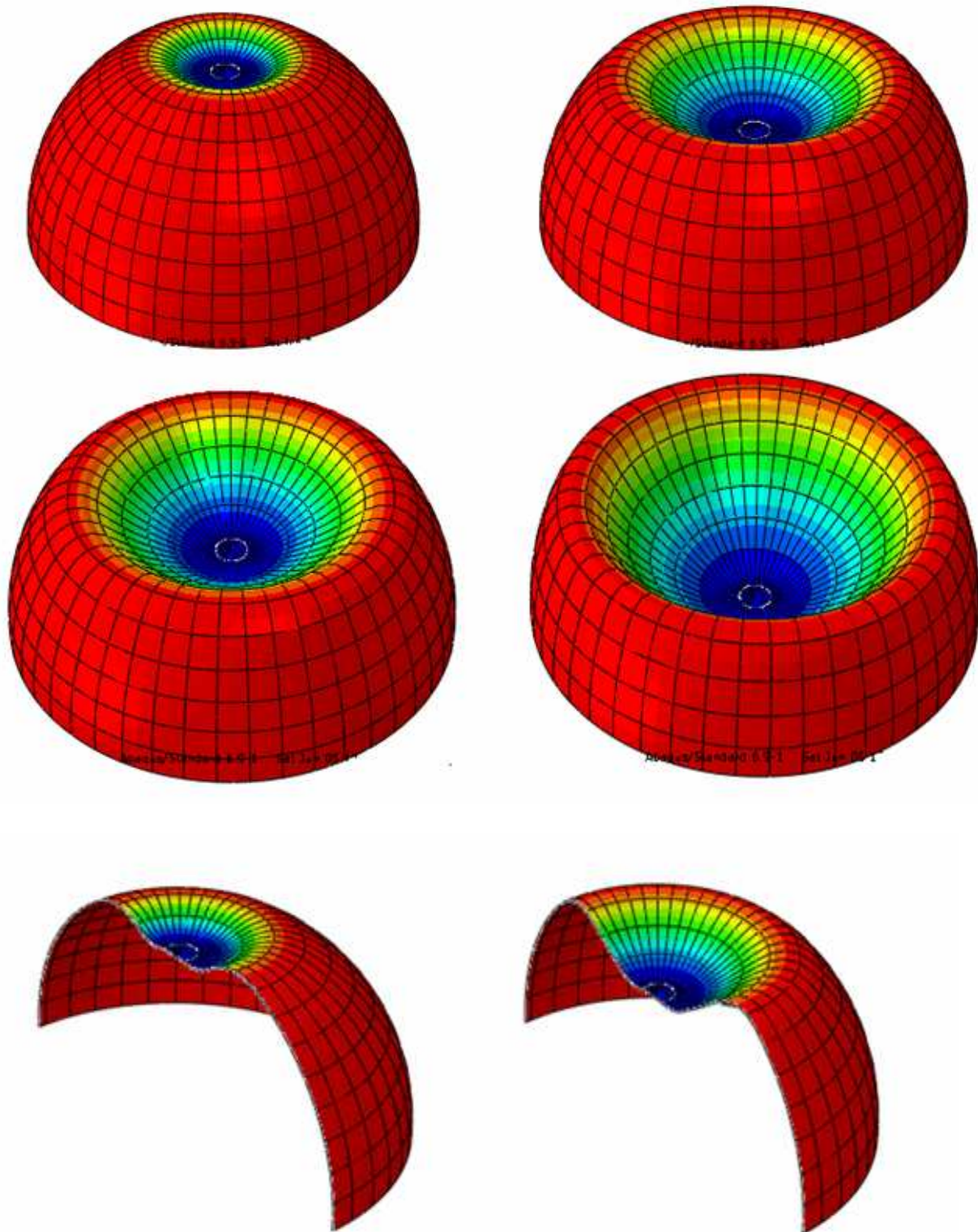


Figure 1. 11: Deformation pattern of the hemispherical shell using 8 node axisymmetric rectangular shell element.

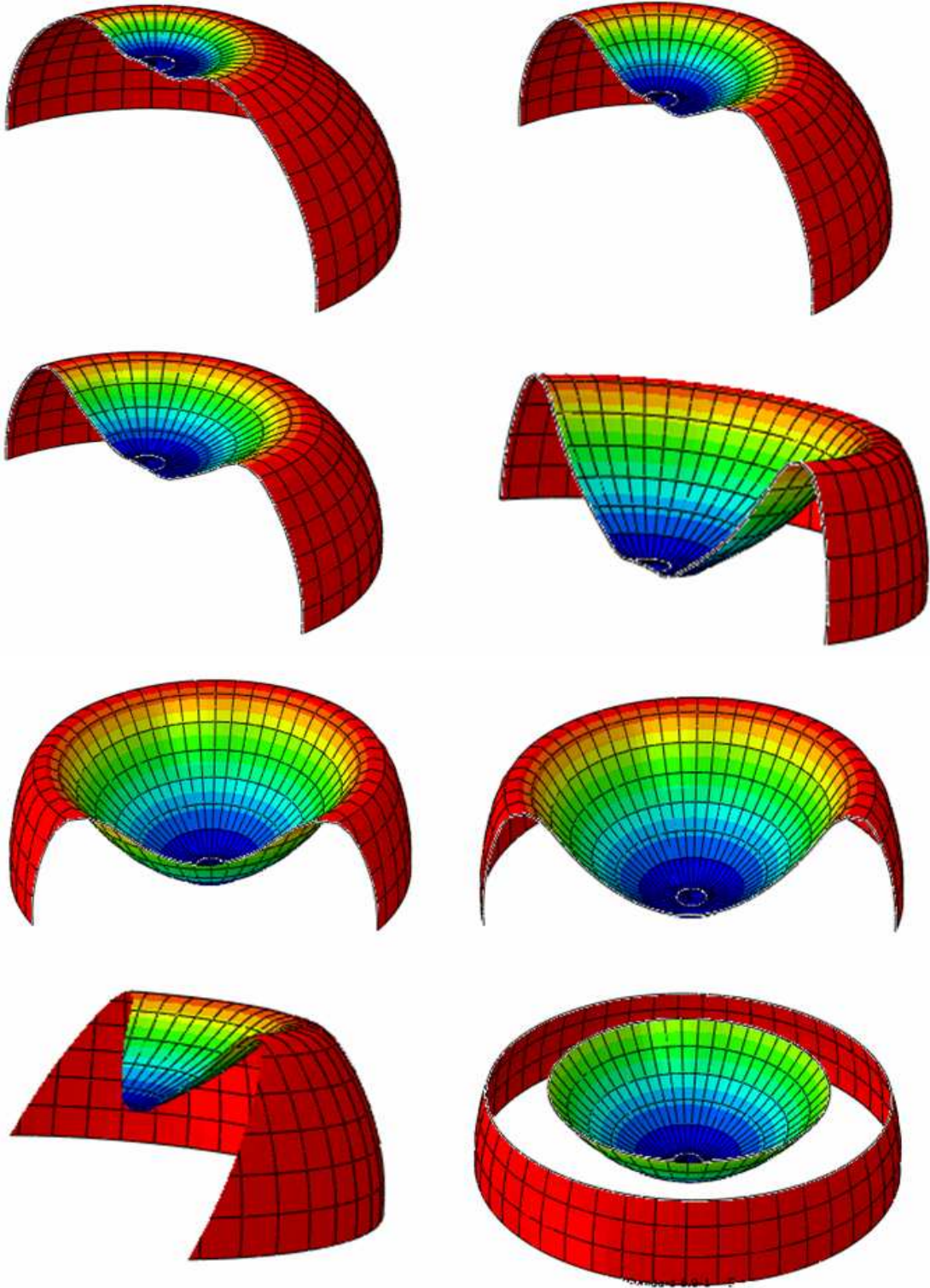


Figure 1. 12: Different cuts of the deformed moderately thick shell $R/t_0 \leq 100$.

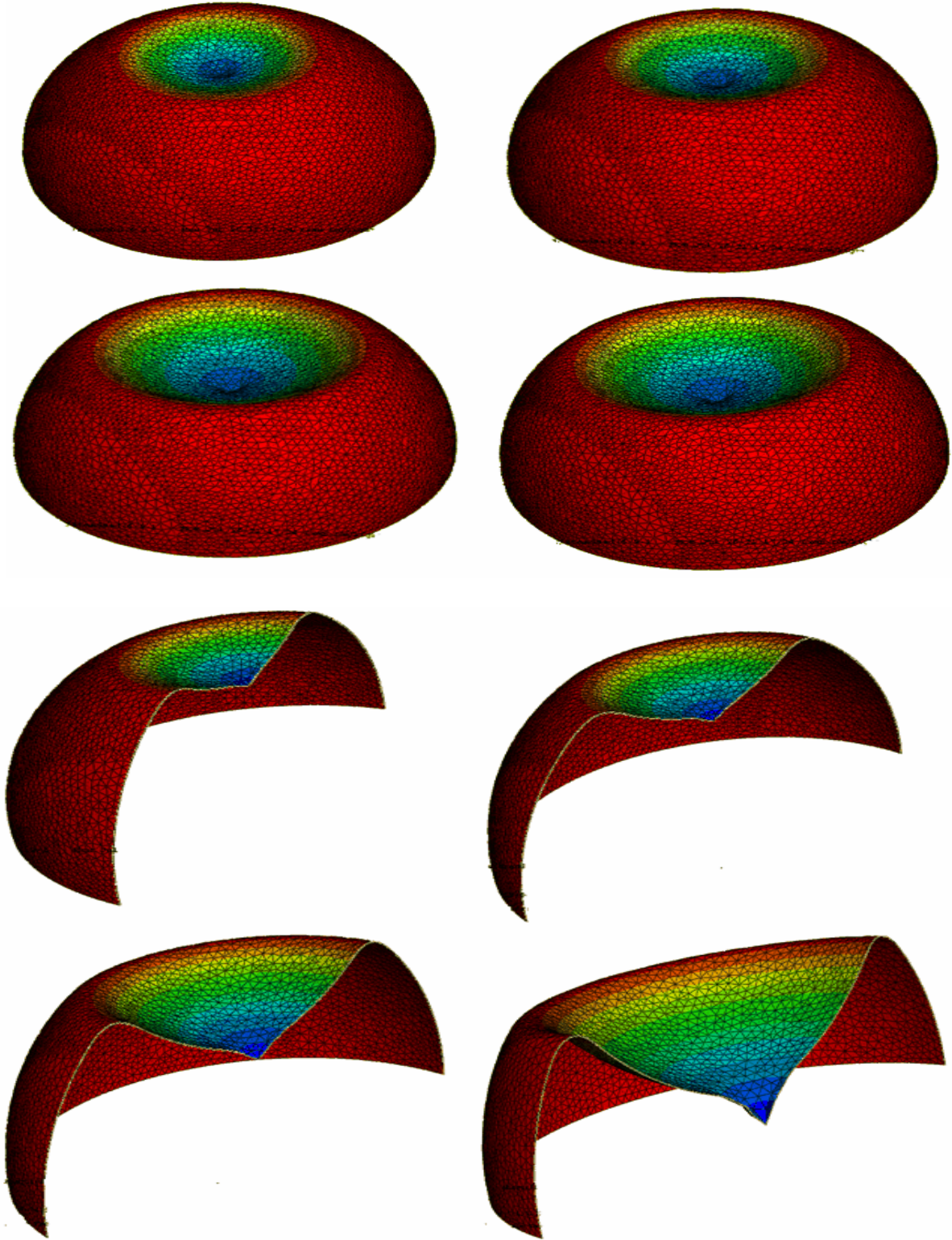


Figure 1. 13: Deformation pattern of the moderately thick shell $R/t_0 \leq 100$ using six node triangular shell element.

1.4.2 Numerical Results

The numerical results for moderately thick shells ($R/t_0 < 100$) were identical in the case of axisymmetric and general 3D models. These results were found to compare well to the analytical and experimental findings. On the other hand a bifurcation from axisymmetric response is observed at some point after initial collapse in thin shells with ($R/t_0 > 100$) and this phenomenon is shown in Figs.1.14-1.17. The level of bifurcation load depends on the effect of geometrical parameters of shell (wall thickness t_0 , radius R , R/t_0 ratio), the material properties as well as the size of the boss.

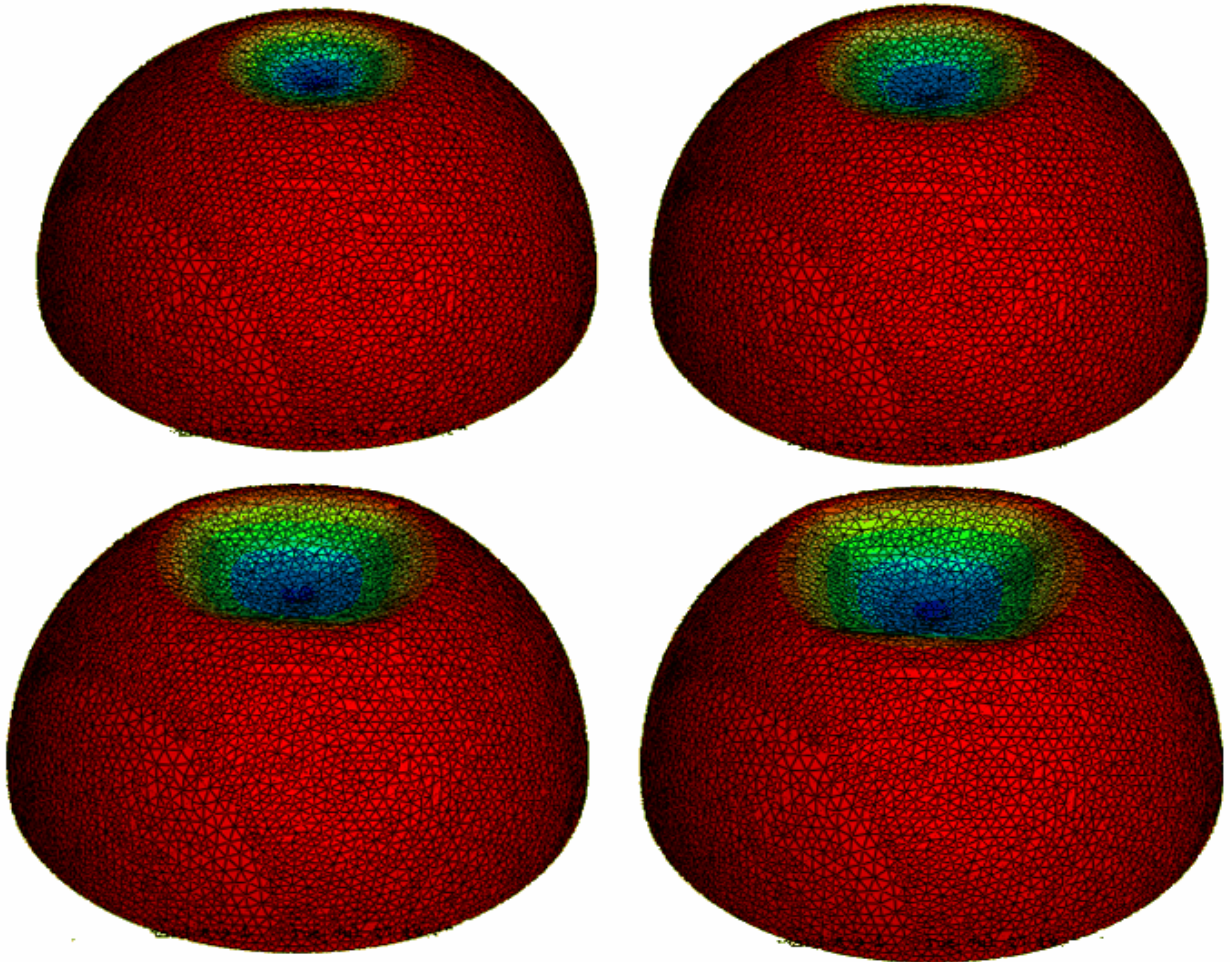


Figure 1. 14: Buckling initiation of thin shell $R/t_0 > 100$ using six node triangular shell elements.

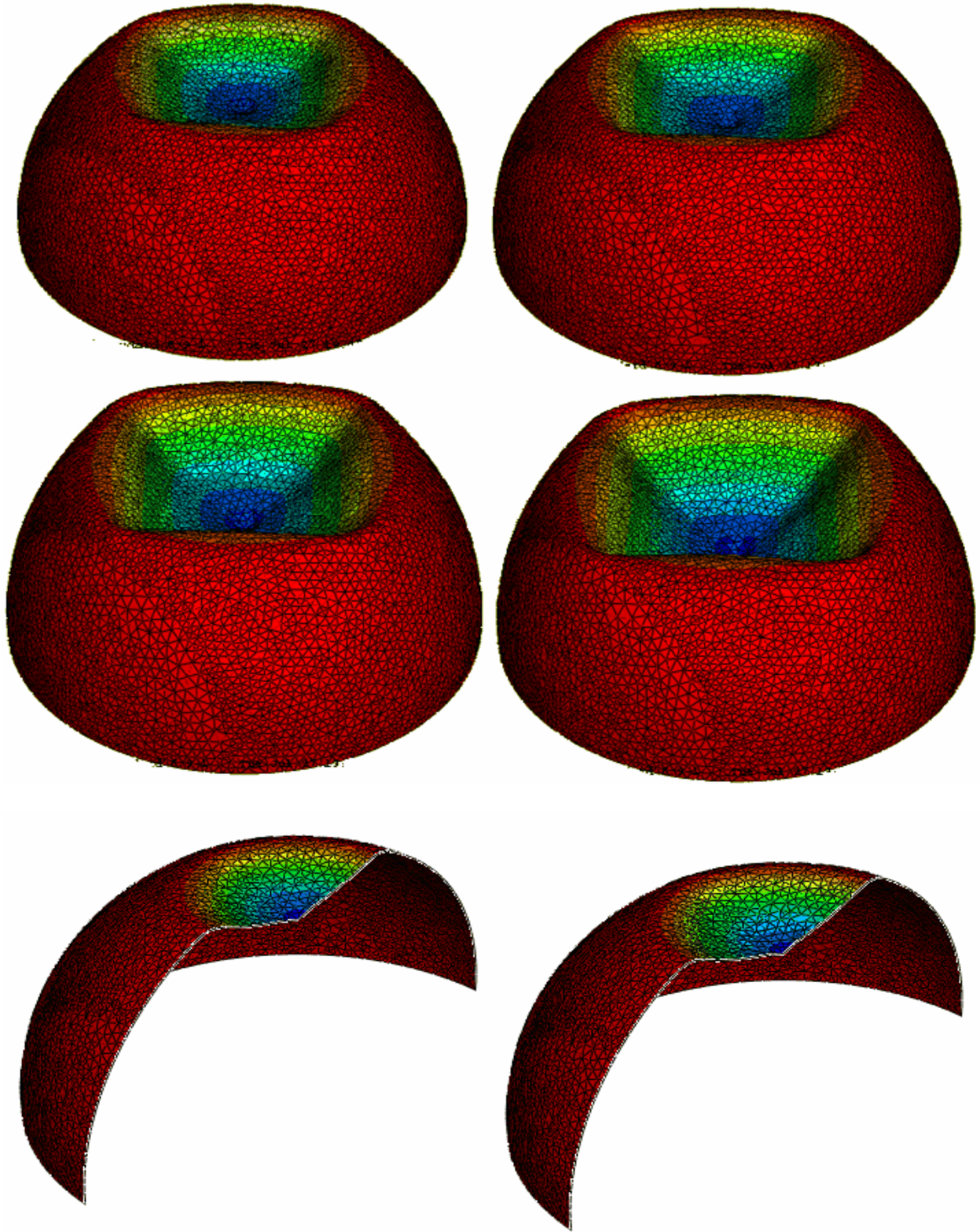


Figure 1. 15: Subsequent deformation of thin shell $R/t_0 \gg 100$ showing the secondary bifurcation phenomenon.

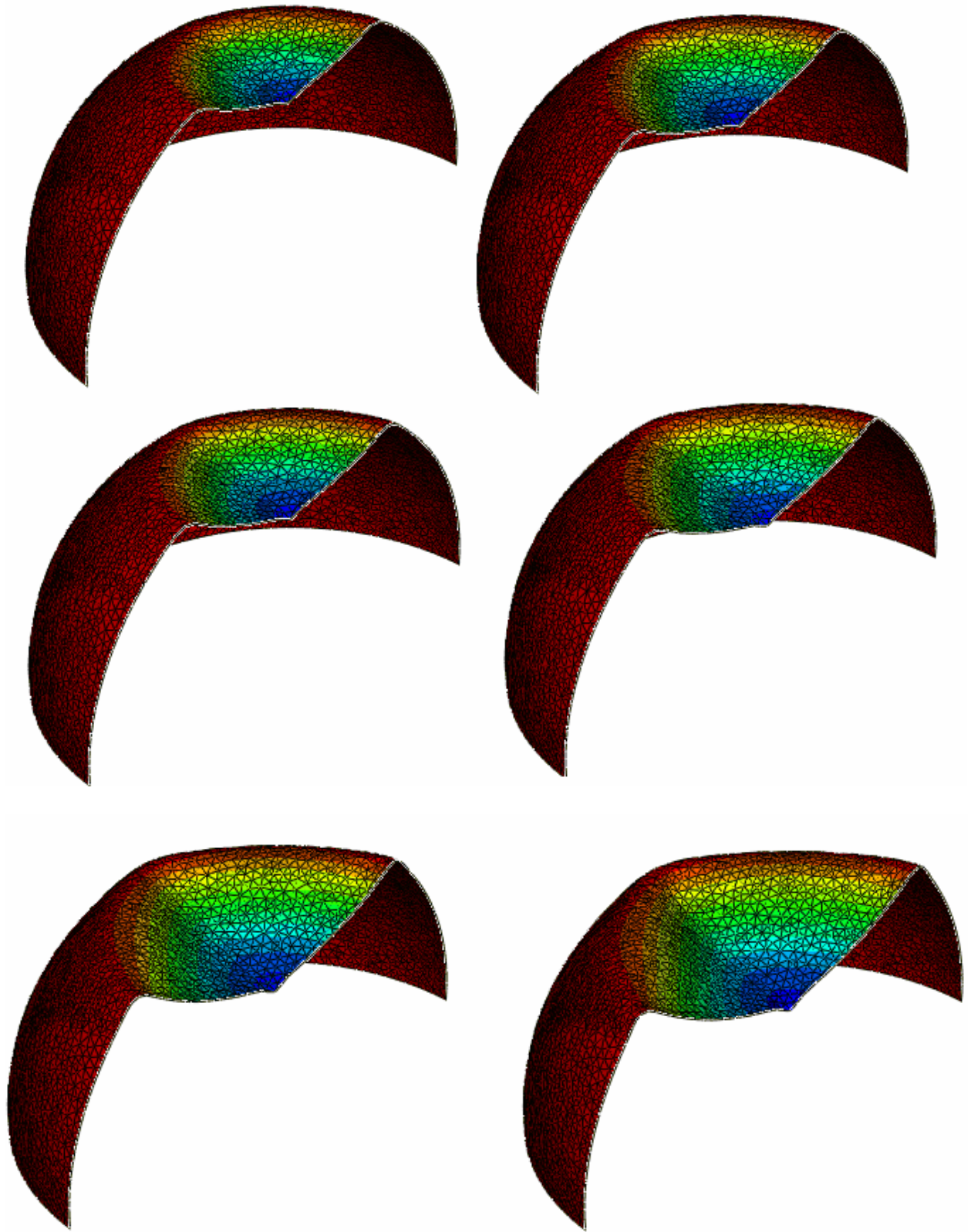


Figure 1. 16: Different cuts of the deformed thin shell $R/t_0 \gg 100$

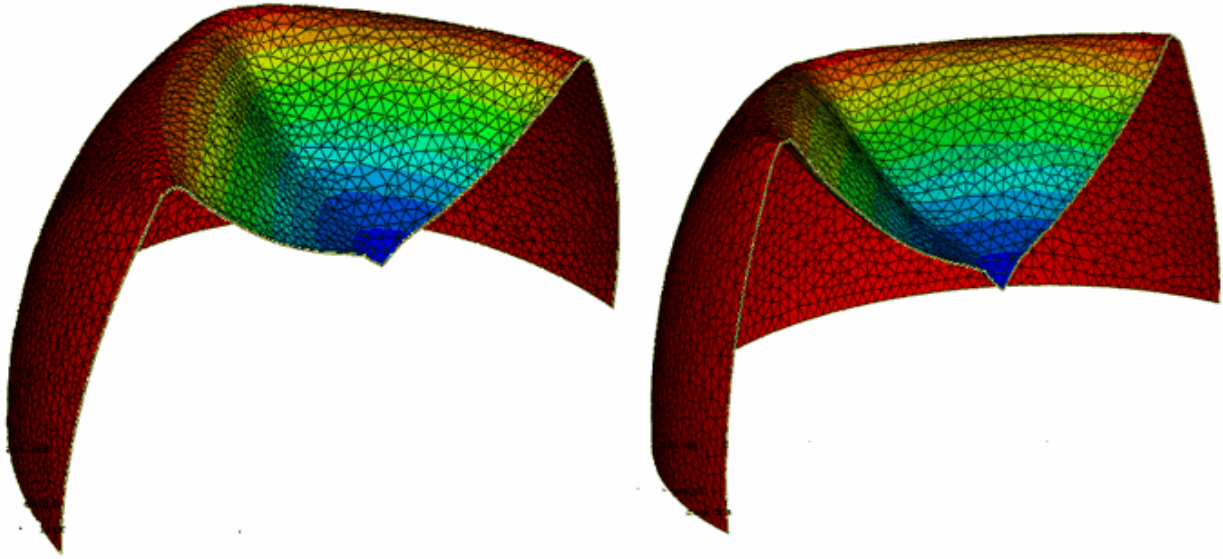


Figure 1. 17: Deformation pattern of the thin shell $R/t_0 \gg 100$ showing the secondary bifurcation phenomenon.

1.5. Experimental Program

1.5.1 Parameters and test setup

Different samples with various R/t_0 ratios were designed, manufactured, and tested, Figs. 1.18. These were made out of Bronze ($E = 120GPa$ and $F_y = 110MPa$), stainless steel ($E = 210GPa$ and $F_y = 315MPa$), and copper ($E = 116GPa$ and $F_y = 132MPa$). The radius of the shells was $R = 50mm$ and $R = 75mm$ respectively. The thickness of the shells were $t_0 = 0.3mm$ and $t_0 = 1mm$. These parameters yield R/t_0 ratio of 250 for Bronze, 166 for Stainless Steel, and 75 for Copper alloy. During testing, these shells were subjected to concentrated loads at the apex by means of rigid flat-based circular rods of three different boss sizes, namely $b = 0.125, 0.25, 0.5mm$ (Fig.1.19).



Figure 1. 18: Different hemispherical shell samples were made for experimental study



Figure 1. 19: Three different boss size used for loading ($b = 1.25, 2.5, 5.0 \text{ mm}$)

The hemispherical shells were rigidly supported against translation around the bottom circumference by using grooved base plate as shown in Fig.1. 20.



Figure 1. 20: Grooved base plate as a support for two sizes of hemispherical shells

The load-deflection curves for the shells were recorded on a Riehle Universal testing machine (Figs.1.21). The materials were selected for manufacturing after tension coupons were tested to ensure that their material behavior corresponds closely to rigid-plastic. This was the case in order to fruitfully compare experimental and theoretical results.



Figure 1. 21: Riehle Universal testing machine for displacement control measurements

The yield stress for each material was found from the load-deflection diagrams for the metal coupons since in forming the shell specimens only a negligible amount of work hardening was involved. Figs.1.22-1.24 shows typical stress strain diagrams for the Copper alloy, Bronze, and Stainless Steel used in experiments.

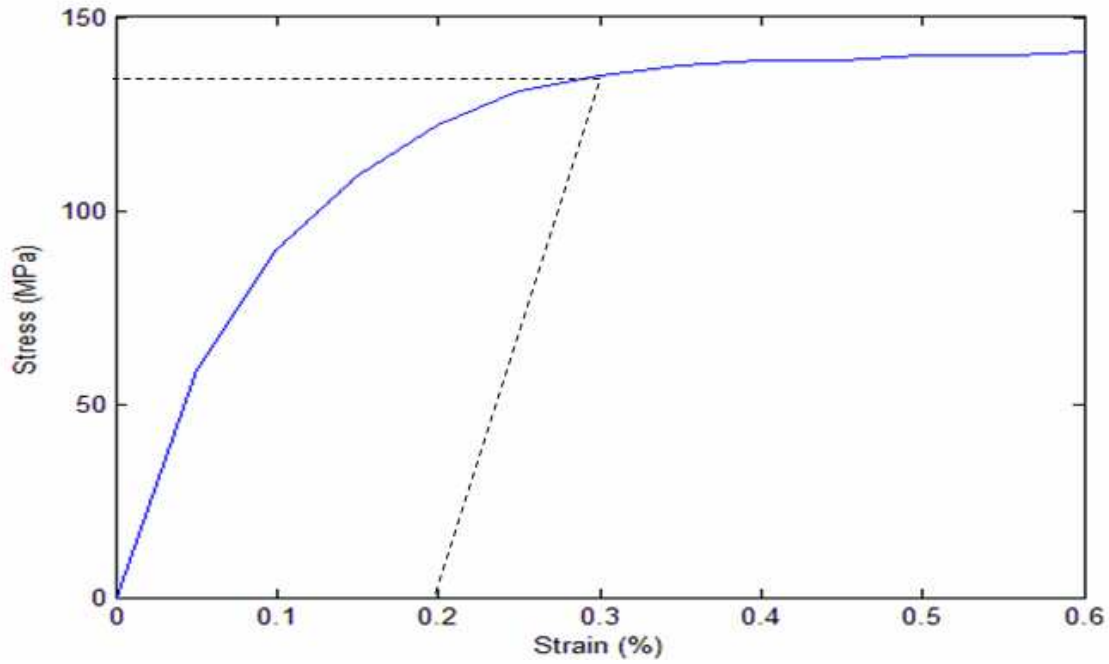


Figure 1. 22: Stress strain diagram for copper alloy.

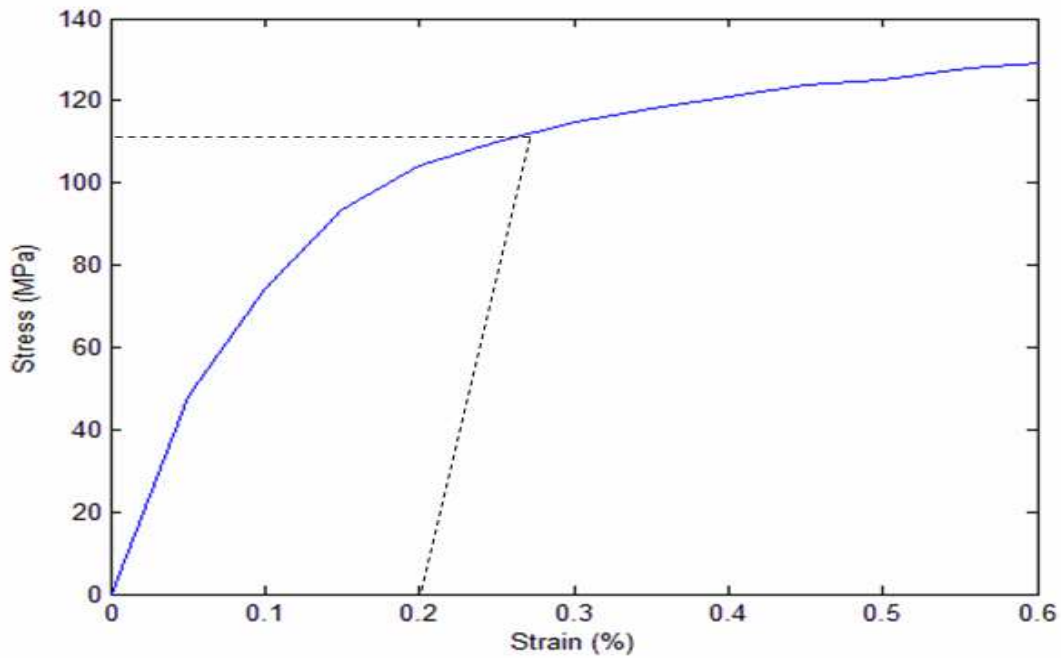


Figure 1. 23: Stress strain diagram for Bronze.

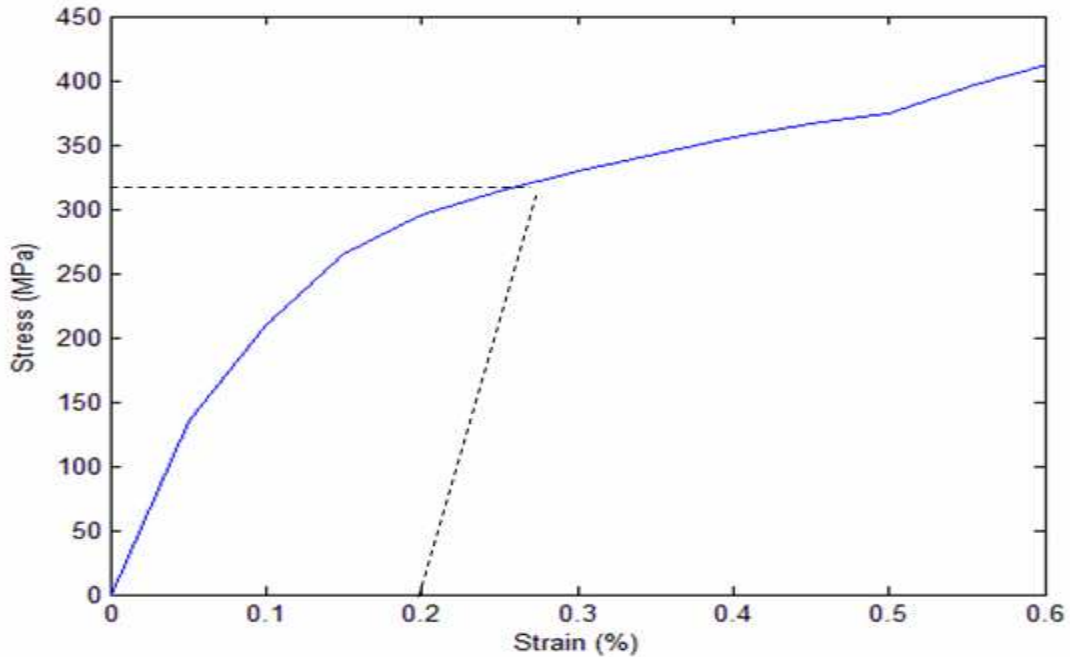


Figure 1. 24: Stress strain diagram for Stainless Steel.

1.5.2 Experimental Results:

It is evident from Fig 1.25 that the deformation of the moderately thick copper alloy shell $R/t_0 \approx 75$ is axisymmetric throughout the different loading stages. On the other hand, the deformation of the thin stainless steel shell $R/t_0 \approx 166$ is axisymmetric upon initial collapse and early subsequent deformation Figs 1.26-1.27. However, Figs1.27-1.28 show the latter bifurcation in deformation as an interesting secondary phenomenon. This phenomenon takes place in thin shells, which have $R/t_0 > 100$, as shown by the numerical results (Fig 1.46).



Figure 1. 25: Deformation of the moderately thick shell (Copper alloy $R/t_0 \approx 75$)



Figure 1. 26: Initial buckling and post buckling of the thin shell (Stainless Steel $R/t_0 \approx 166$).

Similarly, the deformation of the thin bronze shell $R/t_0 \approx 250$ is also axisymmetric upon initial collapse and some short subsequent deformation Figure 1.29. Then, Fig 1.30 shows the degeneration to the secondary bifurcation deformation which is clearly identified in Figs.1.31-1.33.

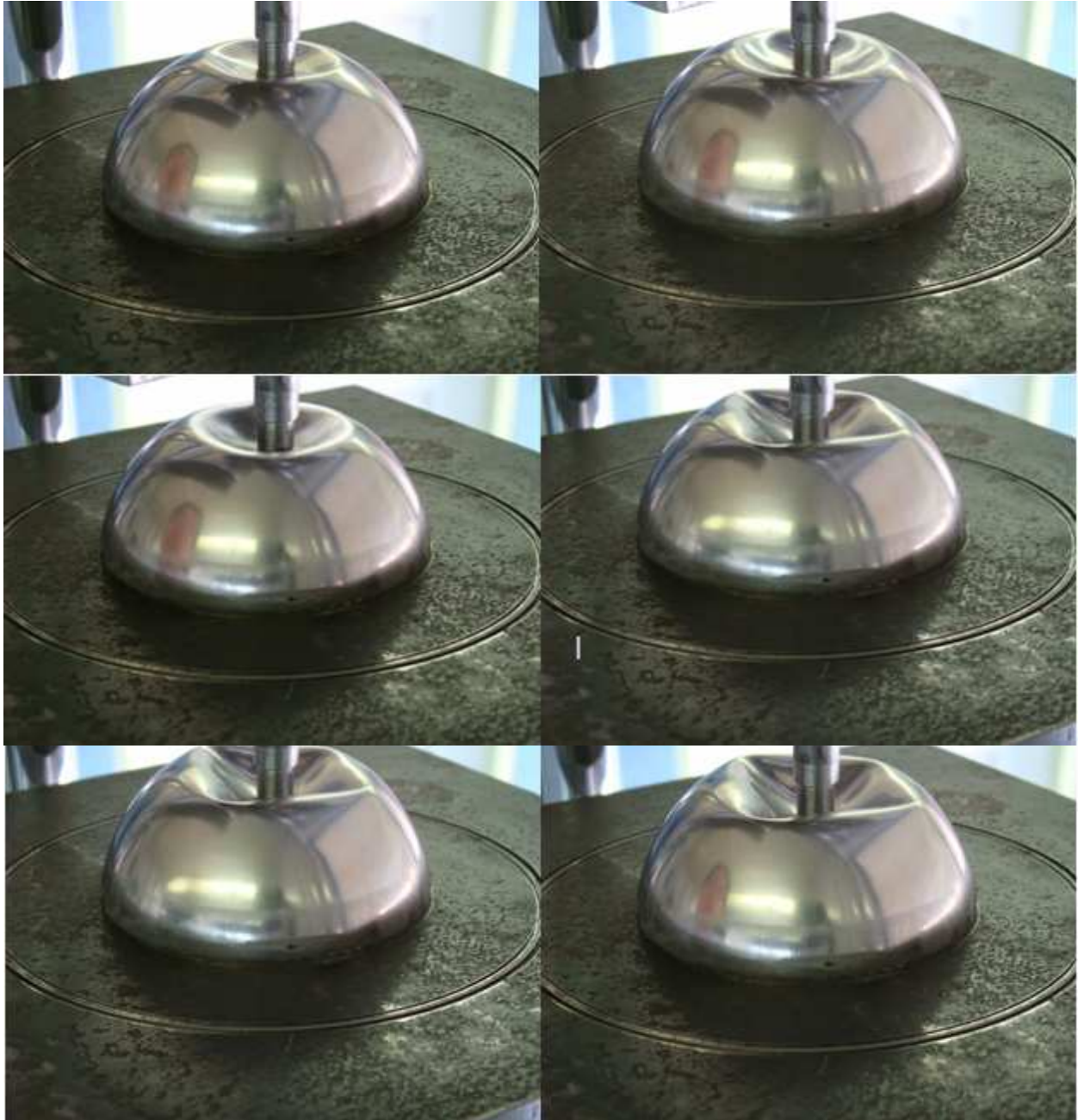


Figure 1. 27: Degeneration of axisymmetric deformation of the thin shell (Stainless Steel $R/t_0 \approx 166$).

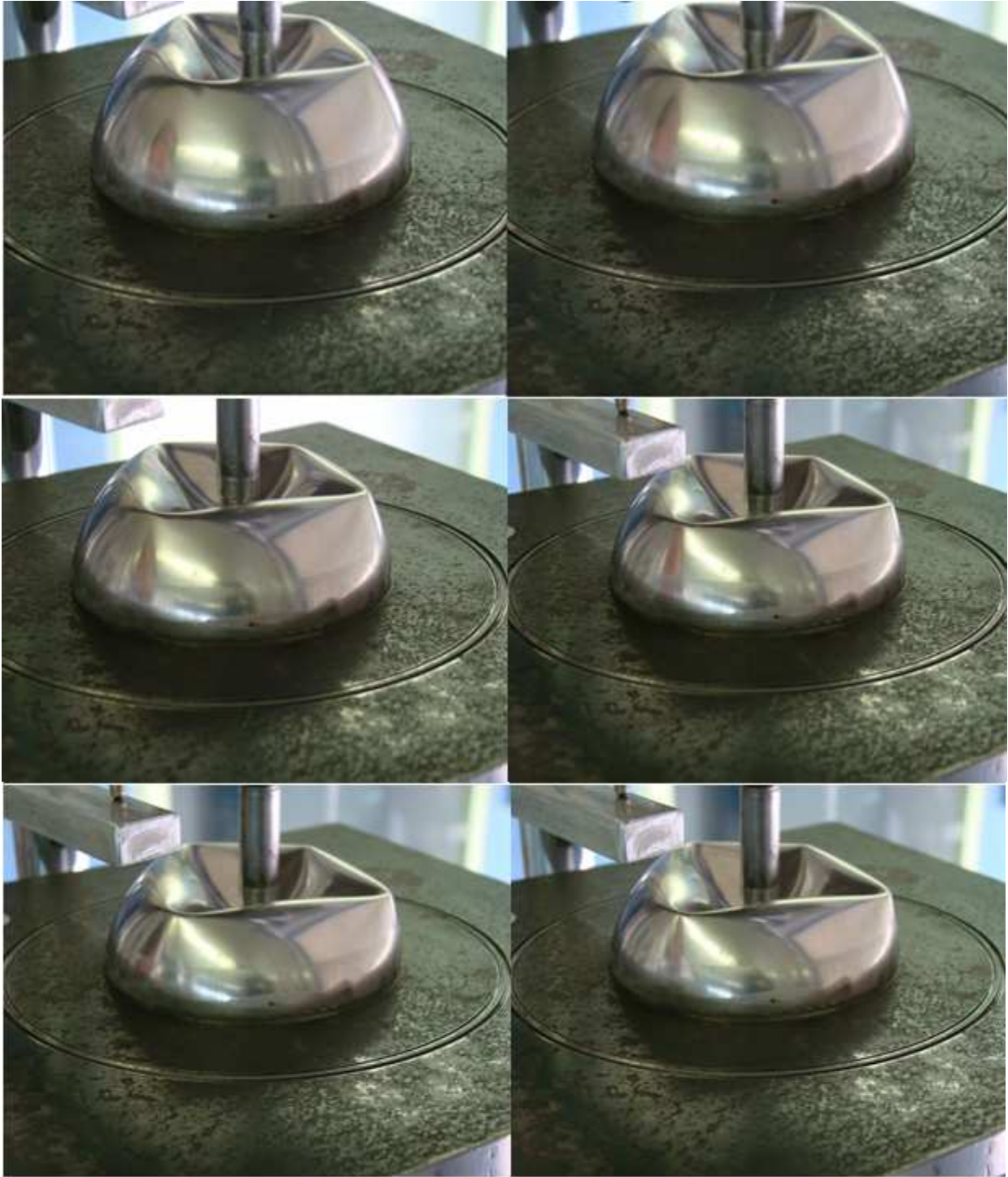


Figure 1. 28: Secondary bifurcation deformation of the thin shell (stainless steel $R/t_0 \approx 166$)

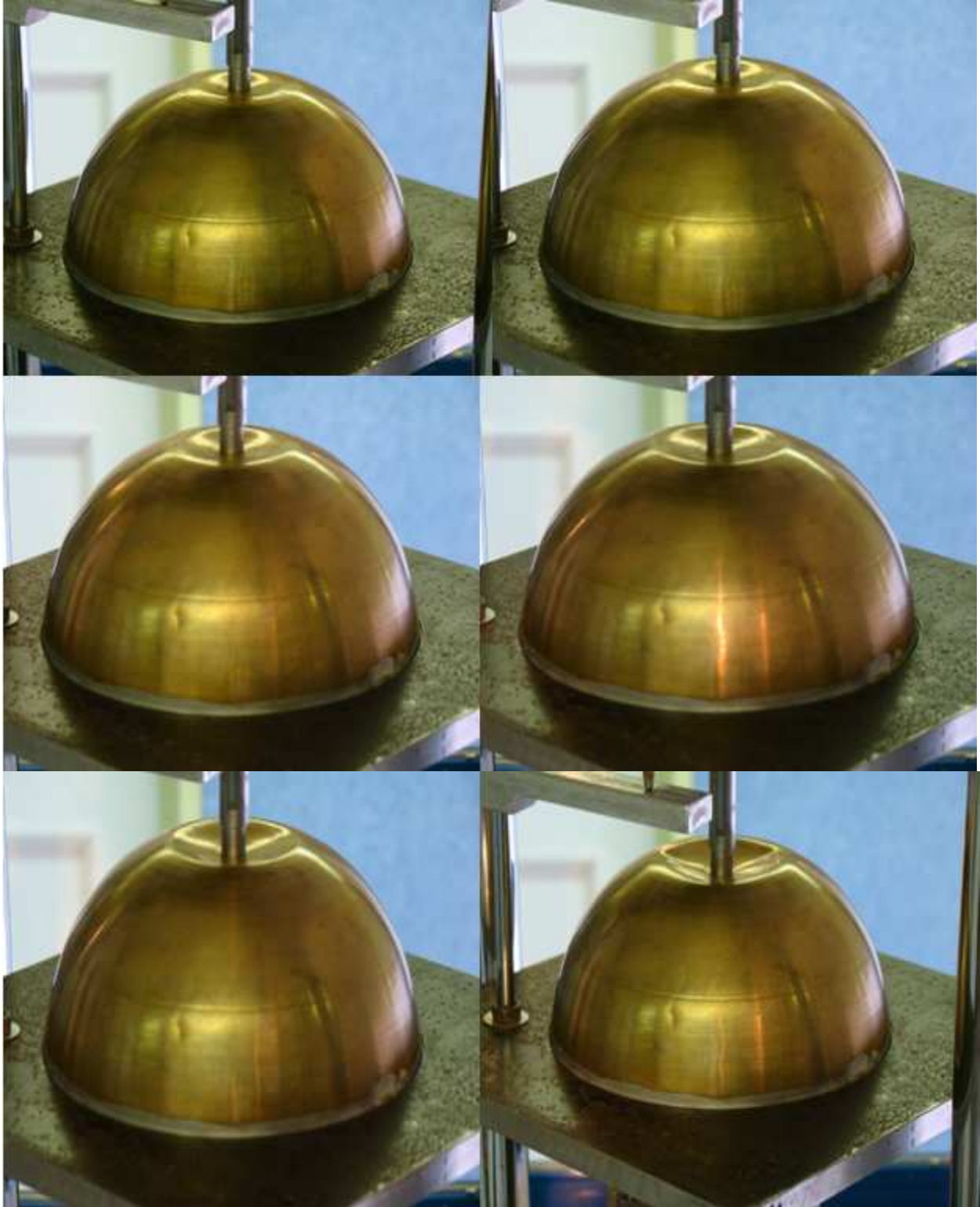


Figure 1. 29: Initial buckling and axisymmetric post buckling of the thin shell (Bronze $R/t_0 \approx 250$)

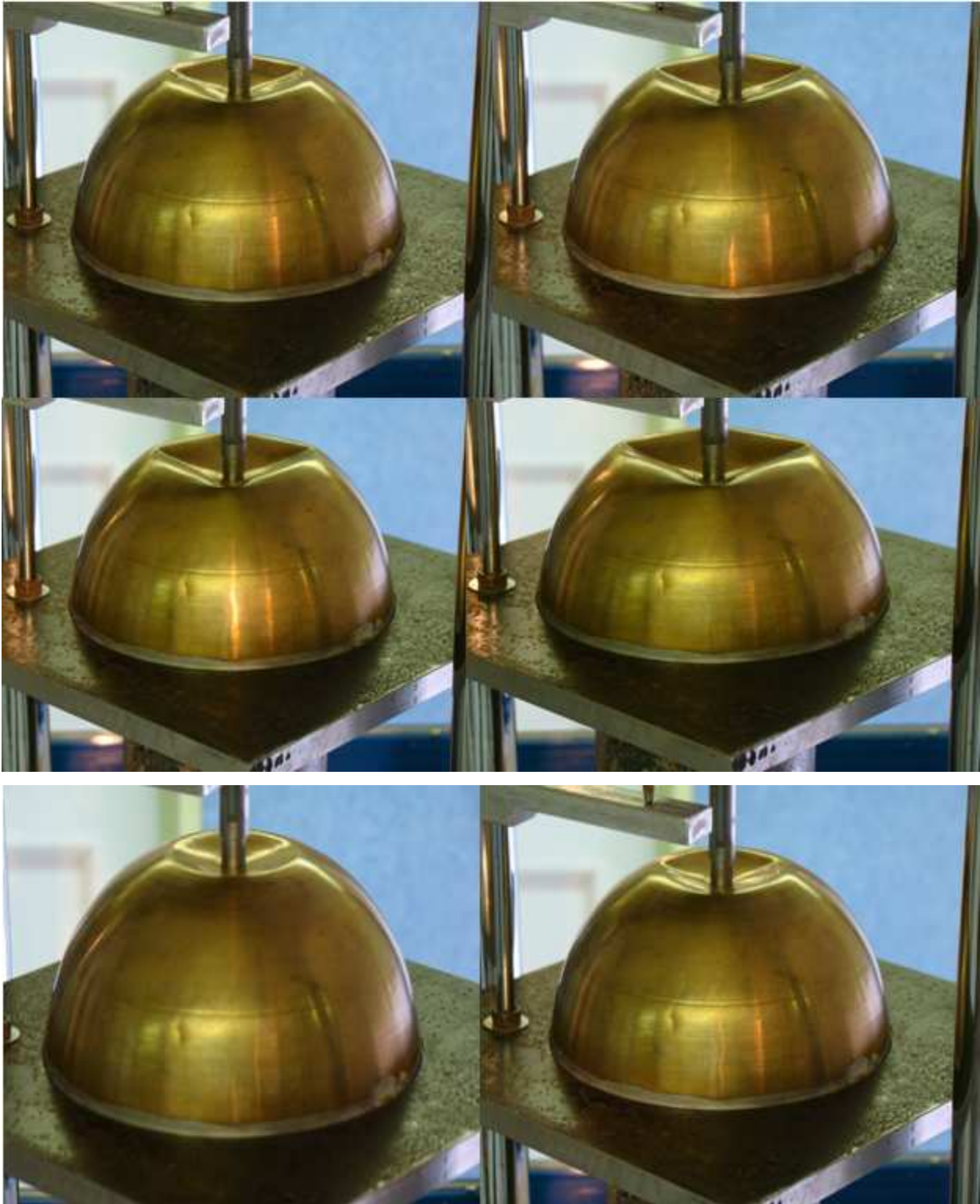


Figure 1. 30: Degeneration of the axisymmetric deformation of the thin shell (Bronze $R/t_0 \approx 250$).



Figure 1. 31: Secondary bifurcation deformation of the thin shell (Bronze $R/t_0 \approx 250$)



Figure 1. 32: Different stages of the triangular with secondary bifurcation (Bronze $R/t_0 \approx 250$)



Figure 1. 33: Final deformation of the thin shell (Bronze $R/t_0 \approx 250$)

1.6 Results and Discussion

As it is seen in Fig.1.25 for relatively thick shell $R/t_0 < 100$, shell deformation pattern as assumed in the analytical solution consists of a cone and torus which spread out axisymmetrically from the apex with increasing load. Therefore, the analytical solution, experimental findings and numerical results are expected to match for large amplitude of deformations, Fig 1.34. However, when $R/t_0 > 100$, the deformation follows the same axisymmetric pattern in the beginning. Then, the annular zone degenerates into various n-sided polygon deformation modes and bifurcation in deformation pattern is observed (Figs.1.26-1.33).

In order to find bifurcation point in thin wall hemispherical shell ($R/t_0 > 100$) for which the bending and membrane stresses are simultaneously important and assuming the boss pressure to be uniformly distributed over the region of contact, new solution has been derived using equilibrium approach.

Figs. 1.34, 1.40, and 1.43 give the load deflection curve for the copper alloy, Bronze, and stainless steel shell respectively. The analytical solution results seem to be always slightly less than the numerical solution because the finite element solution gives a lower bound on the maximum displacements for a given set of forces and gives an upper bound on the maximum stresses for a given set of displacements. The secondary bifurcation response is shown to yield higher loads than the axisymmetric response for the same h/R value Fig 1.40 and 1.43, the axisymmetric analytical solution may still be used for design of thin shells since it is on the conservative side. Figs.1.35, 1.41, and 1.44 show the boss effect on the initial collapse load. Due to ignoring the shell curvature in the small vicinity of the load, the collapse load is always

slightly on the safe side. However, because of the sample imperfection in the experimental study, the experimental findings are on the lower side

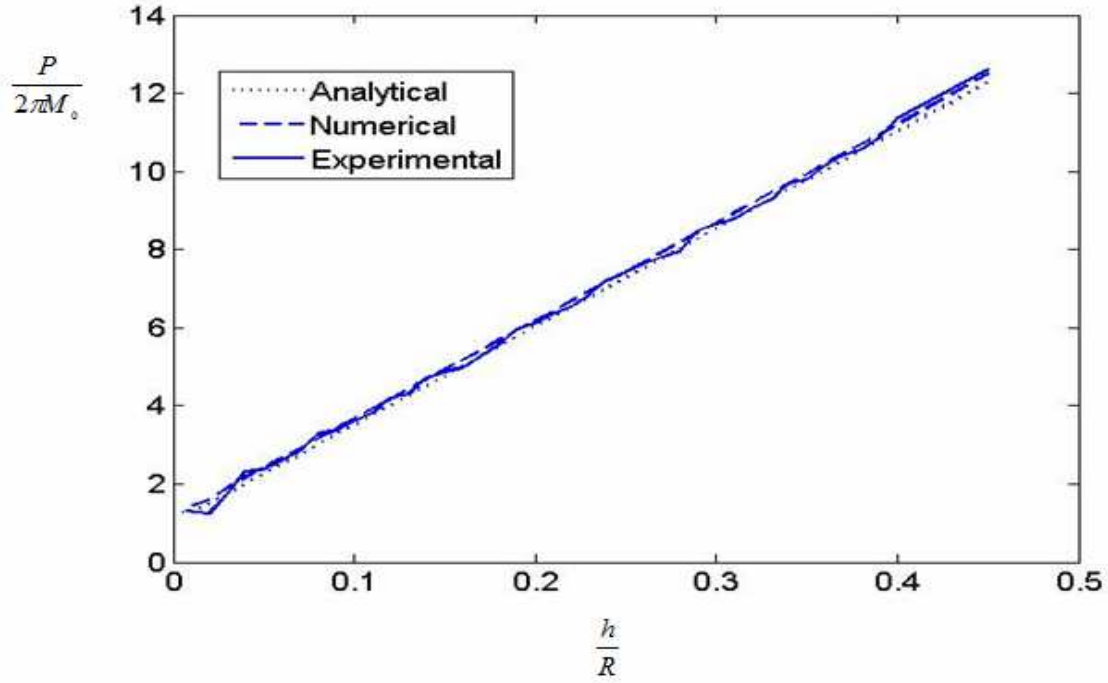


Figure 1.34: Dimensionless Load deflection curve for copper alloy shell ($R/t_0 \approx 75$)

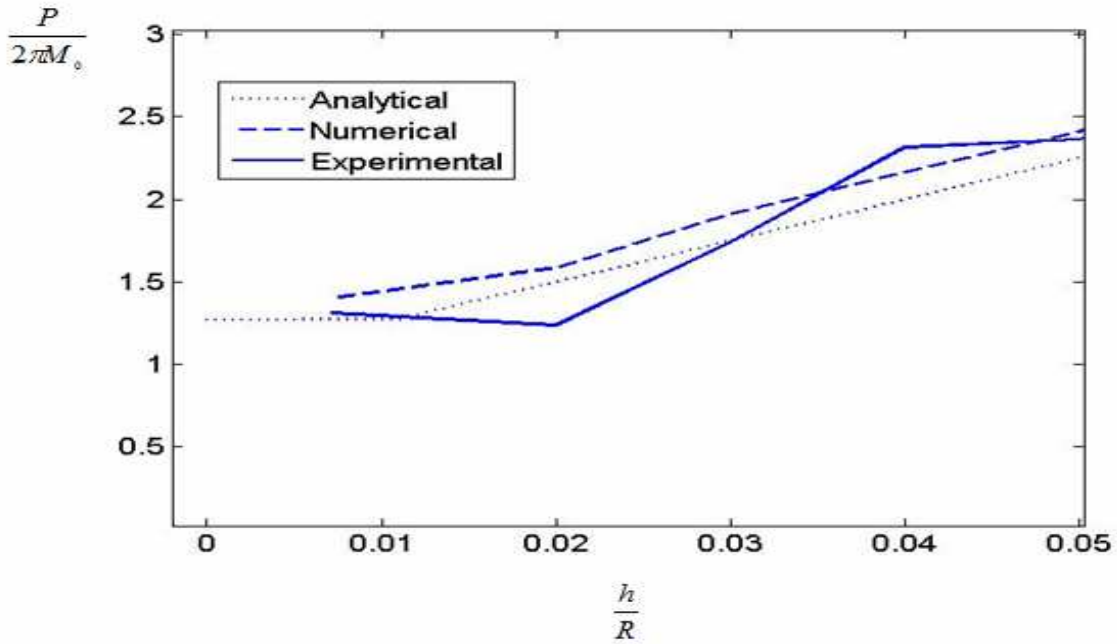


Figure 1.35: Comparison of initial collapse response for copper alloy shell ($R/t_0 \approx 75$)

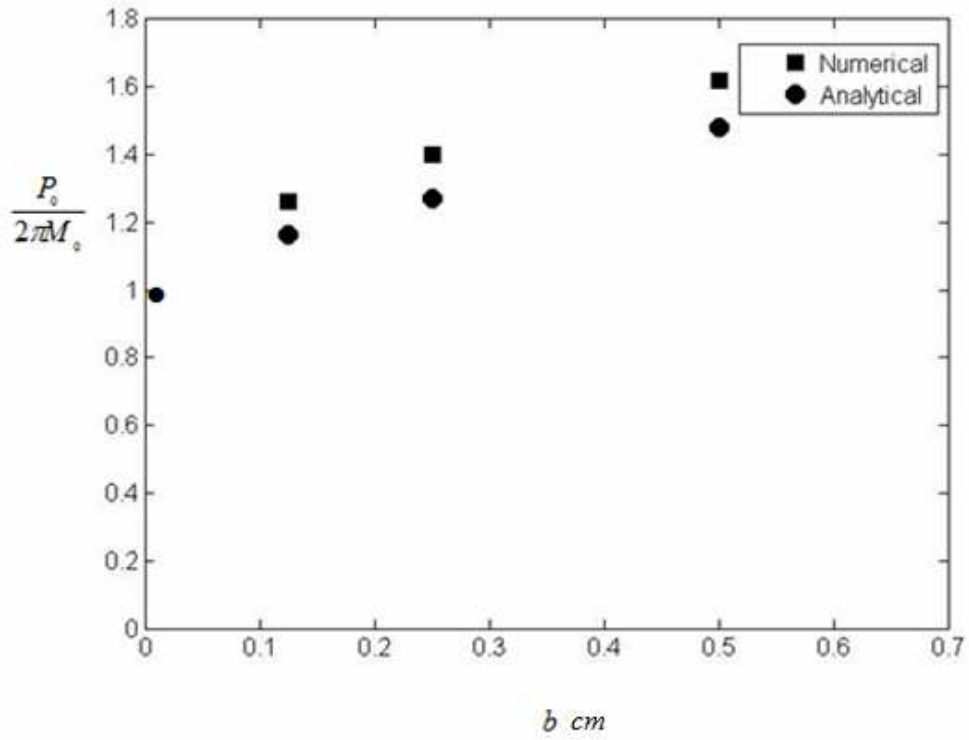


Figure 1. 36: Dimensionless initial collapse load vs boss size for copper alloy shell ($R/t_0 \approx 75$)

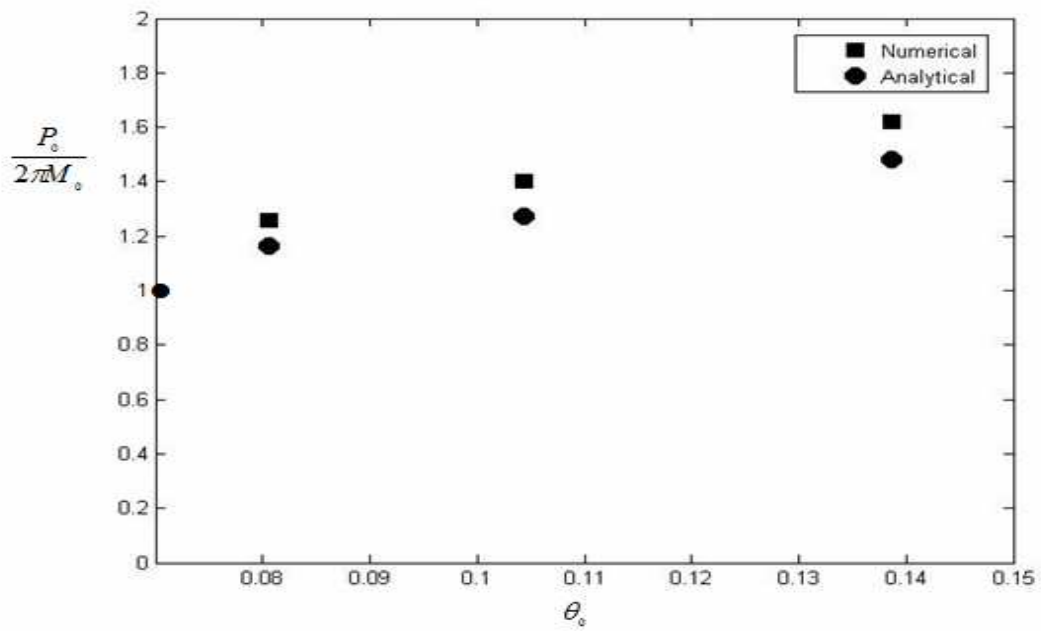


Figure 1. 37: Dimensionless initial collapse load vs initial collapse angle for copper alloy ($R/t_0 \approx 75$)

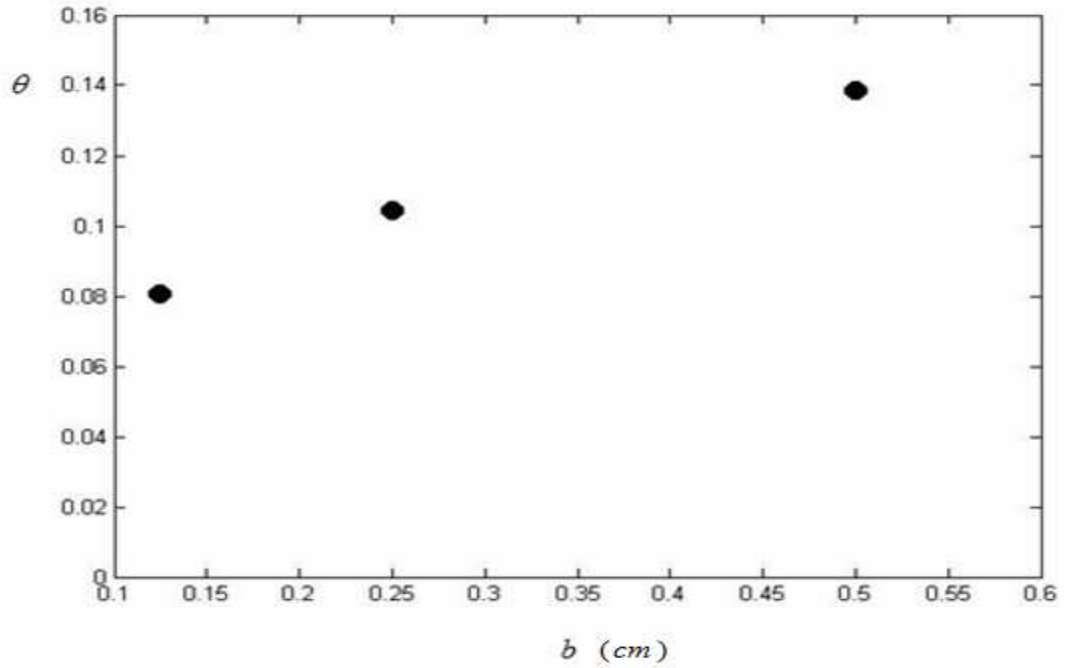


Figure 1. 38: Initial collapse angle vs boss size for copper alloy ($R/t_0 \approx 75$)

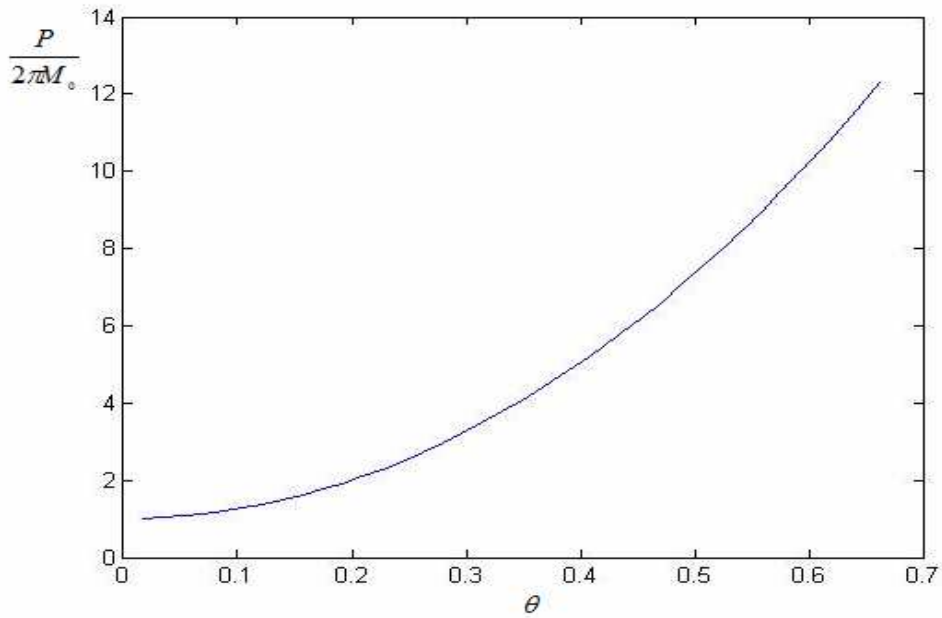


Figure 1. 39: Dimensionless Load vs knuckle meridional angle in rad for copper alloy shell ($R/t_0 \approx 75$).

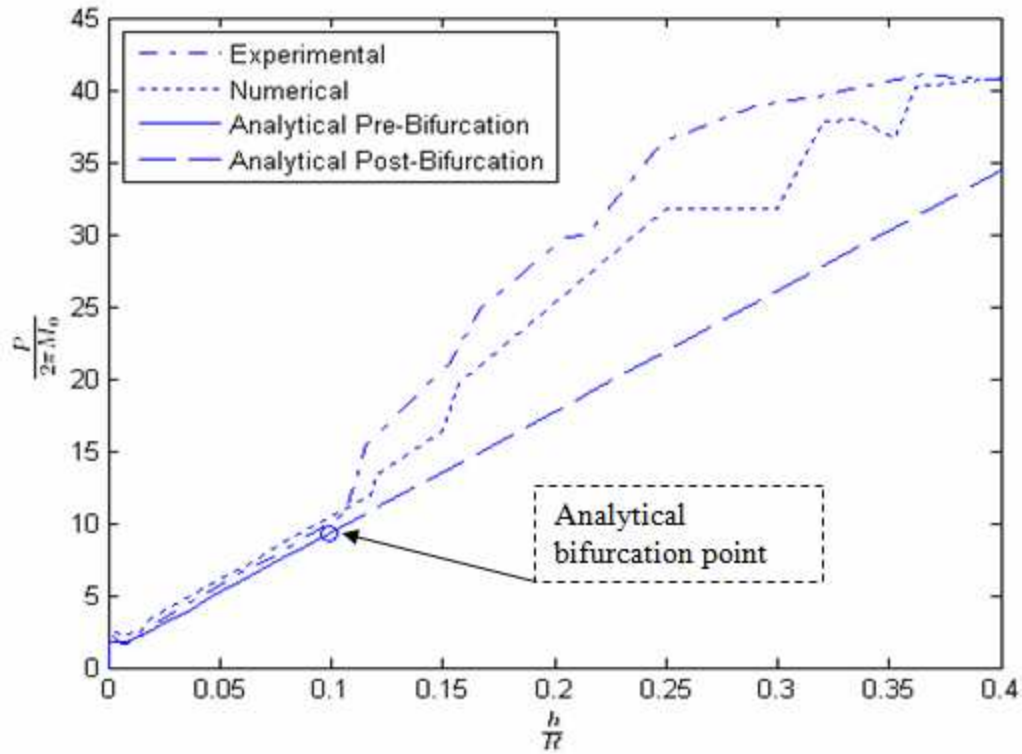


Figure 1.40: Dimensionless Load deflection curve for Bronze shell ($R/t_0 \approx 250$)

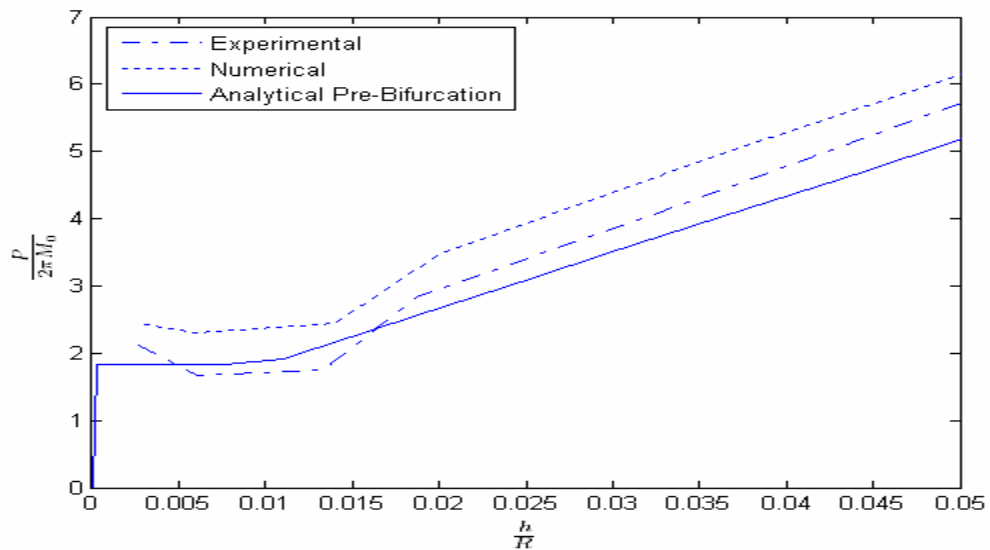


Figure 1.41: Comparison of initial collapse response for Bronze shell ($R/t_0 \approx 250$)

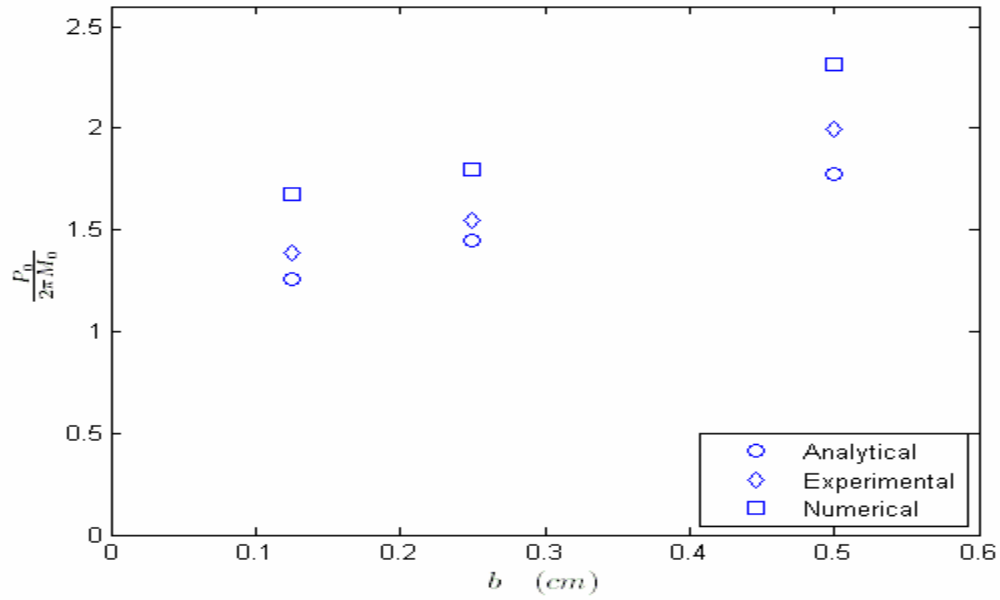


Figure 1.42: Dimensionless initial collapse load vs boss size for Bronze shell ($R/t_0 \approx 250$)

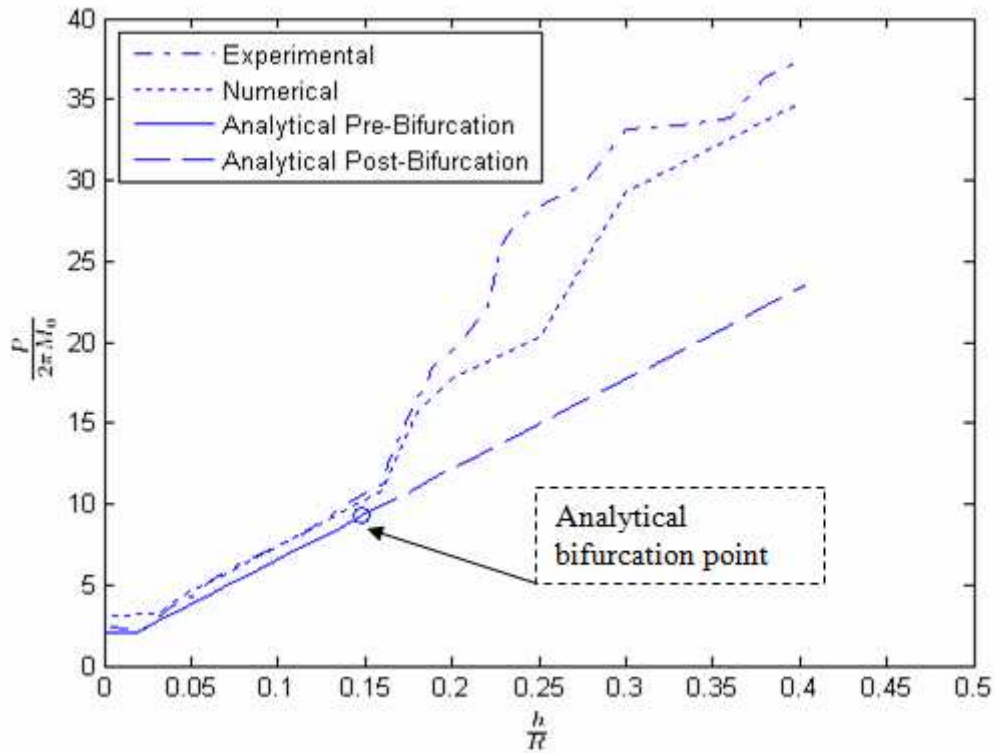


Figure 1.43: Dimensionless Load deflection curve for Stainless Steel shell ($R/t_0 \approx 166$)

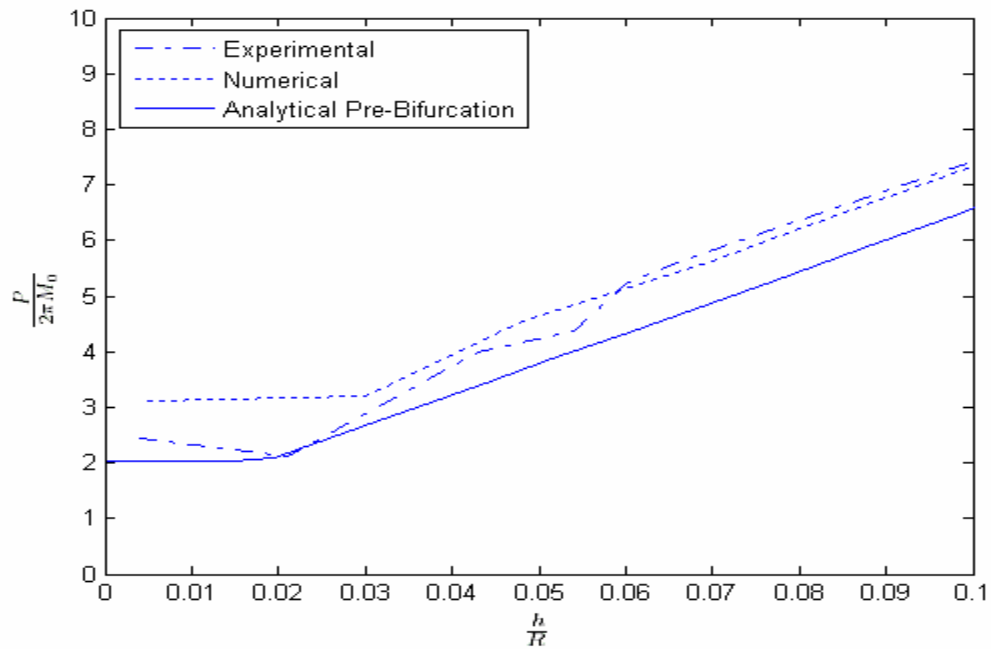


Figure 1. 44: Comparison of initial collapse response for Stainless Steel shell ($R/t_0 \approx 166$)

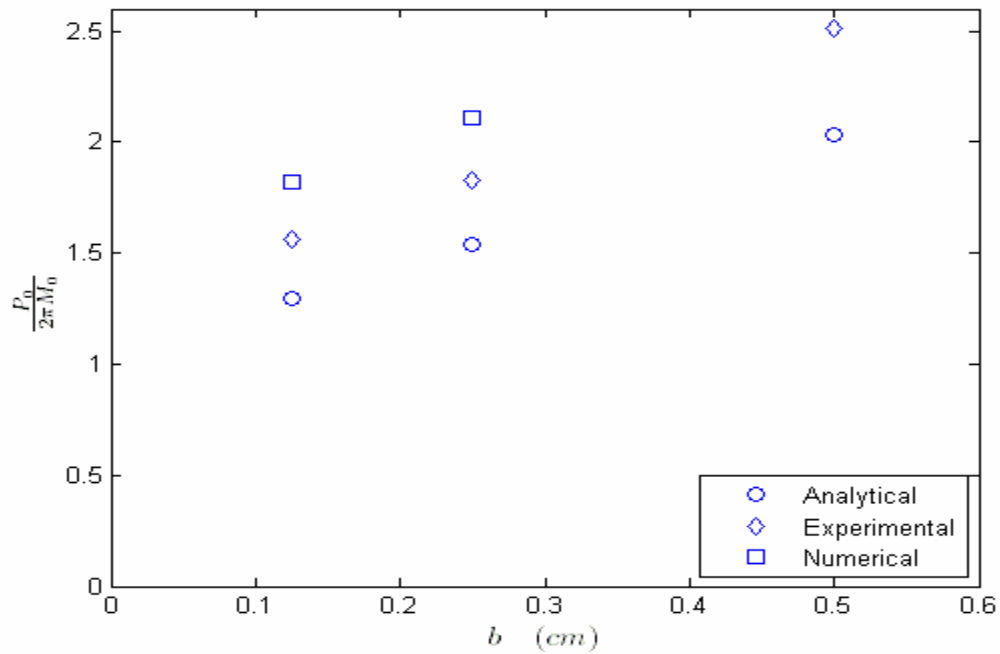


Figure 1. 45: Dimensionless initial collapse load vs boss size for Stainless Steel shell ($R/t_0 \approx 166$)

(h/R) vs (R/t)

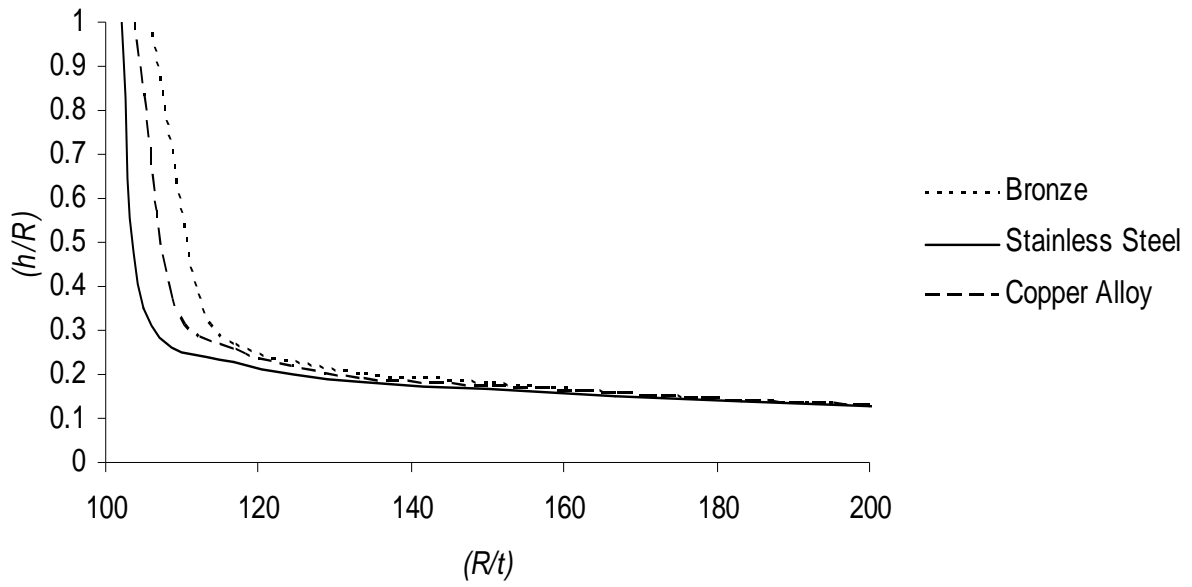


Figure 1. 46: Numerical bifurcation point for Bronze, Stainless Steel, and Copper alloy versus (R/t_0) .

1.7 Conclusions

In this research the effect of the geometry change on the plastic buckling behavior of hemispherical metal shells loaded inwardly at the apex has been studied theoretically, numerically and experimentally. An analytical expression has been derived for plastic buckling of hemispherical shell in a form which is especially convenient for application due to its simplicity. In addition, it shows that a quite simple model of deformation at equilibrium is sufficient to make predictions concerning postbuckling behavior of a moderately thick hemispherical shell subjected to a concentrated load on top. The initial buckling load has been shown to be highly depending on the radius of the loading boss. A formulation is used to evaluate this effect based on the initial collapse of a simply-supported circular plate under concentrated rigid boss. The results of initial buckling load formulation due to ignoring the shell curvature in small vicinity of the loading actuator are always slightly on the safe side. It is found that the shell carrying capacity after initial collapse increases continuously with the deflection. The hemispherical shell deformation can be represented by a mathematical model consisting of a cone and a torus which spread out symmetrically from the apex with increasing load. The whole region of the shell forming the cone must be plastic to make this deformation possible. The analytical solution results are shown to closely match those of numerical and experimental values. It is also evident that larger boss size corresponds to higher initial collapse load and larger dimple size. This solution is rigorously applicable for shells having smaller values of R/t_0 (not exceeding approximately 100). This is because the symmetry of the propagating annular zone about the vertical axis cannot be assumed throughout the load-deflection response for large, R/t_0 . For R/t_0 greater than 100, the outer part of the

annular zone turns out to be unstable after a certain deformation level where the plastic part of the shell degenerates into an n-sided polygon. For thin shell which R/t_0 is larger than 100, the bifurcation point is approximately found using analytical solution as well. On the other hand, for very thin shells ultimate load carrying capacity is limited by punch strength of the shell material.

Notation used in this chapter

- a Radius of Circular Plate
- c Radius of Circular Plate used to model behavior at bifurcation point
- b Radius of Rigid Boss
- t_0 Initial Shell Thickness
- t Current Shell Thickness
- M_0 Shell Plastic Moment/Unit Length in shell
- M_ϕ Meridional Moment/Unit Length in shell
- M_β Circumferential Moment/Unit Length in circular plate
- M_r Radial Moment/Unit Length in circular plate
- M_t Tangential Moment/Unit Length in shell
- N_ϕ Meridional Force/Unit Length in shell
- N_β Circumferential Force/Unit Length in shell
- Q Transverse Shear Force /Unit Length in shell
- P_0 Shell initial Collapse Load
- P Shell Current Load
- R Shell Radius
- θ Knuckle Meridional Angle
- ϕ Toroid Angle
- ρ Knuckle Radius
- h Vertical deflection of the apex of the hemispherical shell

CHAPTER 2 - Nondestructive Method to Predict the Buckling Load in Elastic Spherical Shells

2.1 Introduction and Purpose of this chapter

As the variety and the quantity of shells increase, the determination of shell behavior becomes more and more important. One of the most important things is to determine the buckling load of shells either experimentally or theoretically.

The critical load for an axially loaded elastic structure is the load at which straight (undeformed) and the deformed form of a structure are both possible. Therefore, a small increment of this critical load causes a sudden deformation called buckling. In an initially straight member, if the weight of member is neglected and no eccentricity exists, until the buckling load is attained there is no transverse deformation theoretically. But this definition of critical load holds true only in a theoretical sense. Because, in reality, due to the manufacturing imperfections, a very small eccentricity or non homogeneity, which are unavoidable for most cases from the first point of application of the load, transverse deformations begins. When the critical load has been attained there will be excessive deformations. Therefore, the theoretical minimum buckling load is not a reliable one, since the actual critical load is less than that. Theoretically speaking, there are an infinite number of critical loads, but in practice only the smallest one is necessary, since, at this load or slightly below that load buckling should be expected. Accordingly, the target is to determine this minimum buckling load either theoretically or experimentally.

The modern design technique goes into the model investigation, especially, for complicated structures as shells. Since in most cases, the true behavior of the shell is not known or very difficult to know, the best thing is to make some assumptions and then to verify these assumptions by means of model tests. Accordingly, this chapter is investigating a possibility of nondestructive method for finding the critical buckling load in spherical shells. For this purpose, Southwell's nondestructive method for columns is extended to spherical shells subjected to uniform external pressure acting radially, and then by means of experiments, it is shown that the theory is applicable to spherical shells with an arbitrary symmetrical loading. In addition, Southwell's nondestructive technique for columns is extended to the framed columns. Therefore, a procedure is developed that the critical loads of columns in a multi-story frame can be determined by using lateral deflections obtained through matrix formulation.

2.2 Southwell Method in Columns

If x is measured along the line of the thrust, and y defines the transverse deflection, which is very small everywhere meaning that the small deformation theory is applicable, and assuming P has a constant intensity over the span length L , writing the sum of the forces in horizontal and vertical directions and the moments about an arbitrary point, (equilibrium equations) the condition of equilibrium for the bent configuration may be obtained, Fig .2.1. Summing up the forces in vertical direction and equating to zero;

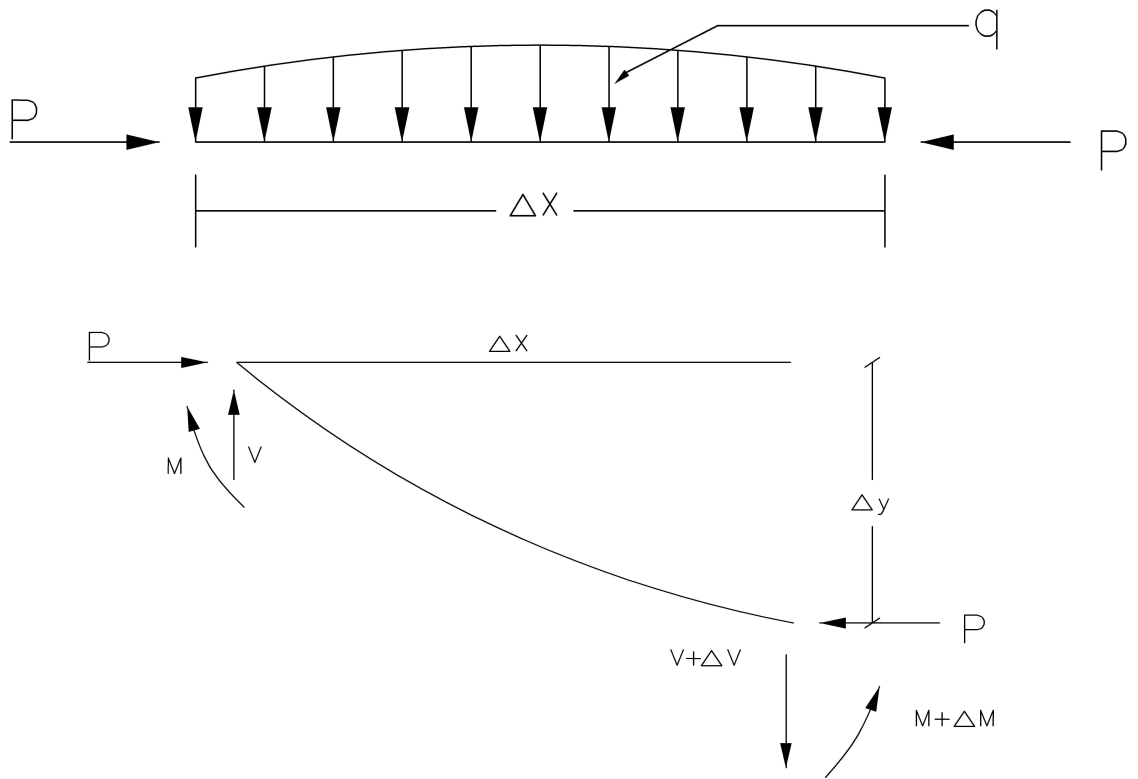


Figure 2. 1: Column under compression force

$$+\downarrow \sum F_y = 0 \rightarrow -V + (V + \Delta V) + q\Delta x = 0 \quad (2.1)$$

therefore, after taking the limit:

$$q = -\frac{dV}{dx} \quad (2.2)$$

The sum of the moments,

$$M - (M + \Delta M) + (V + \Delta V)\Delta x + q\frac{\Delta x^2}{2} + P(\Delta y) = 0 \quad (2.3)$$

taking the limit,

$$V + P \frac{dy}{dx} = \frac{dM}{dx} \quad (2.4)$$

but since $EI \frac{d^2y}{dx^2} = -M$

$$\frac{d^2M}{dx^2} = \frac{dV}{dx} + P \frac{d^2y}{dx^2} = -q + P \frac{d^2y}{dx^2} \rightarrow (EIy'')'' + Py'' = q \quad (2.5)$$

where EI is the flexural rigidity, P is the axial force and q is the lateral load. In the case of zero lateral load, it is possible to write equilibrium equation as:

$$EIy'' + Py = 0 \quad (2.6)$$

calling, $\alpha^2 = P/EI$, the general solution equation will be:

$$y = A \sin \alpha(x - x_0) \quad (2.7)$$

where A and x_0 are two arbitrary constants of integration.

The condition that y must vanish at both ends of the strut will be realized if, $\sin \alpha l = 0$ which is possible for $\alpha = 0$, but in that case, the strut will remain straight or in other words, there will not be any deformation. The further solutions are $\alpha = \frac{n\pi}{l}$ where $n = 1, 2, 3, \dots$

Substitution of this value into the equation $\alpha^2 = \frac{P}{EI}$ yields $\frac{P}{EI} = \frac{n^2 \pi^2}{l^2}$ or by substituting the values of n ,

$$\frac{Pl^2}{EI\pi^2} = 1, 4, 9, \dots, n^2 \quad (2.8)$$

For practical purposes, only the smallest value of that critical load is needed. Therefore, using the smallest value of n , which is one,

$$P_{cr} = \frac{\pi^2 EI}{L^2} \quad (2.9)$$

Suppose now that the strut is not quite straight initially, and let y_0 be the initial transverse deflection of the strut. Then the equation of equilibrium for zero lateral loads will be;

$$EI(y'' - y_0'') + py = 0 \rightarrow y'' + \alpha^2 y = y_0'' \quad (2.10)$$

Provided that y vanishes at both ends of the strut. A general solution may be obtained by expressing both y and y_0 in terms of Fourier's series. Therefore;

$$y = \sum_{n=1}^{\infty} w_n \sin \frac{n\pi x}{L} \quad (2.11)$$

$$y_0 = \sum_{n=1}^{\infty} \bar{w}_n \sin \frac{n\pi x}{L} \quad (2.12)$$

Differentiating them with respect to x twice,

$$y'' = -\sum_{n=1}^{\infty} \frac{n^2 \pi^2}{L^2} w_n \sin \frac{n\pi x}{L} \quad (2.13)$$

$$y_0'' = -\sum_{n=1}^{\infty} \frac{n^2 \pi^2}{L^2} \bar{w}_n \sin \frac{n\pi x}{L} \quad (2.14)$$

Substituting back into the differential equation (2.10),

$$w_n = \frac{\bar{w}_n}{1 - \frac{L^2 \alpha^2}{n^2 \pi^2}} \quad (2.15)$$

If P_n is the n -th critical load, then $P_n = \frac{\pi^2 n^2 EI}{L^2}$. Therefore,

$$w_n = \frac{\bar{w}_n}{1 - \frac{P}{P_n}} \quad (2.16)$$

As P approaches to its first critical value P_1 , w_1 will be very largely magnified, while w_2 will be approximately in the ratio four over three, w_3 nine over eight and so on.

This result explains why as the load is increased, every strut appears to bent into a sine wave of one bay, other harmonics are present, but they are very little magnified by the load, whereas the first harmonic soon becomes large. Also in that case, from the differential equation it is possible to notice that the deflection begins from the first application of the load, since the differential equation is not homogeneous anymore due to the consideration of the initial imperfections, which are almost unavoidable in practice.

The deflection of the strut at its centre may be written as;

$$\delta = \sum_{n=1}^{\infty} w_n \sin \frac{n\pi}{L} \times \frac{L}{2} = w_1 - w_3 + w_5 - \dots \quad (2.17)$$

or

$$\delta \cong w_1 = \frac{\bar{w}_1}{1 - \frac{P}{P_1}} \quad (2.18)$$

Thus provided that the above mentioned assumptions hold true, the load-deflection curve is a rectangular hyperbola having the axis of P , and the horizontal line $P = P_{cr}$ as asymptotes.

(See Fig. 2.2a)

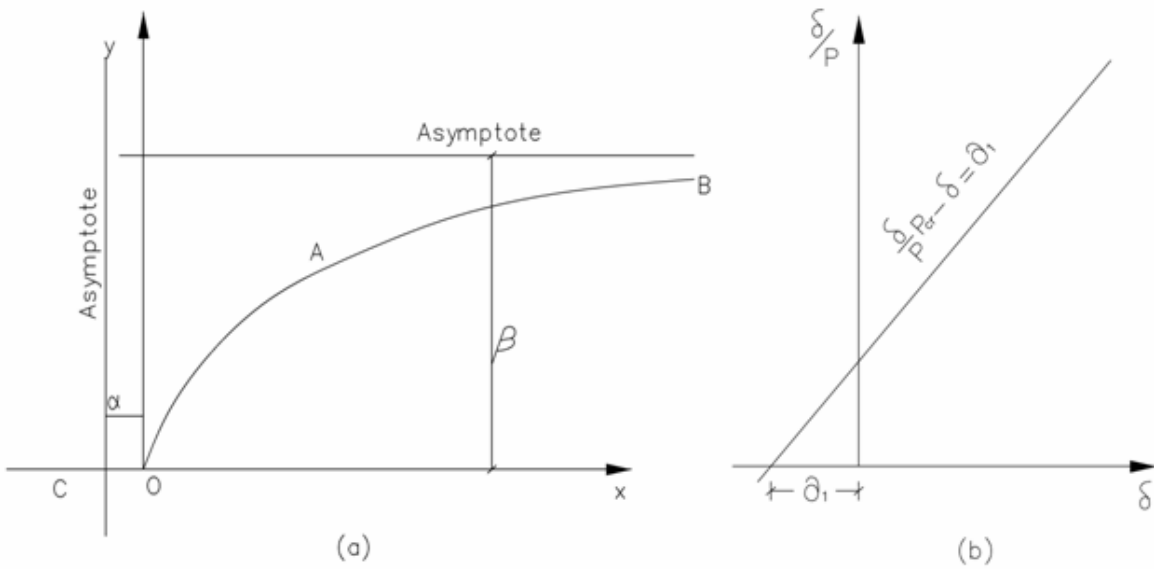


Figure 2. 2: Load Deflection curve in Southwell Method

Now, if a hyperbola passes through the origin and has asymptotes of equations.

$$\begin{aligned} x + \alpha &= 0 \\ y - \beta &= 0 \end{aligned} \tag{2.19}$$

The equation of this hyperbola will be:

$$xy - \beta x + \alpha y = 0 \tag{2.20}$$

or dividing by y ;

$$x - \beta \frac{x}{y} + \alpha = 0 \tag{2.21}$$

calling $\frac{x}{y} = v$ the equation of the hyperbola becomes;

$$x - \beta v + \alpha = 0 \tag{2.22}$$

which is a straight line. Therefore, if x is plotted against v , the inverted slope $\frac{dx}{dv}$ is the measure of the smallest critical load (See Fig 2.2b).

If instead of having an initial curvature, an initial eccentricity e has appeared since in the case of a single lateral load Q the deflected shape may be defined as;

$$y = \frac{1}{\pi^3} \frac{QL^3}{EI} \sum_{n=1}^{\infty} \frac{1}{n \left(n^2 - \frac{P}{P_n} \right)} \sin \frac{n\pi c}{L} \sin \frac{n\pi x}{L} \quad (2.23)$$

where c is the distance between the support and the point of application of the load. Making c infinitely small, the condition of bending by a couple is obtained. Therefore, using the notation $M = Qc$;

$$y = \frac{2}{\pi^3} \frac{ML^2}{EI} \sum_{n=1}^{\infty} \frac{1}{n \left(n^2 - \frac{P}{P_n} \right)} \sin \frac{n\pi x}{L} \quad (2.24)$$

is obtained. For two moments applied at both ends, by superposition;

$$y = \frac{2}{\pi^3} \frac{ML^2}{EI} \sum_{n=1}^{\infty} \frac{1}{n \left(n^2 - \frac{P}{P_n} \right)} \left[\sin \frac{n\pi x}{L} + \sin \frac{n\pi(L-x)}{L} \right] \quad (2.25)$$

and the deflection at the midspan is:

$$\delta = \frac{4}{\pi^3} \frac{ML^2}{EI} \left[\frac{1}{1 - \frac{P}{P_1}} - \frac{1}{3 \left(9 - \frac{P}{P_3} \right)} + \dots \right] \quad (2.26)$$

Since due to symmetry, the even terms do not appear.

If the couples at both ends are caused due to the small eccentricity e of the applied axial loads

P , then calling $Pe = M$

$$\delta = \frac{4Pe}{\pi P_1} \left[\frac{1}{1 - P/P_1} - \frac{1}{3(9 - P/P_3)} + \dots \right] \quad (2.27)$$

As P reaches P_1 the ratio P/P_1 reaches to unity. So, while the first term approaching to infinity, the others approach to zero therefore,

$$\delta = \frac{4Pe}{\pi P_1} \frac{1}{1 - P/P_1} \quad (2.28)$$

or in a more compact form,

$$\delta = \frac{4e}{\pi} \frac{1}{P_1/P - 1} \quad (2.29)$$

For a more general case of combination of both an eccentricity and curvature:

$$\delta = \left(\bar{w}_n + \frac{4e}{\pi} \right) \frac{1}{P_1/P - 1} \quad (2.30)$$

which is analogous to the original equation:

$$\delta = \frac{\bar{w}_1}{1 - P/P_1} \quad (2.31)$$

The main advantage of the method lies in its generality and simplicity. In all ordinary examples of elastic instability the equation

$$EI \left(y'' - y_0'' \right) + Py = 0 \quad (2.32)$$

governs the deflection as controlled by its initial value, provided that both are small. It follows that the deflection is related with the applied load by an approximate equation of the hyperbolic form

$$\delta \cong w_1 = \frac{\bar{w}_1}{1 - P/P_{cr}} \quad (2.33)$$

2.3 Agreement of Test Results in Columns

As stated in the preceding section, the relation between measured load and deflection will not be hyperbolic if the deflections are so large that the elasticity of the material is impaired; moreover, when the deflections are large the approximations will not hold true. On the other hand, if both the deflections and loads are small, the exact measurements will not be possible. Thus, some scatter of the observational points must be expected. Moreover, in this range w_1 (the first term of the Fourier series) does not necessarily dominate the expression for deflection (Southwell 1932).

The data required for a satisfactory test is related values of load and central deflection for columns which have been loaded as axially as possible.

The recorded observations of this nature are given by T. Von Karman (1909) in an inaugural dissertation published in 1909. In his paper, the experimental struts are classified in three groups, described relatively as slender, medium or thick. Slender struts having a $1/k$ ratio greater than 90 and for medium struts the slenderness ratio ranges between 45 and 90, and thick struts are those for which the slenderness ratio is less than 45.

In the slender group, Von Karman tested eight struts, numbered 1, 2, 3a, 3b, 4a, 4b, 5, and 6. These have been analyzed by R. V. Southwell (1932) in Table 2.1 and Fig. 2.3 exhibiting the relation of x to v . In some instances the initial observations have been rejected in estimating the best fitting straight lines; such observations are distinguished in the table by asterisks. The

remaining observations have been analyzed by the method of least squares by R.V. Southwell, in order that the best fitting lines might be determined without introduction of personal judgment.

Table 2.2, gives the values of slope as determined from the best fitting lines. This table shows that the agreement with theory in regard to the critical load is in fact very close. The actual value of the modulus of elasticity, measured by Karman is 2170000 kgf/cm^2 .

As applied to the struts in Karman's medium and thick groups, the method failed for the reason that practically every observation related to deflections, which can be shown to have involved in elastic failure of the material. It, thus, appears that the method has given good results in every case where these could be expected, but that only trial can show whether in any instance sufficient observations can be taken of deflection which on the one hand are large enough to give reasonable certainty of ν , and on the other hand, are not so large that material is still elastic.

One of the struts tested by Prof. Robertson (1912) was loaded with such small eccentricity by R. V. Southwell as to provide a fair test of the method. Table 2.3 presents the analysis of this case, and related values.

As it is seen from that figure, the plotted points fall on two distinct straight lines; the first, covering values of the measured deflection ranging from 7 to 18 thousands of an inch, indicated an initial deflection of about 0.01 inch and a critical load of 14.5 tons, which is some ten percent in excess of the value 12960 *kgs* obtained from Euler's theoretical expression when modulus of elasticity is given the value 13.3 tons/in^2 , which was measured by Prof. Robertson. The second test representation values of the measured deflection in excess of 18 thousandths of an inch (of which 0.0064 inch is the amplitude of the first harmonic in the Fourier series for the

specified eccentricity of 0.005 inch) and a critical load of about 12.9 tons, which is less than half percent in error as compared with the theoretical figure.

Table 2. 1: Nos. 1, 2, 3a, 3b, 4a, 4b, 5 and 6. Mild steel: Modulus of

$$\text{Elasticity} = 2170000 \frac{\text{kgf}}{\text{cm}^2}$$

Strut No:1

P , end load in kilograms	x , measured deflection (mm)	$v = \frac{x}{P} \times 10^6$
2260	0.01	4.43
3020	0.025	8.28
3170	0.04	12.62
3320	0.06	18.07
3470	0.09	25.94
3620	0.25	69.06

Strut No:2

P , end load in kilograms	x , measured deflection (mm)	$v = \frac{x}{P} \times 10^6$
4520	0.02	4.43
4830	0.05	10.35
5130	0.11	21.44
5280	0.24	45.45

Strut No:3a

P , end load in kilograms	x , measured deflection (mm)	$v = \frac{x}{P} \times 10^6$
6030	0.01	1.66
7540	0.03	3.98
8290	0.11	13.27
8520	0.52	61.03

Strut No:3b

P , end load in kilograms	x , measured deflection (mm)	$v = \frac{x}{P} \times 10^6$
7840	0.02	2.55
8140	0.05	6.14
8290	0.07	8.44
8445	0.11	13.03
8600	0.21	24.42

Strut No:4a

P , end load in kilograms	x , measured deflection (mm)	$v = \frac{x}{P} \times 10^6$
9050	0.02	2.21
9660	0.025	2.59
10260	0.03	2.92
10560	0.07	6.63
10710	0.10	9.34
10860	0.13	11.97
11010	0.25	22.71
11160	0.73	65.41

Strut No:4b

P , end load in kilograms	x , measured deflection (mm)	$v = \frac{x}{P} \times 10^6$
3020	0.03	9.93
4530	0.05	11.04
6030	0.07	11.51
7540	0.09	11.94
8300	0.12	14.46
9050	0.15	16.58
9805	0.23	23.46

9960	0.26	26.10
10110	0.29	28.8
10260	0.33	32.16
10410	0.41	39.39
10560	0.52	49.24
10710	0.71	66.29
10860	1.46	134.44

Strut No:5

P , end load in kilograms	x , measured deflection (mm)	$v = \frac{x}{P} \times 10^6$
9050	0.01	1.105
10560	0.03	2.84
10860	0.05	4.67
11160	0.07	6.27
11470	0.10	8.72
11770	0.15	12.74
12070	0.22	18.23
12370	0.30	24.25
12520	0.45	35.94

Strut No:6

P , end load in kilograms	x , measured deflection (mm)	$v = \frac{x}{P} \times 10^6$
10560	0.01	0.95
12070	0.04	3.31
12370	0.08	4.85
12670	0.10	7.89
12970	0.15	1.57

13270	0.25	8.84
13430	0.34	25.32
13580	0.74	54.49

Table 2. 2: T. Von Karman's tests

Strut No:	A deduced from best fitting line in Fig. 3 (mm)	P , estimated from slop of best fitting line in Fig. 3	P , as given by theoretical formula kgf
1	0.005	3712	3790
2	0.005	5453	5475
3a	0.005	8590	8645
3b	0.005	8758	8610
4a	0.003	11220	10980
4b	0.030	11090	10920
5	0.010	12815	12780
6	0.010	13750	13980

Table 2. 3: Robertson's Strut No:5. Mild steel: Effective length- 22.25 inches.

Diameter-0.999 inches.

Slenderness- 89.1

Eccentricity-0.005 inches.

P , end loads in tons	x , measured deflection in thousandths of an inch.	$v = \frac{x}{P}$
1.62	1.0	0.617
1.79	1.5	0.838
2.14	1.7	0.794
2.48	2.2	0.887
2.82	2.4	0.851
2.99	2.6	0.869

3.16	2.8	0.886
3.34	3.0	0.898
3.50	3.27	0.934
3.68	3.64	0.989
3.86	4.00	1.037
4.02	4.24	1.060
4.19	4.46	1.063
4.36	4.68	1.078
4.53	4.81	1.063
4.70	4.94	1.051
4.90	5.07	1.028
5.13	5.66	1.106
5.56	6.32	1.140
5.99	6.97	1.163
6.42	7.80	1.218
6.84	8.95	1.310
7.27	9.84	1.358
7.70	11.18	1.450
8.12	12.75	1.572
8.55	14.08	1.647
8.98	15.88	1.768
9.4	18.34	1.951
9.83	21.91	2.222
10.25	26.27	2.563
10.68	32.47	3.040
11.11	41.17	3.706

2.4 An Extension of the Southwell Method for columns in a Frame structure

This section shows an approach whereby the critical loads of columns in a multi-story frame can be determined by using lateral deflections obtained through matrix formulation. The deflection data of columns in a multi-story frame are obtained by including the effect of presence of axial loads in the member and structure stiffness matrices. Effects of initial bending moments are also included. The results prove that Southwell plotting technique used to determine the critical load of single column is also applicable to framed columns.

2.4.1 Formulation of the Governing Equations

For a single column, formulations can be made directly to obtain the critical load. Simple formulations can also be extended to simple portal frames as done by Zweig (1968). When the problem arises to analyze and design a tall building subjected to gravity and lateral loads, however, use of modern matrix methods becomes necessary.

Because of large number of degrees of freedom involved in a multi-story building frame, one is confronted with a correspondingly large number of equations which can be repeatedly solved only by use of matrix method. When buckling is involved then efficient matrix formulations can be made using slope deflection equations modified by stability functions.

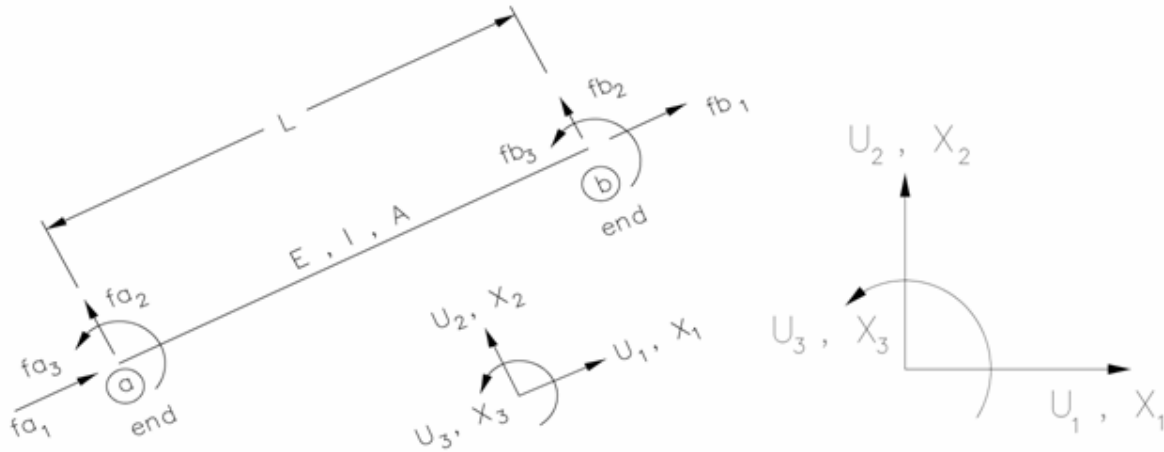


Figure 2. 3: Notation for member and structure

With reference to a notation system shown in Fig.2.3, member stiffness equations 1, 2, 3, and 4 are formed using equations of equilibrium (Bleich (1952)).

The axial force equation is given by:

$$f_{a_1} = \frac{EA}{L}(u_{b_1} - u_{a_1}) \quad (2.34)$$

The shear force equation is given by

$$f_{a_2} = \left(\frac{6EI}{L^2}\right)\beta_3 u_{a_3} + \left(\frac{6EI}{L^2}\right)\beta_3 u_{b_3} - \left(\frac{12EI}{L^3}\right)\beta_5 (u_{b_2} - u_{a_2}) \quad (2.35)$$

The bending moment equations are given by

$$f_{a_3} = \left(\frac{4EI}{L}\right)\beta_1 u_{a_3} + \left(\frac{2EI}{L}\right)\beta_2 u_{b_3} - \left(\frac{6EI}{L^2}\right)\beta_3 (u_{b_2} - u_{a_2}) \quad (2.36)$$

$$f_{b_3} = \left(\frac{2EI}{L}\right)\beta_2 u_{a_3} + \left(\frac{4EI}{L}\right)\beta_1 u_{b_3} - \left(\frac{6EI}{L^2}\right)\beta_3 (u_{b_2} - u_{a_2}) \quad (2.37)$$

where f is the end force, u is the end displacement, the subscripts i and j refer to the particular end of the member and the direction respectively, β_i represents corresponding stability functions E, A, I and L are modulus of elasticity, cross sectional area, moments of inertia and length of the member respectively.

Stability functions β_i have been widely publicized (Gregory (1968)).

They may be concisely expressed as (see appendix C)

$$S = \frac{\alpha(1 - 2\alpha \cot 2\alpha)}{\tan \alpha - \alpha} \quad (2.38)$$

$$C = \frac{2\alpha - \sin 2\alpha}{\sin 2\alpha - 2\alpha \cos 2\alpha} \quad (2.39)$$

$$\beta_1 = S/4 \quad (2.40)$$

$$\beta_2 = SC/2 \quad (2.41)$$

$$\beta_3 = S(1+C)/6 \quad (2.42)$$

$$\beta_4 = \alpha \cot \alpha$$

$$\beta_5 = \beta_3 \cdot \beta_4 \quad (2.43)$$

where $\alpha = \frac{1}{2} \sqrt{\frac{P}{P_E}}$ with P being the axial load on a given structural member and

P_E being the Euler Load for that particular member.

By use of appropriate transformation matrices, the member stiffness equations are transformed to a global coordinate system. Structure stiffness equations are then formed by using the equations of compatibility.

The steps leading to the computer program are summarized as follows:

a) For a given frame adopt numbering system for members and joints, formulate the member equations, transform them to the structure coordinate system, and formulate the structure stiffness matrix by using compatibility equations.

b) Adopt a proportionate multiplier of load, λ , for a given external loading pattern. Then for any value of λ , formulate an external force vector. In the external force vector, the fixed end moments of each member must be modified for the presence of axial load in that member. This is done by deriving the appropriate stability function corresponding to the particular lateral loading on the member.

The stability function corresponding to a uniformly distributed load over the complete length of a member is derived as $\frac{1}{\beta_3}$. This function is used to modify the fixed end moments in the force vector due to the loading of this frame.

c) For any value λ of a loading pattern, initial solution necessitates all β_i be set to unity (i.e. axial forces = 0). By using an invert subroutine, solve the system of equations for the unknown displacements. With the displacements and using equation 1, a vector of axial forces of members is obtained. For each member, β_i values are calculated and equations (2.35), (2.35) and (2.36) are modified in order to reformulate the member and structure equations.

d) The iteration is continued until elements of force vectors and displacement vectors of two successive iterations are correspondingly close to one another. The control point in continuing further iterations is the test value of the determinant of the stiffness matrix.

If the values of the determinant are positive, then according to the principle of positive definiteness for stability, further iteration becomes possible.

e) Once the final set of displacements and forces for a value of λ are obtained, then they are stored further use.

f) Steps c, d and e are repeated for a different value of λ .

Solutions for the structure are completed; end displacements and end forces have been obtained. Now, it is possible to further study the members.

2.4.2 Member Formulations and Solutions

For a straight prismatic member, the general equation of equilibrium is given by

$$\int_0^L \left(EIu_2^{IV} + f_{a_1}u_2'' - q \right) dx = 0 \text{ let } f_{a_1} = P \quad (2.44)$$

where q is the intensity of the lateral load on the member.

Solution of equation (2.44) is

$$u_2 = A \cos \frac{2\alpha}{L} x_1 + B \sin \frac{2\alpha}{L} x_1 + Cx_1 + D + \frac{1}{2} \times \frac{q}{P} x_1^2 \quad (2.45)$$

In the member axis system (x_1, x_2, x_3) of each member, the boundary conditions, the final end forces and displacements corresponding to each value of λ of a loading pattern (obtained in step e of the procedure) are:

End a		End b	
Displacements	Forces	Displacements	Forces
$u_{a_i} = \begin{bmatrix} u_{a_1} \\ u_{a_2} \\ u_{a_3} \end{bmatrix}$	$f_{a_i} = \begin{bmatrix} f_{a_1} \\ f_{a_2} \\ f_{a_3} \end{bmatrix}$	$u_{b_i} = \begin{bmatrix} u_{b_1} \\ u_{b_2} \\ u_{b_3} \end{bmatrix}$	$f_{b_i} = \begin{bmatrix} f_{b_1} \\ f_{b_2} \\ f_{b_3} \end{bmatrix}$

Using these, the coefficients of equations of equation (2.45) can be determined.

Let $r = \sin 2\alpha, t = \cos 2\alpha, w = \frac{2\alpha}{L}$ and $\alpha = \frac{\pi}{2} \sqrt{\frac{P}{P_E}}$ then,

$$\begin{bmatrix} 1 & 0 & 0 & 1 \\ 0 & w & 1 & 0 \\ t & r & L & 1 \\ -wr & wt & 1 & 0 \end{bmatrix} \begin{bmatrix} A \\ B \\ C \\ D \end{bmatrix} = \begin{bmatrix} u_{a_2} \\ u_{a_3} \\ u_{b_2} - \frac{qL^2}{P} \\ u_{b_3} - \frac{qL}{P} \end{bmatrix} \quad (2.46)$$

Knowing the right hand side of equation (2.46), it is possible to determine the coefficients and use them in equation in equation (2.45) to calculate the lateral displacement u_2 at any point x_1 of the member.

2.4.3 Southwell Plot

Using the computer program, for a given frame and a loading pattern, all information regarding the axial forces and displacements at different points of columns are calculated and stored. For every column member, plotting axial load/lateral deflection ratio against axial load for various points within member length yields straight lines converging to one point on the axial load axis. This is the elastic critical load, P_{cr} of the column under the given loading of the frame. The critical load corresponds to that value of the axial load when the displacements approach infinity.

A curve fitting routine greatly reduces the amount of work involved in determining a Southwell Plot which leads to a critical load.

2.4.4 Case Study

In order to demonstrate the procedure, the frame designed by Wood and investigated by Bowles and Merchant (1956) is adopted. A loading pattern is accepted and the solution is carried out. Fig 2.4 gives the dimensions and the cross section profiles of members of the frame. Also, is illustrated the numbering system used in the computer program. Table 2.4 gives the characteristics of the members of this frame according to the numbering system of Fig 2.4.

The loading pattern used is given in Fig. 2.5. In table 2.5 are given the results for member 8 for various values of λ of this loading pattern of the frame. The Southwell Plots are illustrated, and as seen in Fig. 2.5, the $\frac{P}{\Delta_i}$ vs. P curves yield straight lines that converge to the same point defining the critical load, P_{cr} which is equal to 3380 kips.

Table 2. 4: Characteristics of Wood's Frame

Members	$L(in)$	$I(in^4)$	$A(in^2)$	$P_E(ksi)$
1	180	322	20.78	2942.6
2	177	322	20.78	3043.2
3	177	271	18.28	2561.2
4	189	208	14.71	1724.1
5	183	115	10.30	1016.8
6	180	602	22.30	5501.4
7	177	460	19.30	4347.5
8	177	378	18.78	3572.5
9	189	221	17.03	1831.9
10	183	492	10.30	4349.9
11	180	322	20.78	2942.6
12	177	322	20.78	3043.2
13	177	271	18.28	2561.2
14	189	208	14.71	1724.1
15	183	115	10.30	1016.8
16	279	1226	19.12	
17	279	1226	19.12	
18	279	1226	19.12	
19	279	1226	19.12	
20	279	492	13.24	
21	279	1226	19.12	
22	279	1226	19.12	
23	279	1226	19.12	
24	279	1226	19.12	
25	279	492	13.24	

Table 2. 5: Results for Member 8 of Wood’s Frame subjected to the given loading pattern

Pkips , inches

λ	1	2	3	4	5	6
P^1	384.6	769.5	1154.7	1542.3	1929.9	2317.2
Δ_2^2	0.511	1.155	2.001	3.180	5.030	8.369
P/Δ_2	753.2	666.3	577.2	484.9	383.7	276.9
Δ_3	0.726	1.656	2.898	4.654	7.455	12.599
P/Δ_3	529.5	464.7	398.8	33.14	258.9	183.9
Δ_4	0.771	1.774	3.133	5.092	8.251	14.166
P/Δ_4	498.5	433.8	368.6	302.9	233.9	163.6

2.4.5 Discussion Results and Conclusion

In present day practice to design rigidly connected columns of a multi-story frame, one uses the AISC (American Institute for Steel Construction) nomographs (Manual of Steel Construction 2008) to determine the effective column length factor k . In referring to the assumptions behind the nomographs, one finds that primary bending moments inherent in all multistory frame are ignored. In other words, only axial loads are considered.

Here, the effect of primary bending moments (due to loads applied at points other than the joints) are included in the formulations though the use of stability functions to modify the

fixed end moments (for uniformly distributed load, $1/\beta_3$ is used). Therefore, the procedure leads to a more rational evaluation of the critical load.

Once the critical load has been determined, the effective length factor k is given by

$$k = \sqrt{P_E / P_{cr}}$$

For member 8 of the frame in the example, the Euler load P_E is in Table 2.4. Then k is found to be equal to 1.03. AISC nomographs yield k equal to 1.14.

The technique demonstrates that there is an effect of the loading pattern of a frame on the load carrying capacity of a column in that frame. This fact has been long discussed, and the German Codes partially take into account. Zweig (1968) proved that load carrying capacity changes when two different values of external loads are applied to a portal frame.

In conclusion, by using matrix formulations, the Southwell plotting technique is proved to be applicable to determine the critical loads of columns in multistory frames under given loading patterns.

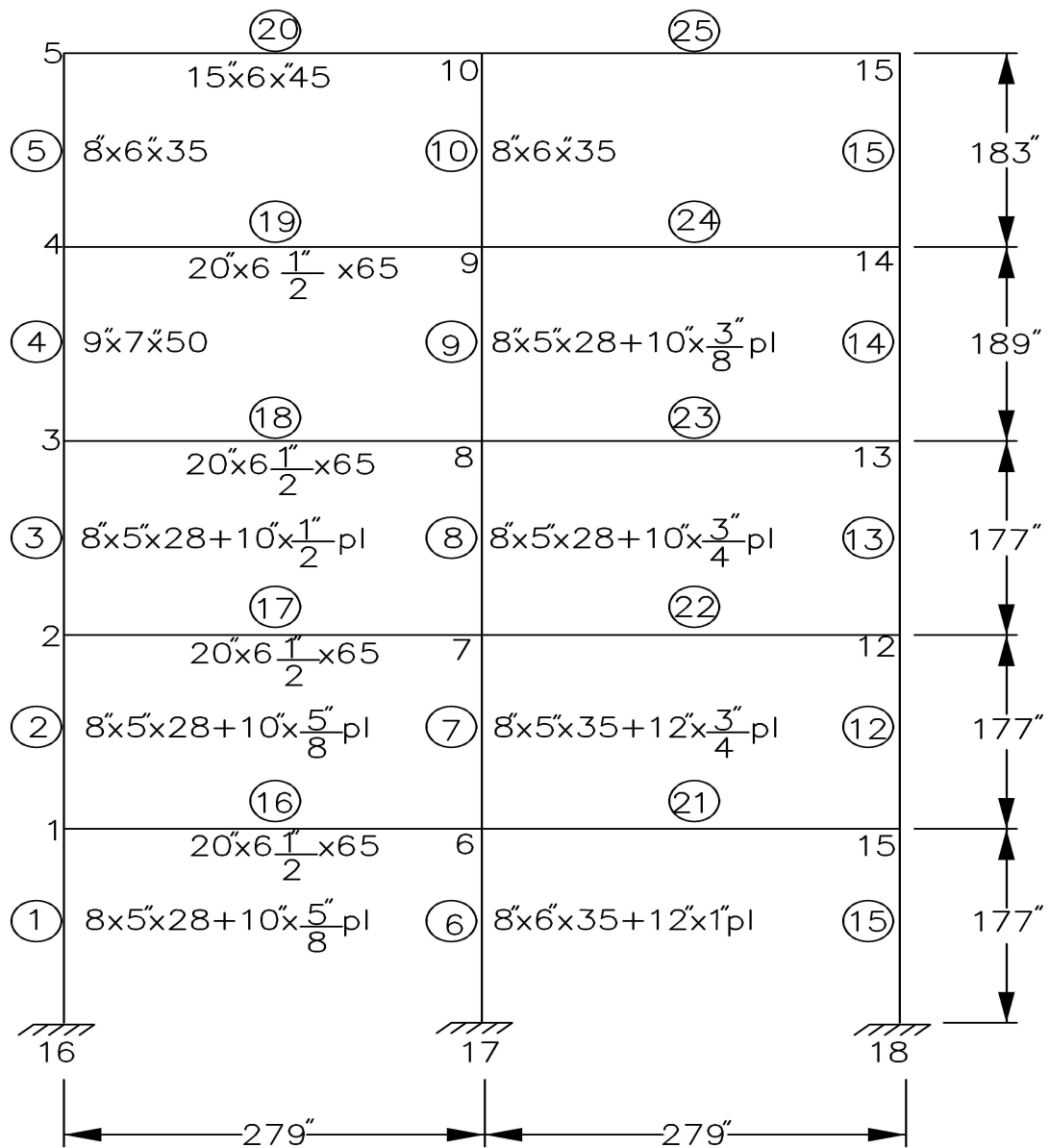


Figure 2. 4: Wood's frame

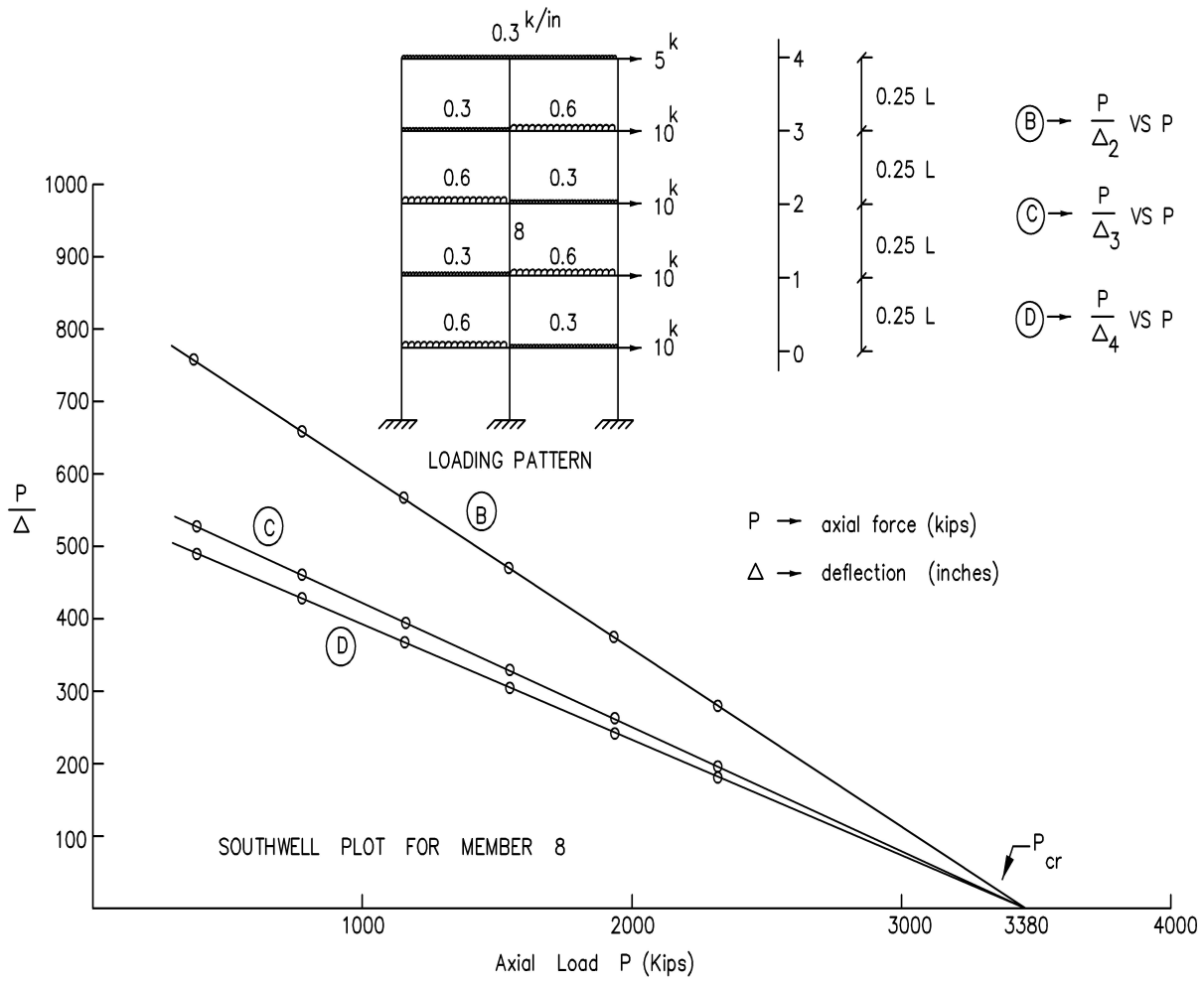


Figure 2. 5: Loading of frame, Soutwell plot for member 8

2.5 The Southwell Method Applied to Shells

To apply the Southwell method of predicting the critical load without disturbing the model, a uniformly compressed spherical shell is considered. If a spherical shell is submitted to a uniform external pressure, it may retain its spherical form, and undergo a uniform compression whose magnitude is in this case;

$$\sigma = \frac{pa}{2t_0} \quad (2.47)$$

So, for values of pressure increasing from zero, the shell will at first deform in a rather uniform manner. This process persists until the external pressure, p , reaches a certain critical value, p_{cr} , called the initial buckling pressure. At this value of pressure the shell no longer deforms in a uniform manner but jumps or snaps into another non-adjacent equilibrium configuration. The pressure to which the shell jumps is called the final buckling pressure. Thus, if the pressure increases beyond a certain limit, the spherical form of equilibrium of the compressed shell may become unstable, and buckling then occurs. In order to calculate this critical pressure, the buckled surface is assumed to be symmetrical with respect to the diameter of the sphere. But before going into the detail of the buckling problem it is advisable first to consider the bending theory of shells.

2.5.1 Deformation of an Element of a Shell of Revolution

In the Fig. 2.6 let $ABCD$ represents an infinitely small element taken from a shell by two pairs of adjacent plans normal to the middle surface of the shell and containing its principle curvature(Timeshenko et.al (1961) and Timeshenko et al. (1959)).

Taking the coordinate axes x and y tangent at an arbitrary point o of the middle surface and the axis z normal to the middle surface, the element may be defined. In bending theory of shells, it is assumed that, the linear elements, which are normal to the middle surface of the shell remain straight and become normal to the deformed middle surface of the shell. Thus the law of variation of the displacements through the thickness of the shell is linear (Novozhilov (1959)).

During bending, the lateral faces of the element $ABCD$ have rotation and displacement; superposing and first considering rotation only with respect to their lines of intersection with the middle surface. The unit elongations of a thin lamina at a distance z from the middle surface are;

$$\varepsilon_x = -\frac{z}{1 - \frac{z}{r_x}} \left(\frac{1}{r'_x} - \frac{1}{r_x} \right) \quad (2.48)$$

$$\varepsilon_y = -\frac{z}{1 - \frac{z}{r_y}} \left(\frac{1}{r'_y} - \frac{1}{r_y} \right) \quad (2.49)$$

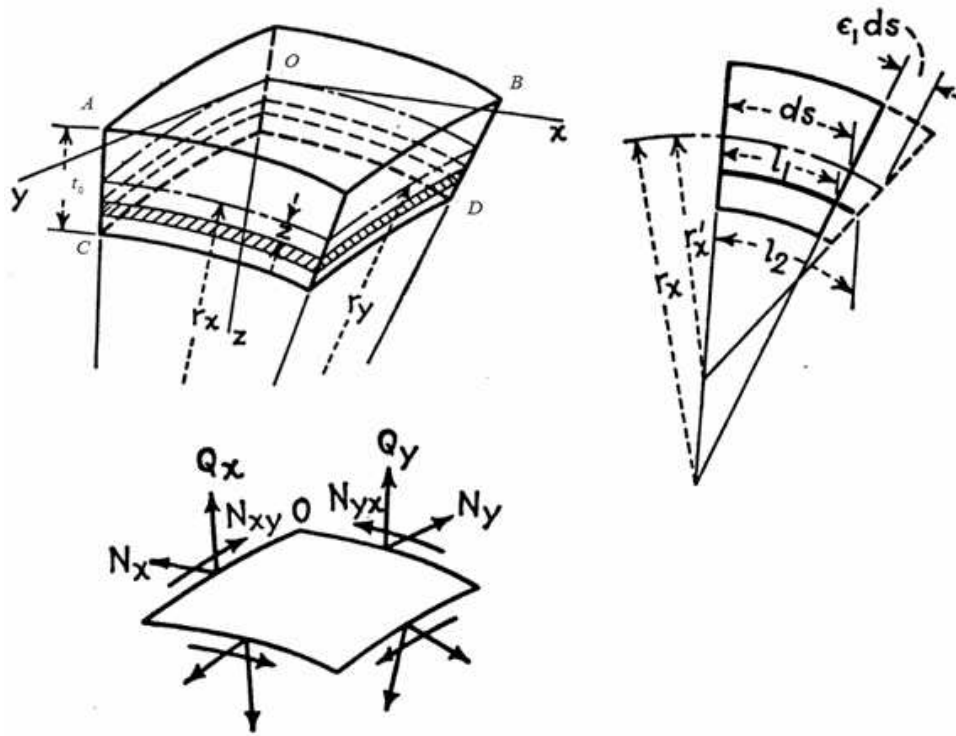


Figure 2. 6: Element taken from a shell by two pairs of adjacent plans normal to the middle surface

If in addition to rotation, the lateral sides of the element are displaced parallel to themselves, owing to stretching l_2 of the middle surface, the elongation of the lamina considered above,

$$\epsilon_1 = \frac{l_2 - l_1}{l_1} \quad (2.50)$$

but since; $l_1 = ds \left(1 - \frac{z}{r_x}\right)$ and, $l_2 = ds(1 + \epsilon_1) \left(1 - \frac{z}{r'_x}\right)$ substituting them back into the

equation (2.50) and summing up with ϵ_x due to the rotation only,

$$\epsilon_x = \frac{\epsilon_1}{1 - \frac{z}{r_x}} - \frac{z}{1 - \frac{z}{r_x}} \left(\frac{1}{(1 - \epsilon_1)r'_x} - \frac{1}{r_x} \right) \quad (2.51)$$

and similarly,

$$\varepsilon_y = \frac{\varepsilon_2}{1 - \frac{z}{r_y}} - \frac{z}{1 - \frac{z}{r_y}} \left(\frac{1}{(1 - \varepsilon_2)r'_y} - \frac{1}{r_y} \right) \quad (2.52)$$

Since the thickness t_0 of the shell always will be assumed small in comparison with the radius of curvature, the quantities $\frac{z}{r_x}$ and $\frac{z}{r_y}$ may be neglected in comparison with unity.

Also neglecting the effect of elongations ε_1 and ε_2 on the curvature the expressions become,

$$\varepsilon_x = \varepsilon_1 - z \left(\frac{1}{r'_x} - \frac{1}{r_x} \right) \quad (2.53)$$

and,

$$\varepsilon_y = \varepsilon_2 - z \left(\frac{1}{r'_y} - \frac{1}{r_y} \right) \quad (2.54)$$

Assuming that, there are no normal stresses between laminas $\sigma_z = 0$ is obtained. Then, from the well known formulae;

$$\sigma_x = \frac{E}{1 - \nu^2} (\varepsilon_x + \nu \varepsilon_y) \quad (2.55)$$

$$\sigma_y = \frac{E}{1 - \nu^2} (\varepsilon_y + \nu \varepsilon_x) \quad (2.56)$$

Therefore, substituting the values of strain components;

$$\sigma_x = \frac{E}{1-\nu^2} (\varepsilon_1 + \nu\varepsilon_2 - z(\chi_x + \nu\chi_y)) \quad (2.57)$$

$$\sigma_y = \frac{E}{1-\nu^2} (\varepsilon_2 - \nu\varepsilon_1 - z(\chi_y + \nu\chi_x)) \quad (2.58)$$

are obtained. Since the thickness of the shell is very small, the lateral sides of the element may be considered as rectangles. Therefore the corresponding normal forces acting to the centroid of the side will be;

$$N_x = \int_{-t_0/2}^{t_0/2} \sigma_x dz = \frac{Et_0}{1-\nu^2} (\varepsilon_1 + \nu\varepsilon_2) \quad \text{for } dy = 1 \quad (2.59)$$

$$N_y = \int_{-t_0/2}^{t_0/2} \sigma_y dz = \frac{Et_0}{1-\nu^2} (\varepsilon_2 - \nu\varepsilon_1) \quad \text{for } dx = 1 \quad (2.60)$$

and the moments, $M_x = \int_{-t_0/2}^{t_0/2} z\sigma_x dz = -D(\chi_x - \nu\chi_y)$, and $M_y = \int_{-t_0/2}^{t_0/2} z\sigma_y dz = -D(\chi_y - \nu\chi_x)$ in which

$$D = \frac{E}{1-\nu^2} \int_{-t_0/2}^{t_0/2} z^2 dz = \frac{Et_0^3}{12(1-\nu^2)}.$$

Now knowing that the shearing stresses are also acting on the lateral sides of the element in addition to the normal stresses. If γ is the shearing strain in the middle surface and $\chi_{xy} dx$ the rotation of the edge BC relative to z -axes, $\tau_{xy} = (\gamma - 2z\chi_{xy})G$ is obtained. Also knowing that

$$Q_x = \int_{-t_0/2}^{t_0/2} \tau_{xz} dz, \quad Q_y = \int_{-t_0/2}^{t_0/2} \tau_{yz} dz, \quad N_{yx} = N_{xy} = \int_{-t_0/2}^{t_0/2} \tau_{xy} dz \quad \text{and} \quad -M_{xy} = M_{yx} = \int_{-t_0/2}^{t_0/2} z\tau_{xy} dz \quad \text{one may find,}$$

$$M_{xy} = -M_{yx} = D(1-\nu)\chi_{xy}, \quad \text{and} \quad N_{xy} = N_{yx} = \frac{t_0 E \gamma}{2(1+\nu)}$$

Thus assuming that during bending of a shell of revolution the linear elements, normal to the middle surface the resultant forces N_x, N_y and N_{xy} and the moments, M_x, M_y , and M_{xy} may be expressed in terms of six quantities; three components of strain $\varepsilon_1, \varepsilon_2$, and γ of the middle surface of the shell and the three quantities χ_x, χ_y , and χ_{xy} representing the changes of curvature and the twist of the middle surface of the shell.

2.5.2 Equations of Equilibrium of a Spherical shell

Due to the symmetrical deformation, one of the displacement components vanishes, and the others are only the functions of angle θ . Therefore;

$$u = f_1(\theta)$$

$$v = 0$$

$$w = f_2(\theta)$$

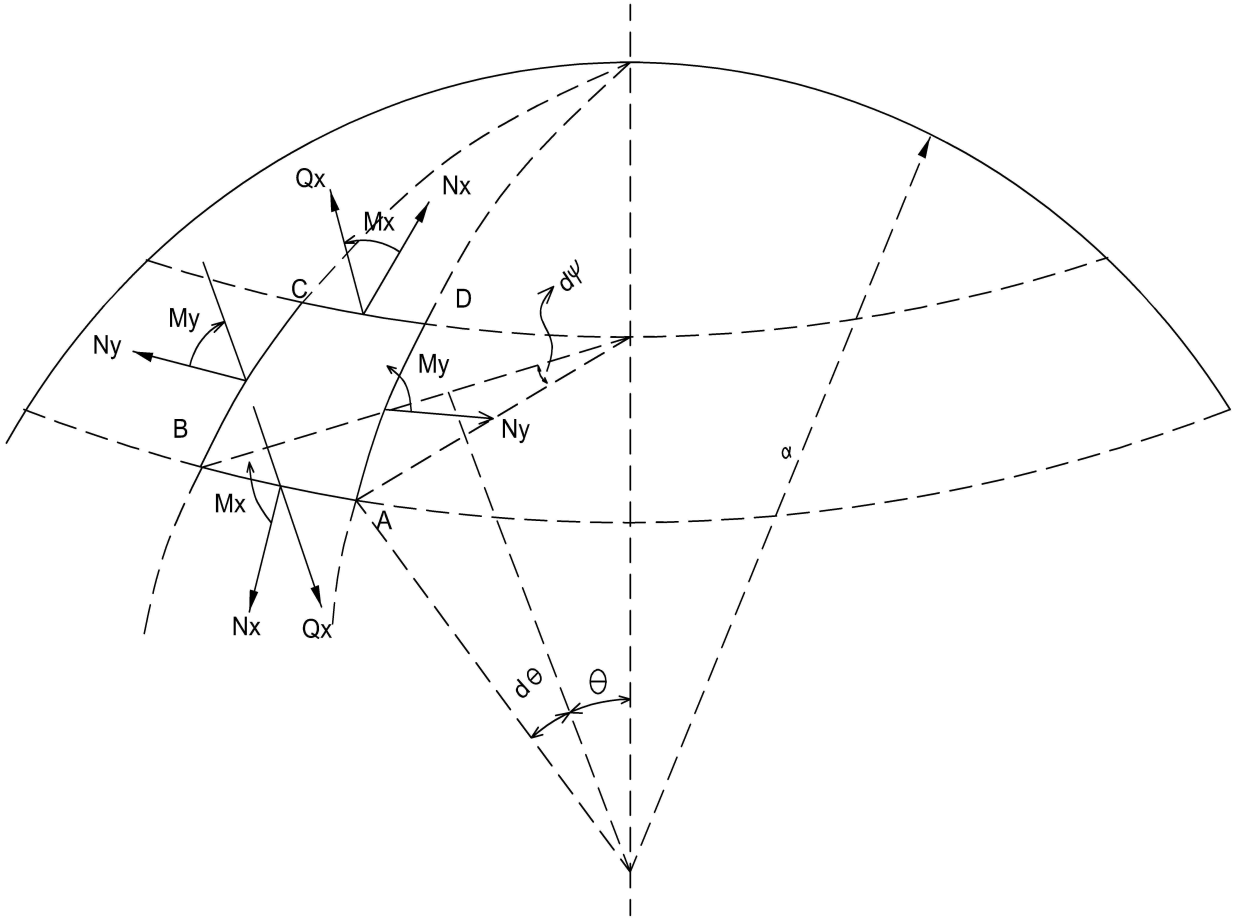


Figure 2. 7: Spherical shell element and corresponding forces

In the case of symmetrical deformation, there are only three equations to be considered as the projections of forces on the x , and z axes and moments of forces with respect the y – axes.

Therefore after simplification, the three equations of equilibrium become;

$$\frac{dN_x}{d\theta} + (N_x - N_y) \cot \theta - Q_x = 0 \quad (2.61)$$

$$\frac{dQ_x}{d\theta} + Q_x \cot \theta + N_x + N_y + pa = 0 \quad (2.62)$$

$$\frac{dM_x}{d\theta} + (M_x - M_y) \cot \theta - Q_x a = 0 \quad (2.63)$$

2.5.3 Equations of Equilibrium for the Case of Buckled Surface of the Shell

In writing the equations of equilibrium for the case of buckled surface of a shell, which is assumed symmetrical with respect to any diameter of the shell, the small changes of the angles between the faces of any element such as $ABCD$ due to the deformation has to be considered. Since there is symmetry of deformation, the rotation will only be with respect to y – axes. For the face OC , this deformation is;

$$\frac{u}{a} + \frac{dw}{ad\theta} \quad (2.64)$$

Thus the angle between the faces OC and AB after deformation becomes;

$$d\theta + \frac{d}{d\theta} \left(\frac{u}{a} + \frac{dw}{ad\theta} \right) d\theta \quad (2.65)$$

The faces AO and BC owing to symmetry of deformation, rotate in their own planes by an angle,

$$-\left(\frac{u}{a} + \frac{dw}{ad\theta} \right) \quad (2.66)$$

Such a rotation in the plane of the face BC has components with respect to the x and z axis equal to; $\left(\frac{u}{a} + \frac{dw}{ad\theta}\right)\cos\theta d\psi$ and, $-\left(\frac{u}{a} + \frac{dw}{ad\theta}\right)\sin\theta d\psi$ respectively. Thus after deformation, the direction of the face BC with respect to the face AD may be obtained by the rotation of the face AO with respect to the x and z axis through the angles, $\sin\theta d\psi + \left(\frac{u}{a} + \frac{dw}{ad\theta}\right)\cos\theta d\psi$ and, $\cos\theta d\psi - \left(\frac{u}{a} + \frac{dw}{ad\theta}\right)\sin\theta d\psi$ respectively.

Using the above derived angles instead of the initial ones; $d\theta$, $\sin\theta d\psi$, and $\cos\theta d\psi$, the equations of equilibrium of the element $OABC$ become;

$$\frac{dN_x}{d\theta} + (N_x - N_y)\cot\theta - Q_x + N_y\left(\frac{u}{a} + \frac{dw}{ad\theta}\right) - Q_x\left(\frac{d^2w}{ad\theta^2} + \frac{w}{a}\right) = 0 \quad (2.67)$$

$$\frac{dQ_x}{d\theta} + Q_x \cot\theta + N_x + N_y + pa + N_x\left(\frac{d^2w}{ad\theta^2} + \frac{du}{ad\theta}\right) + N_y\left(\frac{u}{a} + \frac{dw}{ad\theta}\right)\cot\theta = 0 \quad (2.68)$$

$$\frac{dM_x}{d\theta} + (M_x - M_y)\cot\theta - Q_x a + M_y\left(\frac{u}{a} + \frac{dw}{ad\theta}\right) = 0 \quad (2.69)$$

In this case;

$$\varepsilon_1 = \frac{du}{ad\theta} - \frac{w}{a} \quad (2.70)$$

$$\varepsilon_2 = \frac{u}{a}\cot\theta - \frac{w}{a} \quad (2.71)$$

$$\chi_x = \frac{d^2w}{a^2 d\theta^2} + \frac{du}{a^2 d\theta} \quad (2.72)$$

$$\chi_y = \left(\frac{u}{a^2} + \frac{dw}{a^2 d\theta}\right)\cot\theta \quad (2.73)$$

The differential equation of equilibrium developed have above are based on Love's general theory of small deformations of thin shells which neglects stresses normal to the middle Surface of the shell and assumes that the planes normal to the undeformed middle surface remain normal to the deformed middle surface.

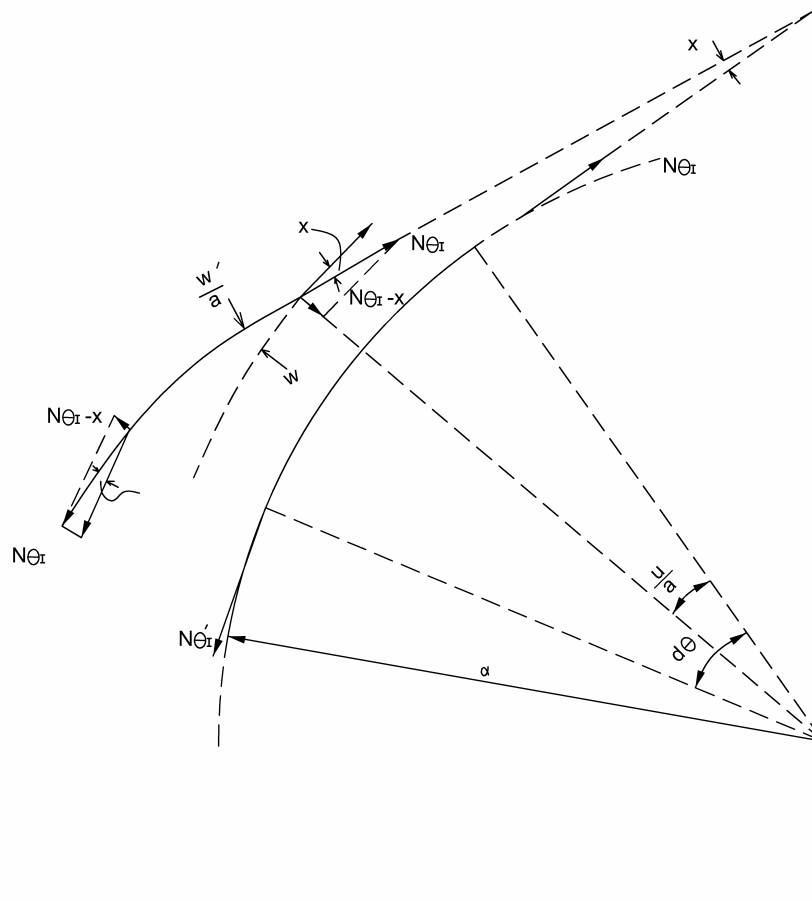


Figure 2. 8: Meridian of a spherical shell before and after buckling

2.5.4 Buckling of Uniformly Compressed Spherical Shells

If a spherical shell is submitted to a uniform external pressure, there will be a uniform compression whose magnitude is;

$$\sigma = \frac{pa}{2t_0}$$

Let u, v and w represent the components of small displacements during buckling from the compressed spherical form, then N_x and N_y differ little from the uniform compressive force

$\frac{pa}{2}$ and they become,

$$N_x = -\frac{pa}{2} + N'_x \quad (2.74)$$

$$N_y = -\frac{pa}{2} + N'_y \quad (2.75)$$

where N'_x and N'_y are the resultant forces due to small displacements u, v and w .

Also, considering the small change of pressure on an element of the surface, due to the stretching of the surface, p becomes $p(1 + \varepsilon_1 + \varepsilon_2)$. Therefore substituting equations (2.74) and 2.75) back into the differential equations of equilibrium (2.67), (2.68), and (2.69) and simplifying and neglecting the small terms, such as the products of N'_x, N'_y and Q_x with the derivations of u, v and w ;

$$\frac{dN'_x}{d\theta} + (N'_x - N'_y) \cot \theta - Q_x - 0.5pa \left(\frac{u}{a} + \frac{dw}{ad\theta} \right) = 0 \quad (2.76)$$

$$\frac{dQ_x}{d\theta} + Q_x \cot \theta + N'_x + N'_y + pa \left(\frac{du}{ad\theta} + \frac{u}{a} \cot \theta - \frac{2w}{a} \right) - 0.5pa \left(\frac{du}{d\theta} + \frac{d^2w}{ad\theta^2} \right) - 0.5pac \cot \theta \left(\frac{u}{a} + \frac{dw}{ad\theta} \right) = 0 \quad (2.77)$$

$$\frac{dM_x}{d\theta} + (M_x - M_y)\cot\theta - Q_x a = 0 \quad (2.78)$$

From the Equation (2.78):

$$Q_x = \frac{dM_x}{ad\theta} + (M_x - M_y)\frac{\cot\theta}{a}$$

Substituting Q_x into the Equations (2.76) and (2.77);

$$N_x' = \frac{Et_0}{1-\nu^2} \left[\frac{du}{ad\theta} - \frac{w}{a} + \nu \left(u \frac{\cot\theta}{a} - \frac{w}{a} \right) \right] \quad (2.79)$$

$$N_y' = \frac{Et_0}{(1-\nu^2)a} \left[u \cot\theta - w + \nu \left(\frac{du}{d\theta} - w \right) \right] \quad (2.80)$$

$$M_x = -\frac{D}{a^2} \left[\frac{du}{d\theta} + \frac{d^2w}{d\theta^2} + \nu \left(u + \frac{dw}{d\theta} \right) \cot\theta \right] \quad (2.81)$$

$$M_y = -\frac{D}{a^2} \left[\left(u + \frac{dw}{d\theta} \right) \cot\theta + \nu \left(\frac{du}{d\theta} + \frac{d^2w}{d\theta^2} \right) \right] \quad (2.82)$$

Now introducing two dimensionless parameters, α and ϕ which are defined as;

$$\alpha = \frac{D(1-\nu^2)}{a^2 Et_0} = \frac{t_0^2}{12a^2} \quad \text{and} \quad \phi = \frac{pa(1-\nu^2)}{2Et_0} \quad \text{and using the elastic law to express the forces and}$$

moments in terms of u and w one obtains;

$$(1+\alpha)\left[\frac{d^2u}{d\theta^2}+\cot\theta\frac{du}{d\theta}-(\nu+\cot^2\theta)'u\right]-(1+\nu)\frac{dw}{d\theta}+\alpha\left[\frac{d^3w}{d\theta^3}+\cot\theta\frac{d^2w}{d\theta^2}-(\nu+\cot^2\theta)\frac{dw}{d\theta}\right] \\ -\phi\left(u-\frac{dw}{d\theta}\right)=0 \quad (2.83)$$

$$(1+\nu)\left[\frac{du}{d\theta}+u\cot\theta-2w\right]+\alpha\left[-\frac{d^3u}{d\theta^3}-2\cot\theta\frac{d^2u}{d\theta^2}+(1+\nu+\cot^2\theta)\frac{du}{d\theta}-\cot\theta(2-\nu+\cot^2\theta)u-\frac{d^4w}{d\theta^4}\right. \\ \left.-2\cot\theta\frac{d^3w}{d\theta^3}+(1+\nu+\cot^2\theta)\frac{d^2w}{d\theta^2}-\cot\theta(2-\nu+\cot^2\theta)\frac{dw}{d\theta}\right]-\phi\left[-u\cot\theta-\frac{du}{d\theta}+4w+\cot\theta\frac{dw}{d\theta}+\frac{d^2w}{d\theta^2}\right]=0 \quad (2.84)$$

These two equations may be simplified by neglecting in comparison with unity in the first term, since the shell is thin, and therefore t_0/a ratio is very small. Also, due largely to angular displacement χ we make good use of this situation by introducing an auxiliary variable U such that $u = -\frac{d\psi}{d\theta}$. Thus, the expressions in the brackets become identical. Then using the symbol

H for the operation;

$$H(\) = \frac{d^2(\dots)}{d\theta^2} + \cot\theta\frac{d(\dots)}{d\theta} + 2(\dots).$$

Equation (2.83) may be written as follows,

$$\frac{d}{d\theta}\left[H(\psi)+\alpha H(w)-(1+\nu)(\psi+w)-\alpha(1+\nu)w-\phi(\psi+w)\right]=0$$

The fourth term, containing the factor, may be neglected in comparison with the third.

Integrating this equation with respect to θ and assuming the constant of integration is equal to zero;

$$H(\psi)+\alpha H(w)-(1+\nu)(\psi+w)-\phi(\psi+w)=0 \quad (2.85)$$

And similarly for Equation (2.84) ;

$$\alpha H H(\psi+w) - (1+\nu)H(\psi) - (3+\nu)\alpha H(w) + 2(1+\nu)(\psi+w) + \phi[-H(\psi) + H(w) + 2(\psi+w)] = 0 \quad (2.86)$$

Now, any regular function of $\cos \theta$ in the interval $-1 \leq \cos \theta \leq 1$ may be expanded in a series of Legendre functions;

$$P_0(\cos \theta) = 1$$

$$P_1(\cos \theta) = \cos \theta$$

$$P_2(\cos \theta) = 0.25(3 \cos 2\theta + 1)$$

.

.

.

$$P_n(\cos \theta) = 2 \frac{1 \times 3 \times 5 \times \dots \times (2n-1)}{2^n n!} \left[\cos n\theta + \frac{1}{1} \times \frac{n}{2n-1} \cos(n-2)\theta + \frac{1 \times 3}{1 \times 2} \times \frac{n(n-1)}{(2n-1)(2n-3)} \cos(n-4)\theta + \dots \right]$$

which satisfy the differential equation,

$$\frac{d^2 P_n}{d\theta^2} + \cot \theta \frac{dP_n}{d\theta} + n(n+1)P_n = 0 \quad (2.87)$$

Thus, performing the operation H ; one obtains,

$$H(P_n) = -\lambda_n P_n \quad (2.88)$$

$$HH(P_n) = \lambda_n^2 P_n \quad (2.89)$$

In which $\lambda_n = n(n+1) - 2$

Assuming general expressions of U and w for any symmetrical buckling of spherical shell,

$$\psi = \sum_{n=0}^{\infty} A_n P_n \quad (2.90)$$

$$w = \sum_{n=0}^{\infty} B_n P_n \quad (2.91)$$

substituting them back,

$$\sum_{n=0}^{\infty} \{A_n [\lambda_n + (1 + \nu) + \phi] + B_n [\alpha \lambda_n + (1 + \nu) + \phi]\} P_n = 0 \quad (2.92)$$

$$\sum_{n=0}^{\infty} \{A_n [\lambda_n^2 + (1 + \nu)(\lambda_n + 2) + \phi(\lambda_n + 2)] + B_n [\alpha \lambda_n^2 + (3 + \nu)\alpha \lambda_n + 2(1 + \nu) - \phi(\lambda_n - 2)]\} P_n = 0 \quad (2.93)$$

The Legendre functions form a complete set of functions. Therefore, the two series can not vanish identically in θ unless each coefficient vanishes;

Thus, for each value of n , the following two homogeneous equations are obtained.

$$A_n [\lambda_n + (1 + \nu) + \phi] + B_n [\alpha \lambda_n + (1 + \nu) + \phi] = 0 \quad (2.93)$$

$$A_n [\alpha \lambda_n^2 + (1 + \nu)(\lambda_n + 2) + \phi(\lambda_n + 2)] + B_n [\alpha \lambda_n^2 + (3 + \nu)\alpha \lambda_n + 2(1 + \nu) - \phi(\lambda_n - 2)] = 0 \quad (2.94)$$

Buckling of the shells become possible if these equations for some value of n , yield for A_n and B_n a solution different than zero, which means a trivial solution or in other words requires having a zero determinant of the system of equations. Thus,

$$(1 - \nu^2)\lambda_n + \alpha \lambda_n [\lambda_n^2 + 2\lambda_n + (1 + \nu)^2] - \phi \lambda_n [\lambda_n + (1 + 3\nu)] = 0 \quad (2.95)$$

A solution of which $\lambda_n = 0$. That corresponds to a value of n equal to unity. Substituting this value of λ_n , one obtains,

$$A_1 = -B_1$$

which corresponding to the displacements,

$$u = -\frac{d\psi}{d\theta} = -A_1 \sin \theta$$

$$w = -A_1 \cos \theta$$

This is a displacement of the sphere as a rigid body displacement “buckling mode” along the axis of symmetry. This must, of course, be excluded when we wish to investigate the elastic instability of the shell.

Now for $\lambda_n \neq 0$ other than zero;

$$\phi = \frac{(1-\nu^2) + \alpha[\lambda_n^2 + 2\lambda_n + (1+\nu^2)]}{\lambda_n + (1+3\nu)} \quad (2.96)$$

which yields for its minimum, or for $\frac{d\phi}{d\lambda_n} = 0$ after simplification;

$$\lambda_n^2 + 2(1+3\nu)\lambda_n - \frac{1-\nu^2}{\alpha} = 0 \quad (2.97)$$

Thus,

$$\lambda_n = -(1-3\nu)\lambda_n + \sqrt{\frac{1-\nu^2}{\alpha}} \quad (2.98)$$

and

$$\phi_{\min} = 2\sqrt{(1-\nu^2)\alpha} - 6\nu\alpha \quad (2.99)$$

But since

$$\phi = \frac{pa(1-\nu^2)}{2Et_0} \quad (2.100)$$

and ϕ_{\min} yields the first critical load p_{cr} ,

$$p_{cr} = \frac{2Et_0\phi_{\min}}{a(1-\nu^2)} = \frac{2Et_0}{a(1-\nu^2)} \left[\sqrt{\frac{1-\nu^2}{3}} \times \frac{t_0}{a} - \frac{\nu t_0^2}{2a^2} \right] \quad (2.101)$$

or neglecting the second term in the parenthesis;

$$p_{cr} = \frac{2Et_0^2}{a^2\sqrt{3(1-\nu^2)}} \quad (2.102)$$

or,

$$\sigma_{cr} = \frac{Et_0}{a\sqrt{3(1-\nu^2)}}$$

In the above derivation a continuous variation of λ_n has been assumed but λ_n is defined so that n is an integer. Hence, to get a more accurate value for the critical load, two adjacent integers as obtained from the equation $\lambda_n = n(n-1) - 2$ should be substituted in the equation of ϕ and the value of λ_n which gives the smaller value for ϕ_n should be used in calculating critical stresses. But this more accurate calculation of the critical load will differ little from that given by the above formula, since the value of λ_n is so large (Timoshenko et al.1961).

Although in the derivation a symmetrical buckling of shells was considered, a more general investigation shows that owing to symmetry of the uniformly compressed spherical shell with respect to any diameter, the formula always can be used for calculating the critical stress.

2.5.5 Southwell Procedure Applied to Shells

The Southwell procedure was first applied to columns by Southwell in 1934. In this part of this chapter, an attempt is made to show that Southwell procedure is also applicable to uniformly compressed spherical shells.

In the derivation of the formula, as it was done for the classical theory of buckling shells (See previous part) it is assumed that the displacements u and w may be expressed as,

$$\psi = \frac{du}{d\theta} = \sum_{n=0}^{\infty} A_n P_n$$

$$w = \sum_{n=0}^{\infty} B_n P_n$$

where P_n is the Legendre functions of the orders n and A_n and B_n are the real constants as before.

Furthermore, as explained in the proceeding section, the manufactural imperfections, which are unavoidable, are considered and it is assumed that they may be expressed as;

$$\psi_0 = \sum_{n=0}^{\infty} A'_n P_n$$

$$w_0 = \sum_{n=0}^{\infty} B'_n P_n$$

Moreover, for the sake of simplicity, it is assumed that the manufactural imperfections of ψ_0 is equal to zero. Thus, it is tried only with the direction w .

When the compressive load q is applied to shell, each point of the middle surface undergoes elastic displacements u and w , and its normal distance from the reference sphere is then becomes $w + w_0$. It is assumed of course, that w_0 is of the order of an elastic deformation,

and then the element of the shell looks like the deformed elements, which are used to establish the differential equations of the buckling problem. Again going through the same procedure one finds that the terms of those equations belong in two groups. (See proceeding section) In those terms which contain the factor ϕ , the quantities u and w describe the difference in shape between the deformed element and an element of true sphere. In these terms w must now be replaced by $w + w_0$. On the other hand, all terms which do not have the factor ϕ , can be traced back to terms of the elastic law, and represent the stress resultants acting on the shell element. Before the application of the load, the shell has been free of stress and the stress resultants depend only elastic displacements u and w . Consequently, in all these terms w is just w and nothing else. Thus one arrives the following set of differential equations:

$$H(\psi + w) + \alpha H(w) - (1 - \nu)(\psi + w) - \phi(\psi + w + w_0) = 0 \quad (2.103)$$

$$\alpha H H(\psi + w) - (1 + \nu)H(\psi) - (3 + \nu)\alpha H(w) + 2(1 + \nu)(\psi + w) + \phi[-H(\psi) + H(w + w_0) + H(w + w_0) + 2(\psi + w + w_0)] = 0 \quad (2.104)$$

In which H denotes the same operator as before;

$$H = \frac{d^2(\)}{d\theta^2} + \cot g \frac{d(\)}{d\theta} + 2(\)$$

Again following the same procedure that is used for the classical buckling theory of spherical shells (see the proceeding section) one obtains the following set of algebraic equations:

$$A_n(\lambda_n + 1 + v + \phi) + B_n(\alpha\lambda_n + 1 + v + \phi) = -B'_n\phi \quad (2.105)$$

$$\begin{aligned} A_n(\alpha\lambda_n^2 + \lambda_n + 2 + v\lambda_n + 2v + \phi\lambda_n + 2\phi) + B_n(\alpha\lambda_n^2 + 3\alpha\lambda_n + v\alpha\lambda_n + 2 + 2v - \phi\lambda_n + 2\phi) = \\ B'_n\phi(\lambda_n - 2) \end{aligned} \quad (2.106)$$

Thus the problem is reduced to solving this set of equations. Eliminating A_n from the above set of equations,

$$\begin{aligned} [\alpha(\alpha-1)\lambda_n^3 + (\phi\alpha - 2\alpha + \phi)\lambda_n^2 + (v\alpha + v^2 + 2\phi v + \phi + 2\phi^2 - 1 - \alpha - 3v\alpha - v^2\alpha + v\phi - \alpha\phi - v\alpha\phi) \\ \lambda_n] B_n = -B'_n\phi[(\alpha+1)\lambda_n^2 + (2v+2\phi)\lambda_n] \end{aligned} \quad (2.107)$$

Therefore the coefficient B_n becomes;

$$B_n = - \frac{B'_n\phi\lambda_n[(\alpha+1)\lambda_n + 2(v+\phi)]}{[-\alpha\lambda_n^2(1-\alpha) + (\phi - 2\alpha + \phi\alpha)\lambda_n + v(3\phi - 2\alpha) + \phi + v^2 - \alpha - 1]\lambda_n} \quad (2.108)$$

After canceling λ_n , and neglecting the small quantities as α, ϕ and their products in comparison with unity;

$$B_n \cong - \frac{B'_n\phi[\lambda_n + 2(v+\phi)]}{-\alpha\lambda_n^2 + (\phi - 2\alpha + \phi\alpha)\lambda_n + v^2 - 1} \quad (2.109)$$

Coming back to the definition of the displacement w one may write the equation,

$$w = \sum_{n=0}^{\infty} B_n P_n \text{ or writing it in detail, } w = B_0 P_0 + B_1 P_1 + B_2 P_2 + \dots$$

Substituting the values of the Legendre Polynomials in their places;

$$w = \left[B_0 + 0.25B_2 + \frac{9}{64}B_4 + \dots \right] + \left[B_1 + \frac{3}{8}B_3 + \dots \right] \cos \theta + [B_2 + \dots] \cos 2\theta + \dots$$

Also according to the definition of;

$$\lambda_n = n(n+1) - 2$$

which is minimum for $n = \frac{1}{2}$ therefore it has the same values for n equals to minus one and zero. Since n must be an integer, it is chosen as zero, which yields, $\lambda = -2$ and corresponds to B_0 which is a function of λ_n and gets smaller when λ_n becomes greater. Thus, it is possible to neglect all the terms and simply write $w \cong B_0$

since the terms which contains $\cos \theta, \cos 2\theta, \dots$ are much more smaller so, buckling is usually expected at the places where θ is large.

Accordingly, it is possible to write;

$$w \cong \frac{B'_0 \phi [-2 + 2(\nu + \phi)]}{4\alpha + (\phi - 2\alpha + \phi\alpha)2 + 1 - \nu^2}$$

or rearranging the terms,

$$w \cong \frac{2B'_0\phi[v + \phi - 1]}{2\phi(1 + \phi) + 1 - \nu^2}$$

Neglecting the small terms as α and ϕ in comparison with unity,

$$w \cong \frac{B'_0(\nu - 1)}{1 + \frac{1 - \nu^2}{2\phi}}$$

Now writing ϕ in detail, $\phi = \frac{q(1 - \nu^2)}{2Em}$ or $\frac{2Em}{1 - \nu^2} = \frac{p}{\phi}$ in which m is the ratio of the

thickness to the radius of the sphere. The classical critical load for a spherical shell as found before is;

$$p_{cr} = \frac{2Em^2}{\sqrt{3(1 - \nu^2)}} \text{ or } p^2_{cr} = \frac{4E^2m^4}{3(1 - \nu^2)} \text{ therefore, } \frac{2Em}{(1 - \nu^2)} = 3 \frac{p_{cr}^2}{2Em^3}$$

Equating the two relations;

$$\frac{q}{\phi} = \frac{3p^2_{cr}}{2Em^3}$$

Thus,

$$\frac{1}{\phi} = \frac{3}{2} \times \frac{q^2_{cr}}{Em^3} \times \frac{1}{p}$$

Substituting back

$$w = \frac{B'_n(\nu - 1)}{1 + \frac{3(1 - \nu^2)p^2_{cr}}{4Em^3q}}$$

or performing the cross multiplication,

$$w + \frac{3(1-\nu^2)}{4Em^3} \times p^2_{cr} \times \frac{w}{q} = B'_n (\nu - 1)$$

Which is the equation of a straight line if one axis is taken as w and the other one as w/p .

Thus the inverse slope of this line gives the critical load with a minus sign. Therefore obtaining the slope of this line experimentally,

$$p^2_{cr} = \frac{-4Em^3}{3(1-\nu^2)S}$$

where S denotes the slope. Thus, the Southwell procedure is applicable for uniformly compressed spherical shells.

2.6. Nonlinear Finite Element Analysis (FEA)

Finite element analysis (FEA) is capable to find the critical load associate with elastic buckling behavior. The first step in elastic buckling analysis is to find the critical load, which should be related to the lowest eigenvalue. All FEA for this investigation was performed using the general purpose program ABAQUS Version 6.7. ABAQUS is a highly sophisticated, general purpose finite element program, designed primarily to model the behavior of solids and structures under externally applied loading. Eight-node shell element was used to model hemispherical shells. This element is a general purpose quadratic shell element. The material of the shells is assumed as homogeneous, isotropic, imcompressible and elastic. In order to check for the accuracy attainable by this method, a number of spherical shells with different kinds of boundary condition and loading were solved (Figs 2.9-2.25).

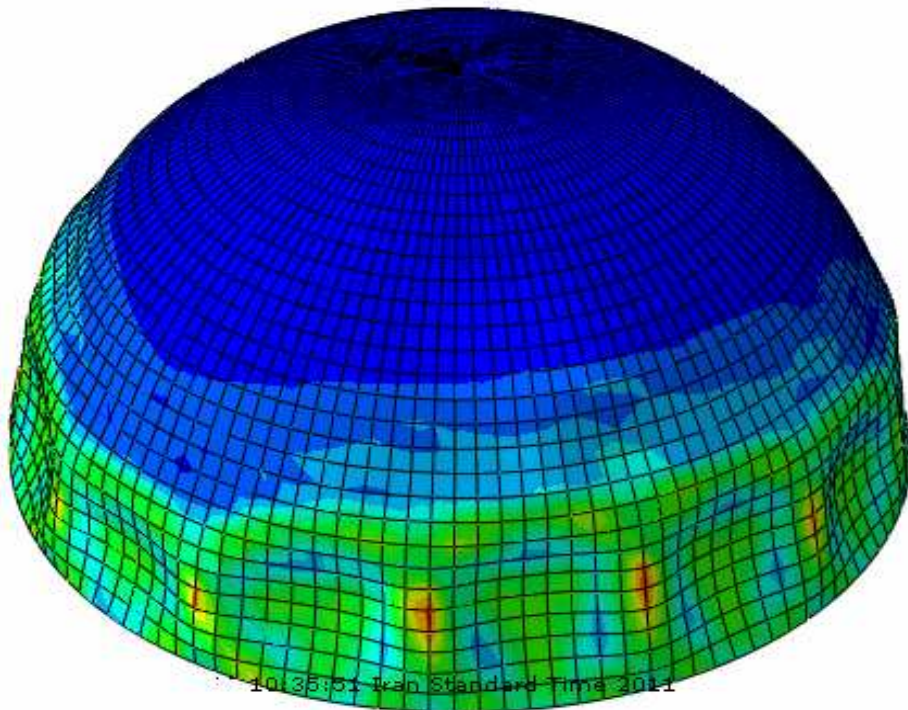
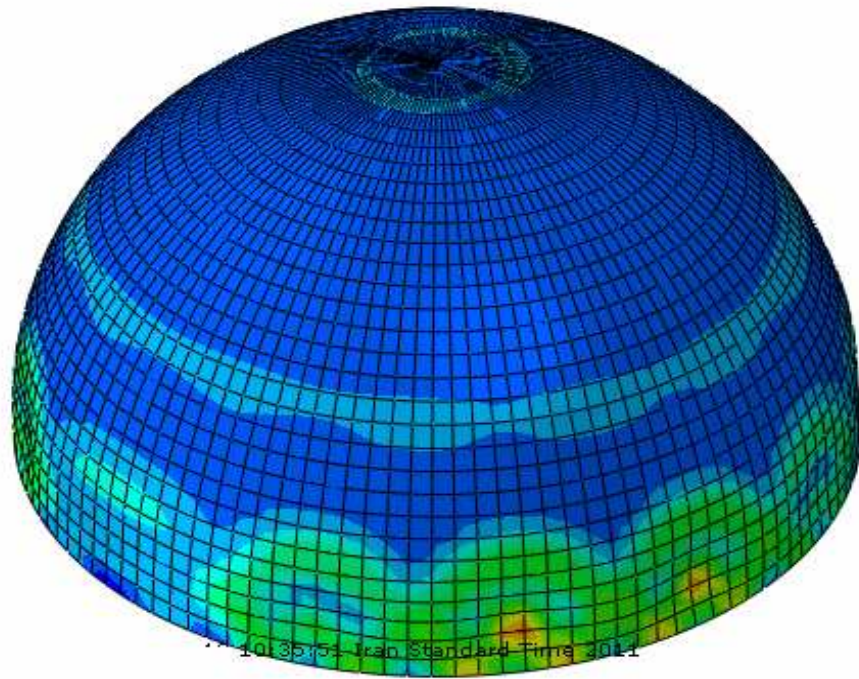


Figure 2. 9: Deformation pattern for hemispherical shell with hinge support under radially uniform pressure

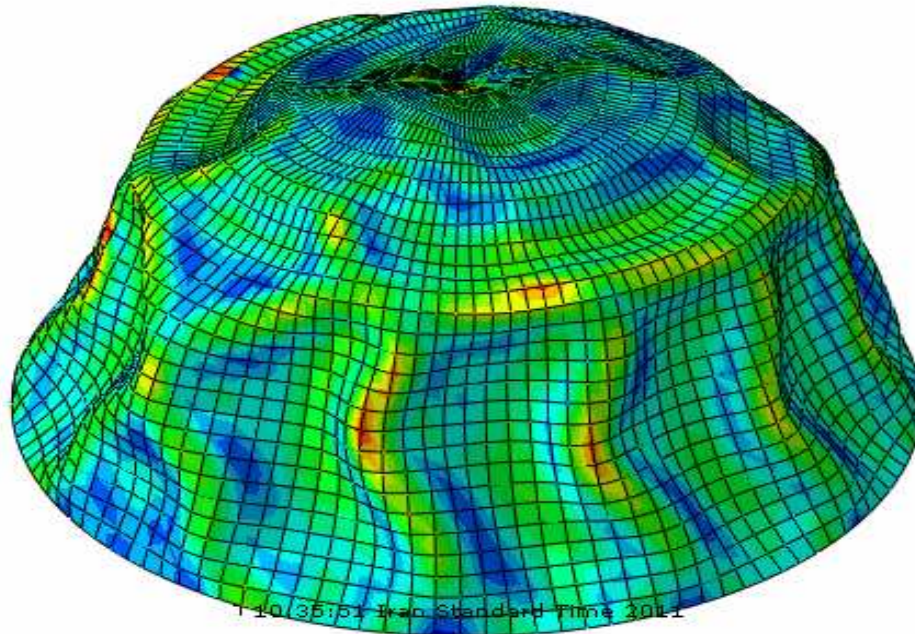
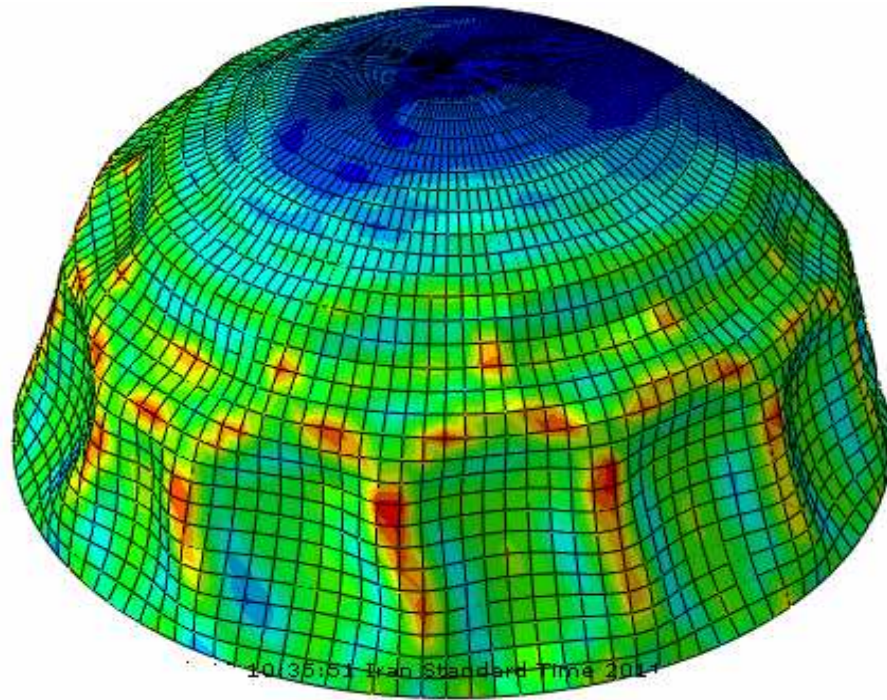


Figure 2. 10: Subsequent deformation of hemispherical shell with hinge support under radially uniform pressure

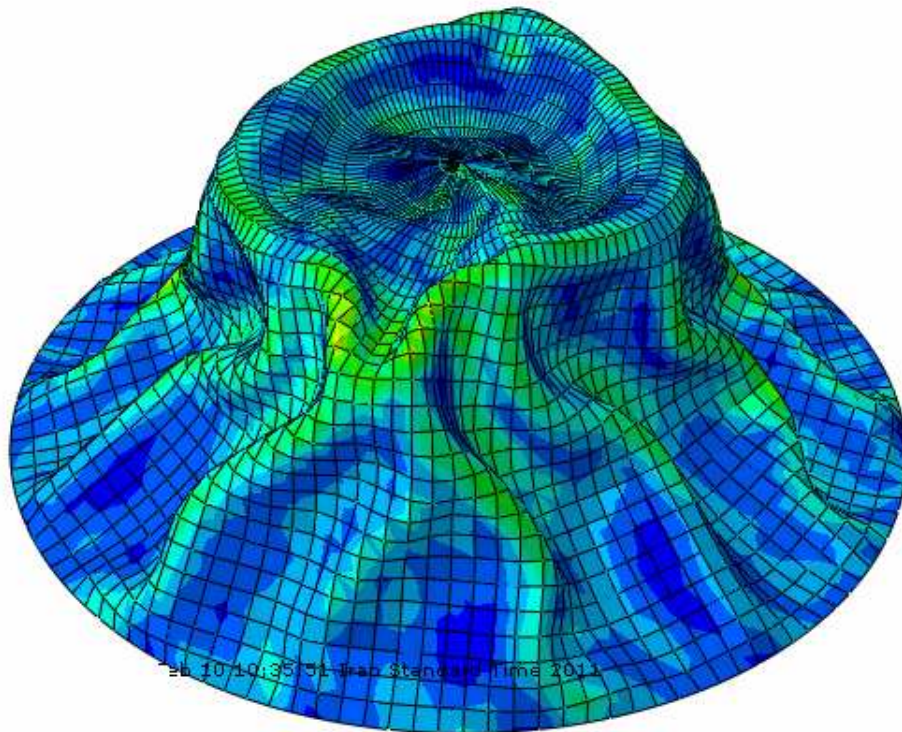
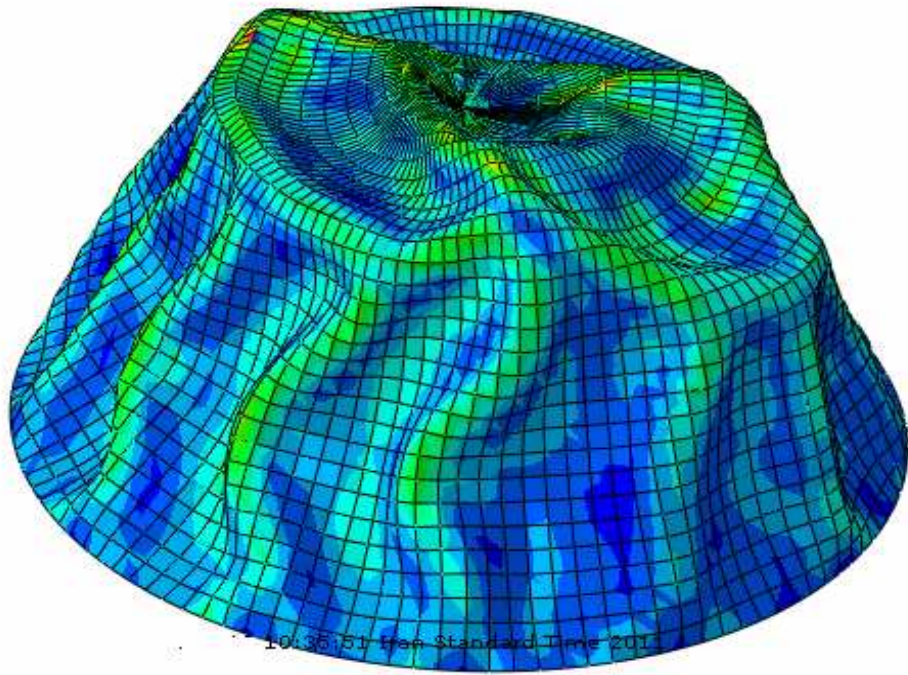


Figure 2. 11: Deformation of hemispherical shell with hinge support under maximum radially uniform pressure

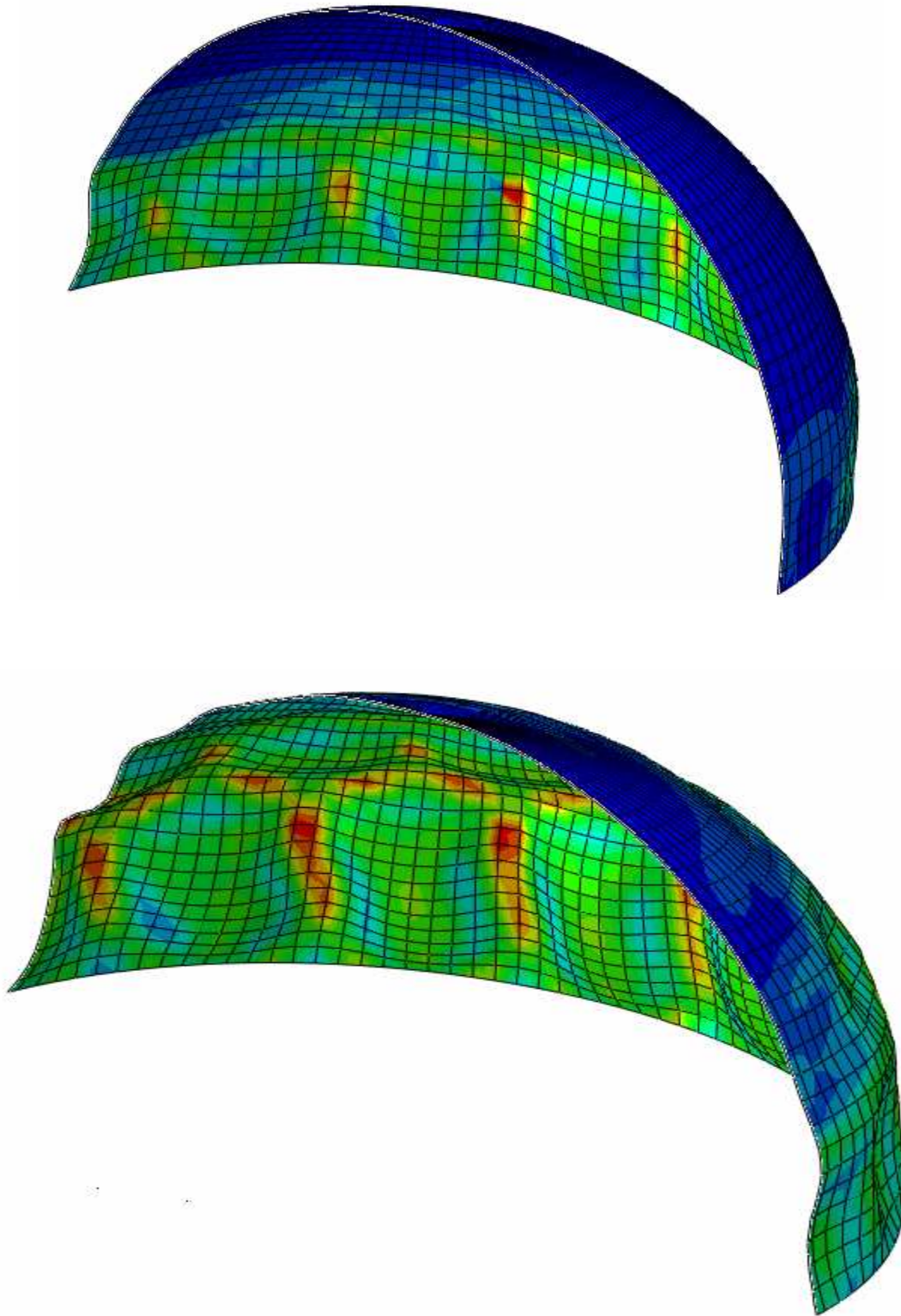


Figure 2. 12: Different cuts of the deformed hemispherical shell with hinge support under radially uniform pressure

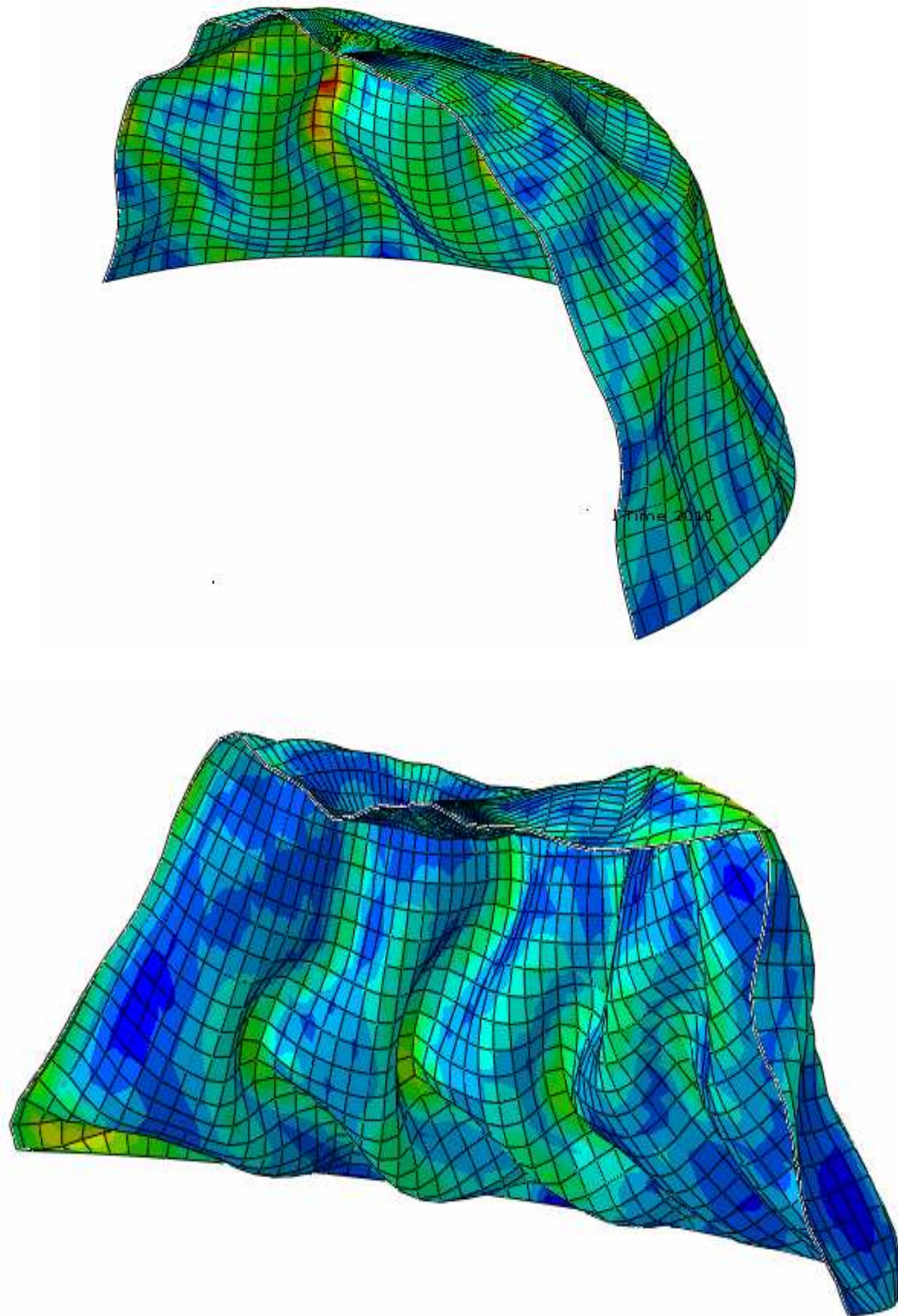


Figure 2. 13: Subsequent deformations in the cuts of the deformed hemispherical shell with hinge support under radially uniform pressure

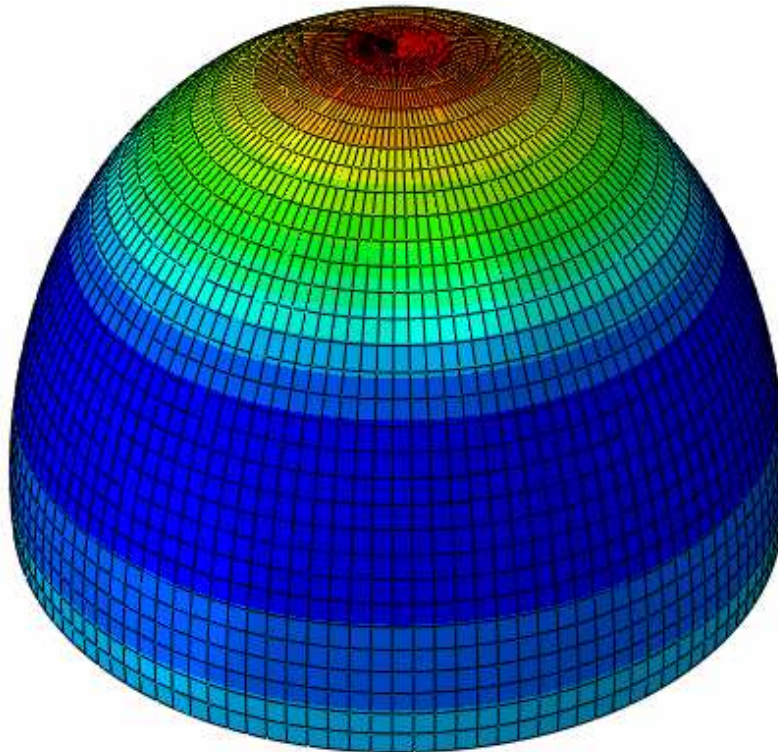
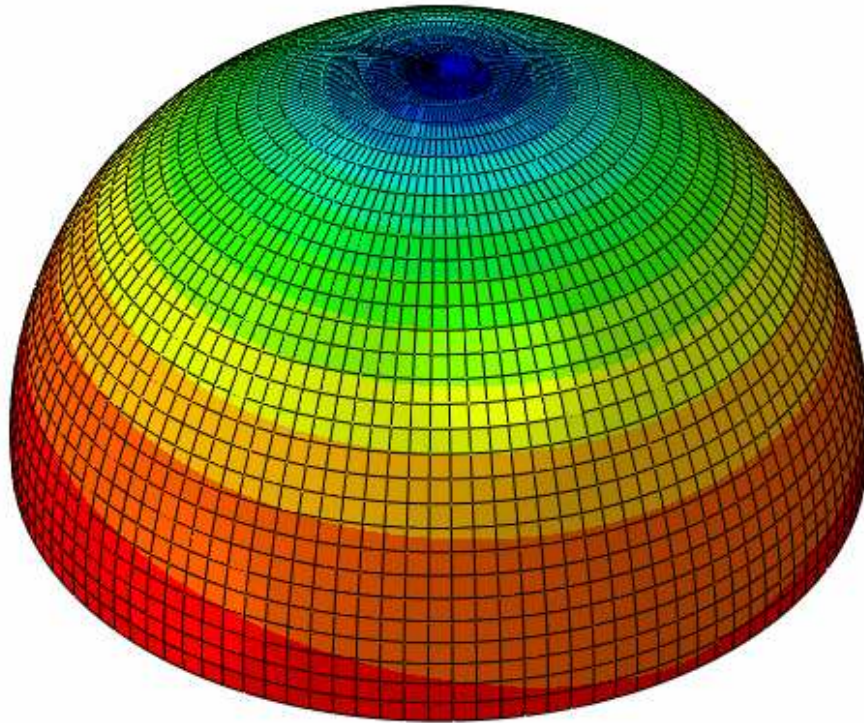


Figure 2. 14: Buckling initiation of the hemispherical shell with roller support under radially uniform pressure

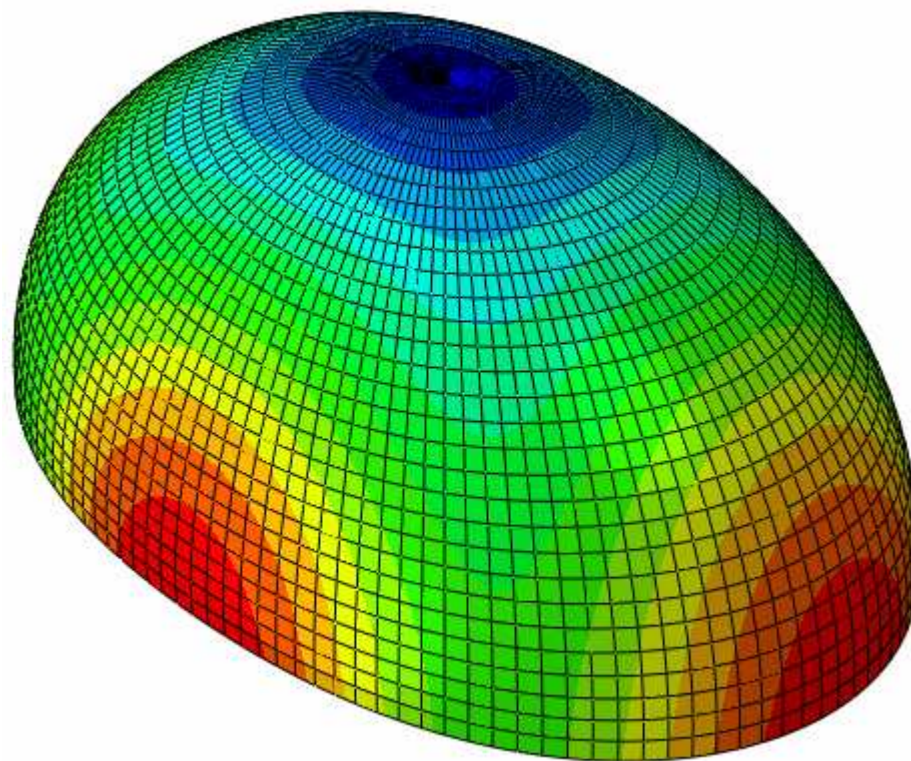
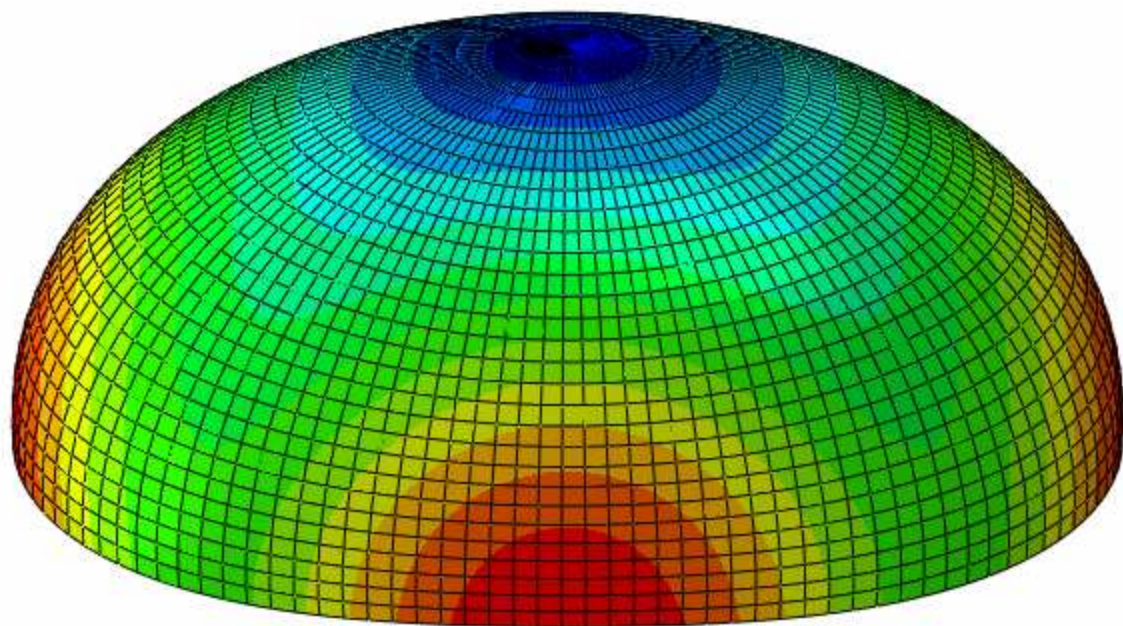


Figure 2. 15: Subsequent deformation of the hemispherical shell with roller support under radially uniform pressure

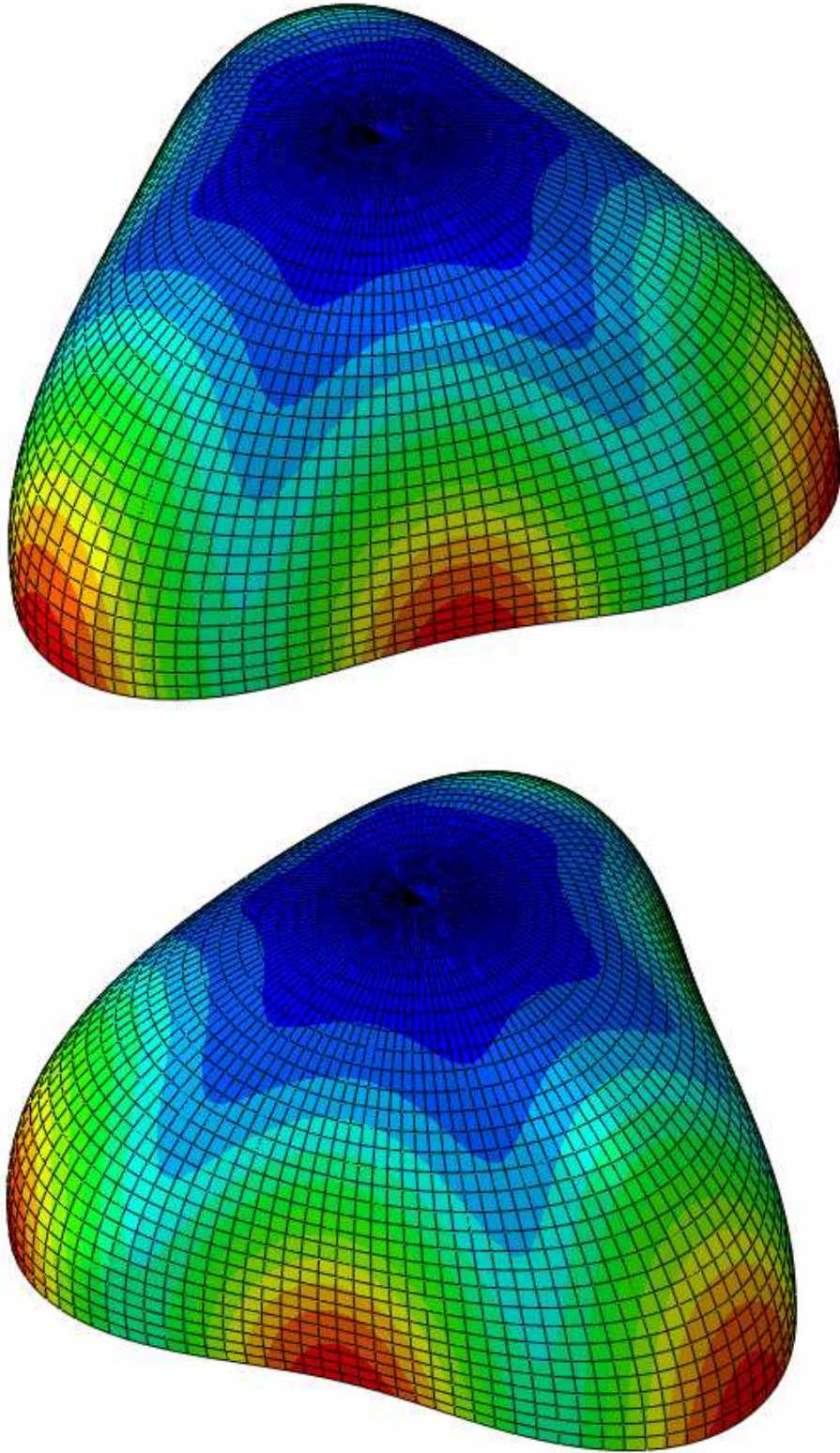


Figure 2. 16: Second mode of the deformation in hemispherical shell with roller support under radially uniform pressure

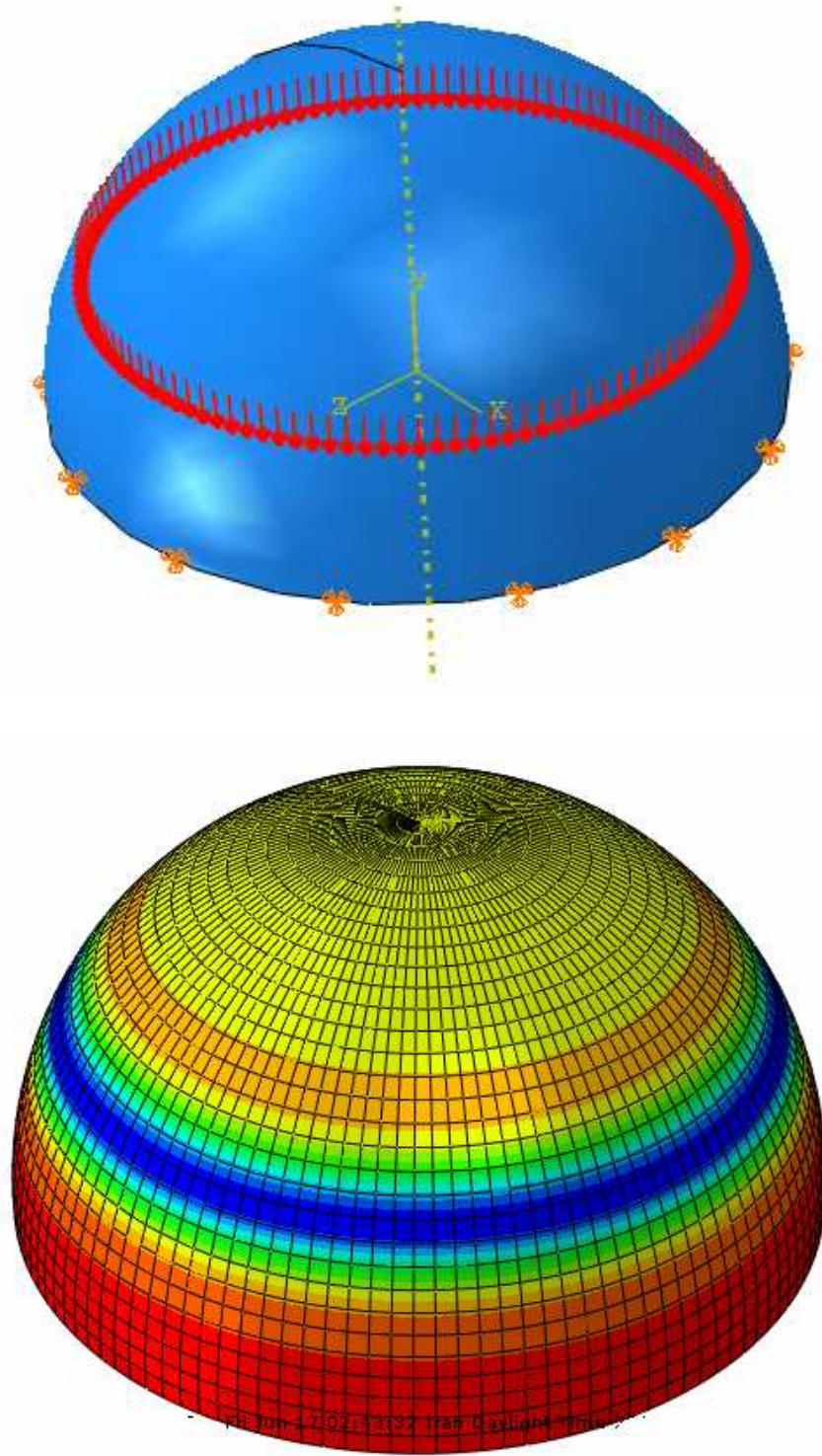


Figure 2. 17: Buckling initiation of the hemispherical shell with hinge support under ring load in

$$R/2$$

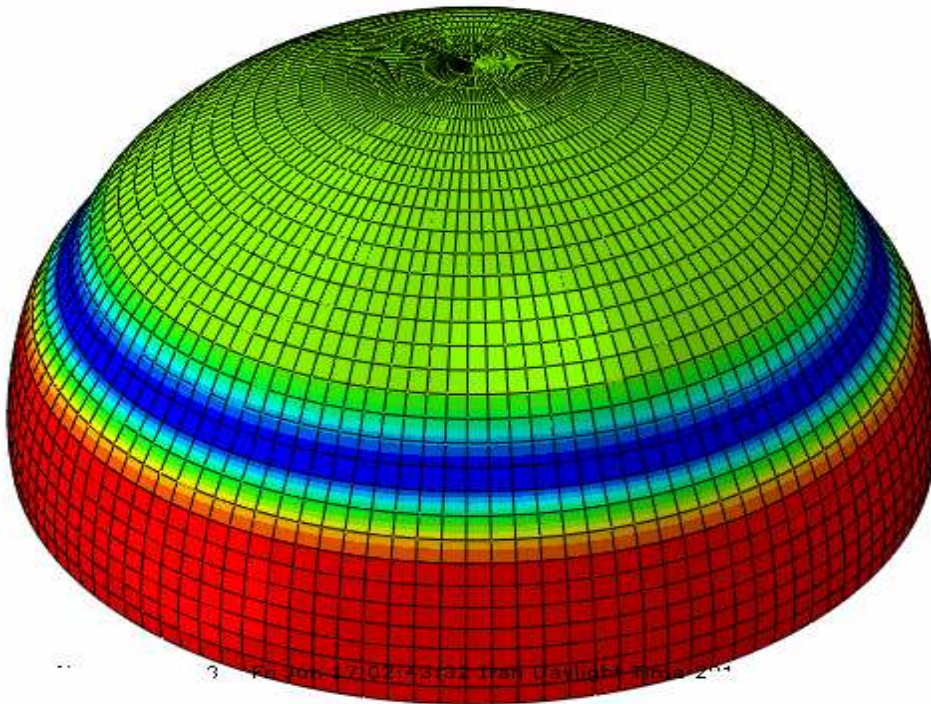
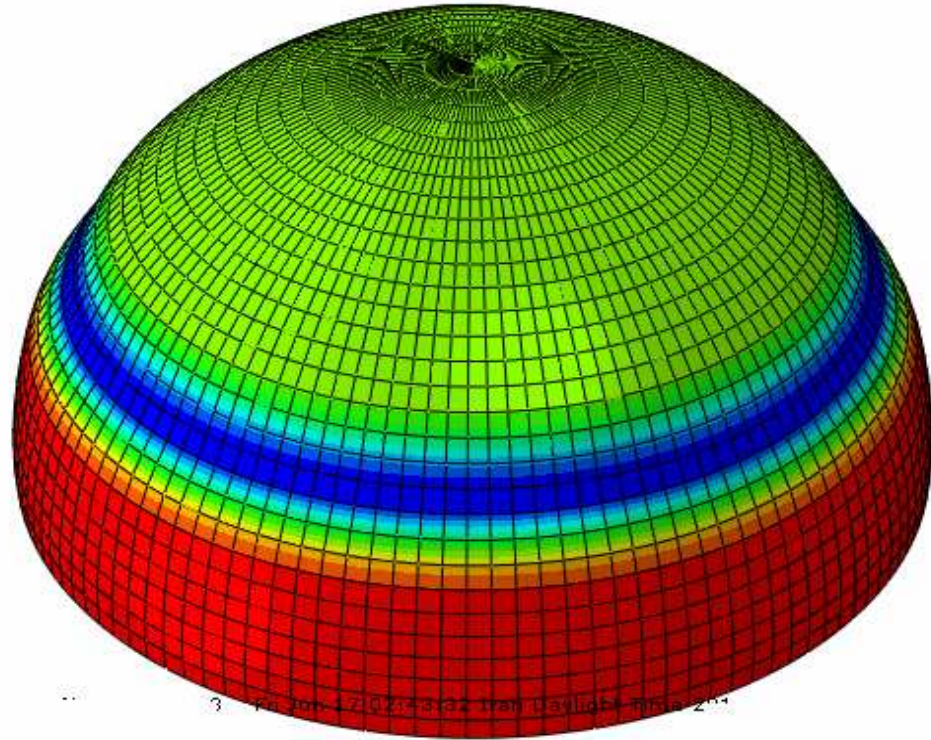


Figure 2. 18: Buckling of the hemispherical shell with hinge support under ring load at $R/2$

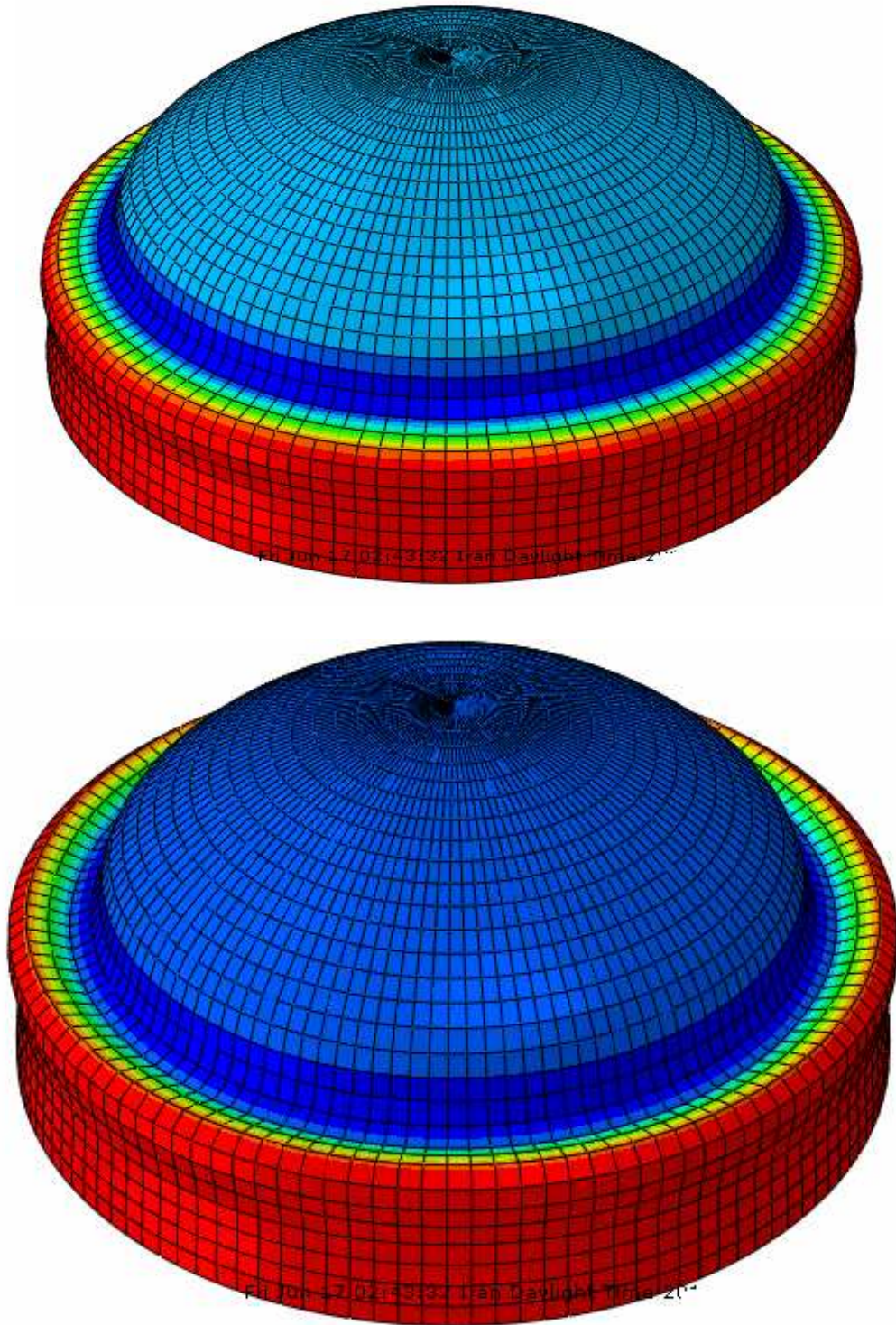


Figure 2. 19: Subsequent deformation of the hemispherical shell with hinge support under ring load at $R/2$

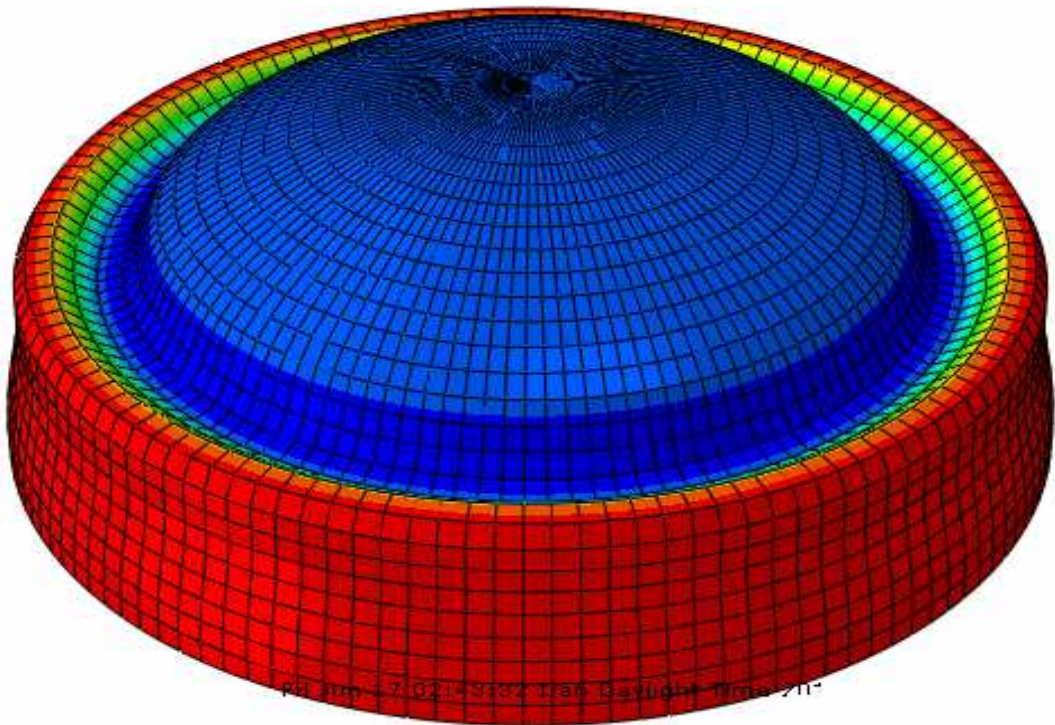
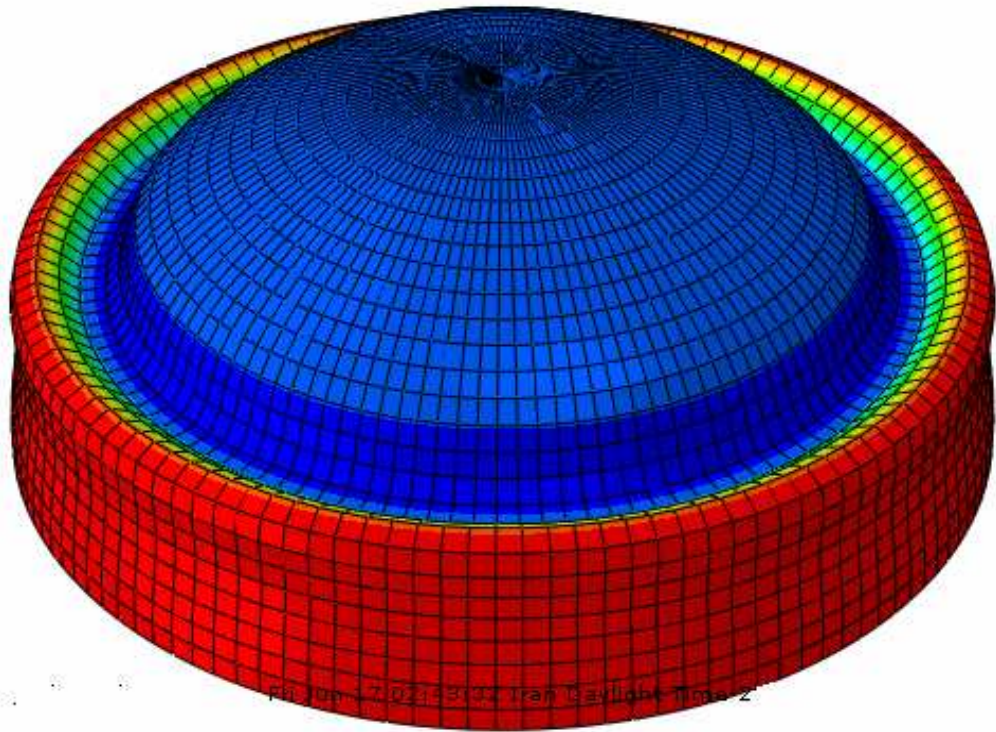


Figure 2. 20: Large deformation of the hemispherical shell with hinge support under ring load distributed at $R/2$

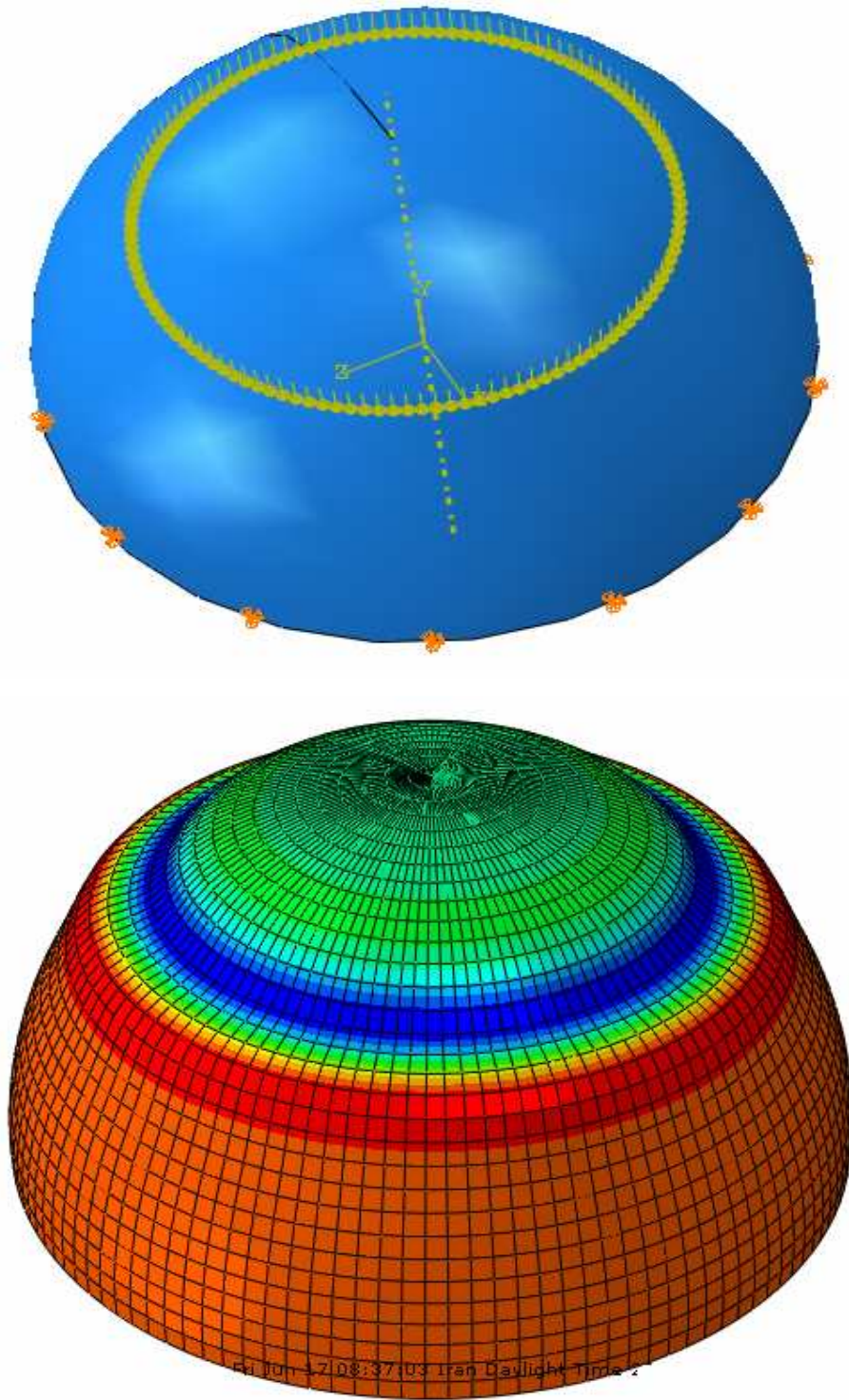


Figure 2. 21: Buckling initiation of the hemispherical shell with hinge support under ring load in

$$\frac{R}{3}$$

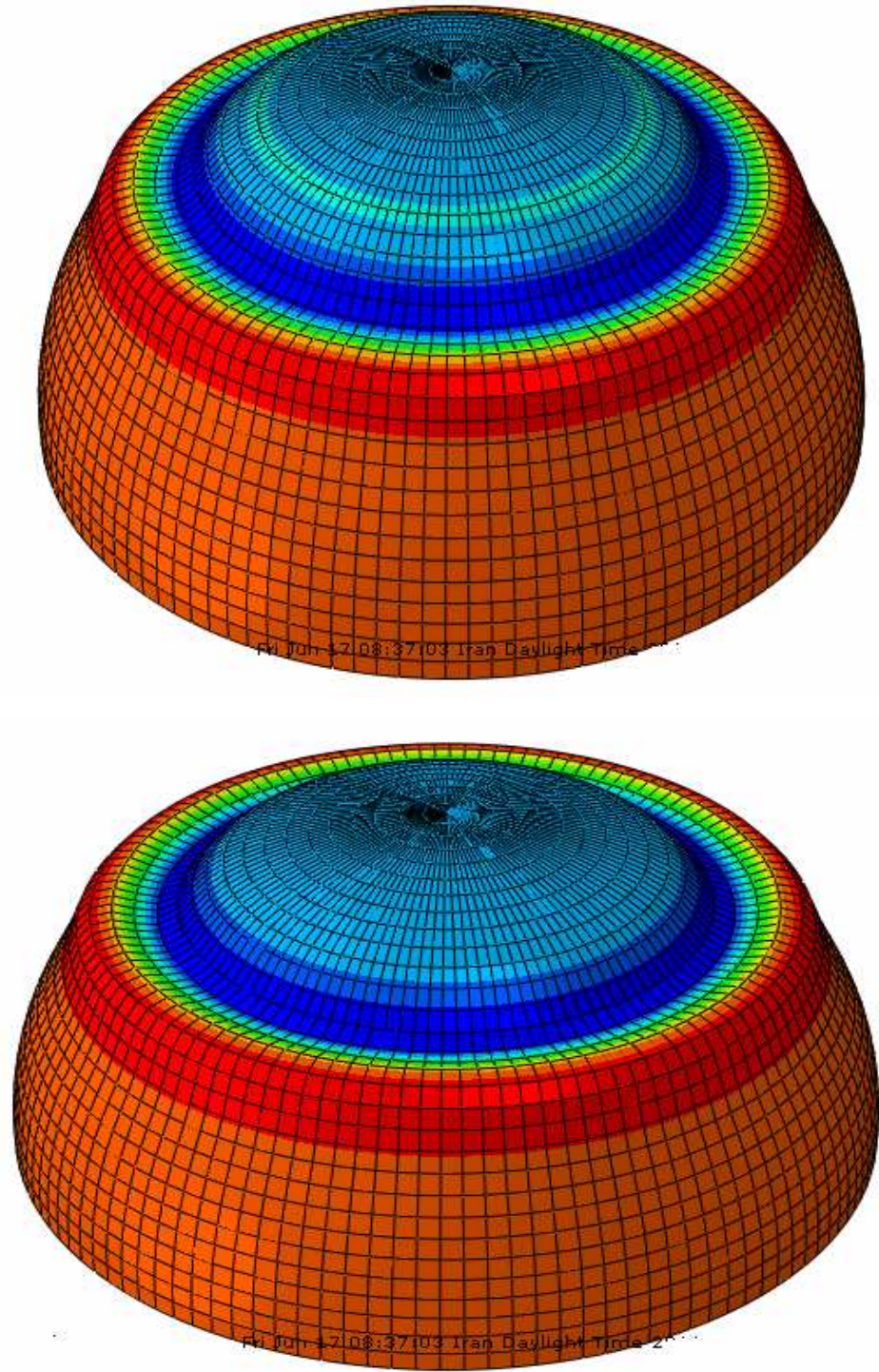


Figure 2. 22: Buckling of the hemispherical shell with hinge support under ring load at $R/2$

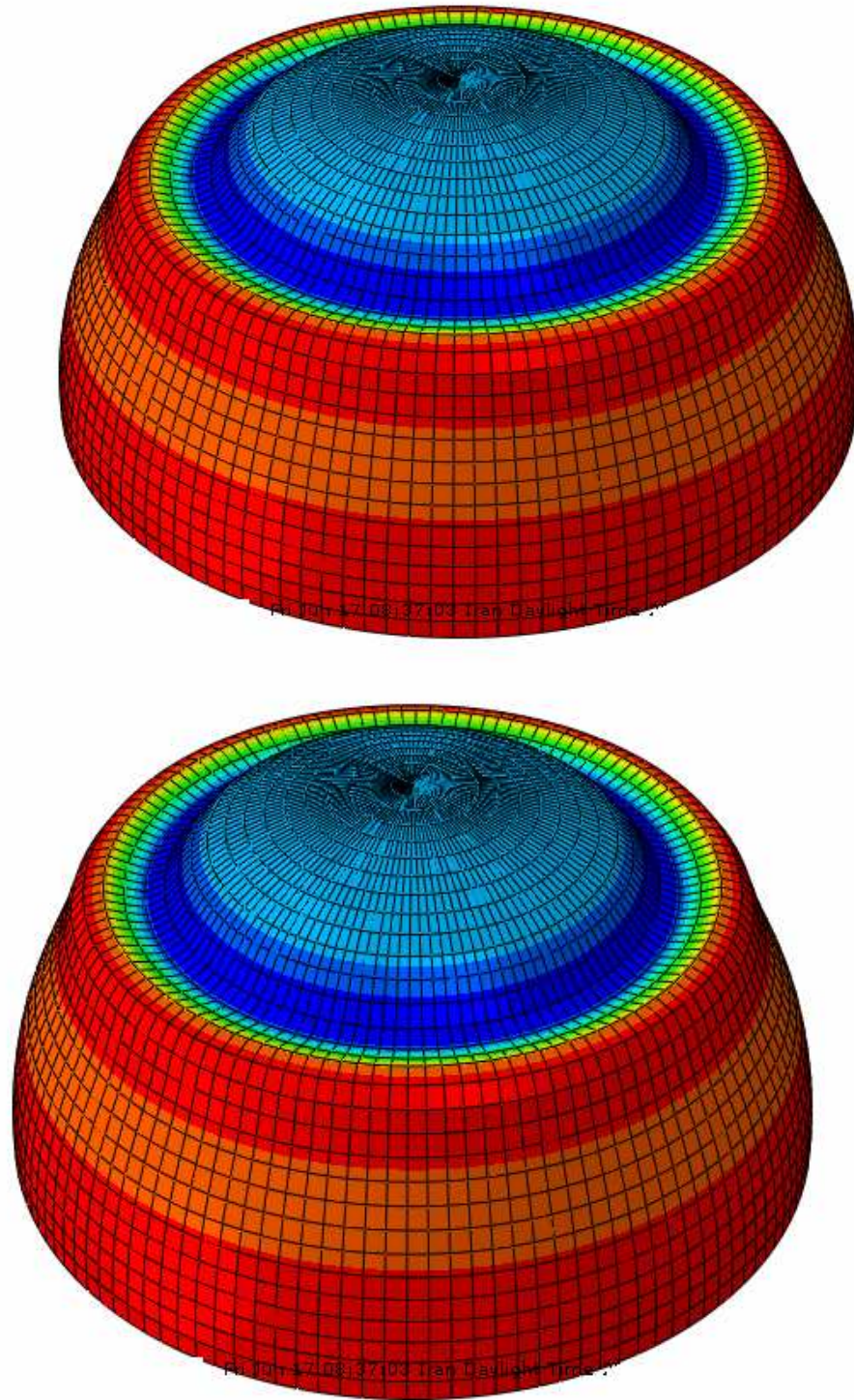


Figure 2. 23: Large deformation of the hemispherical shell with hinge support under ring load distributed at $R/3$

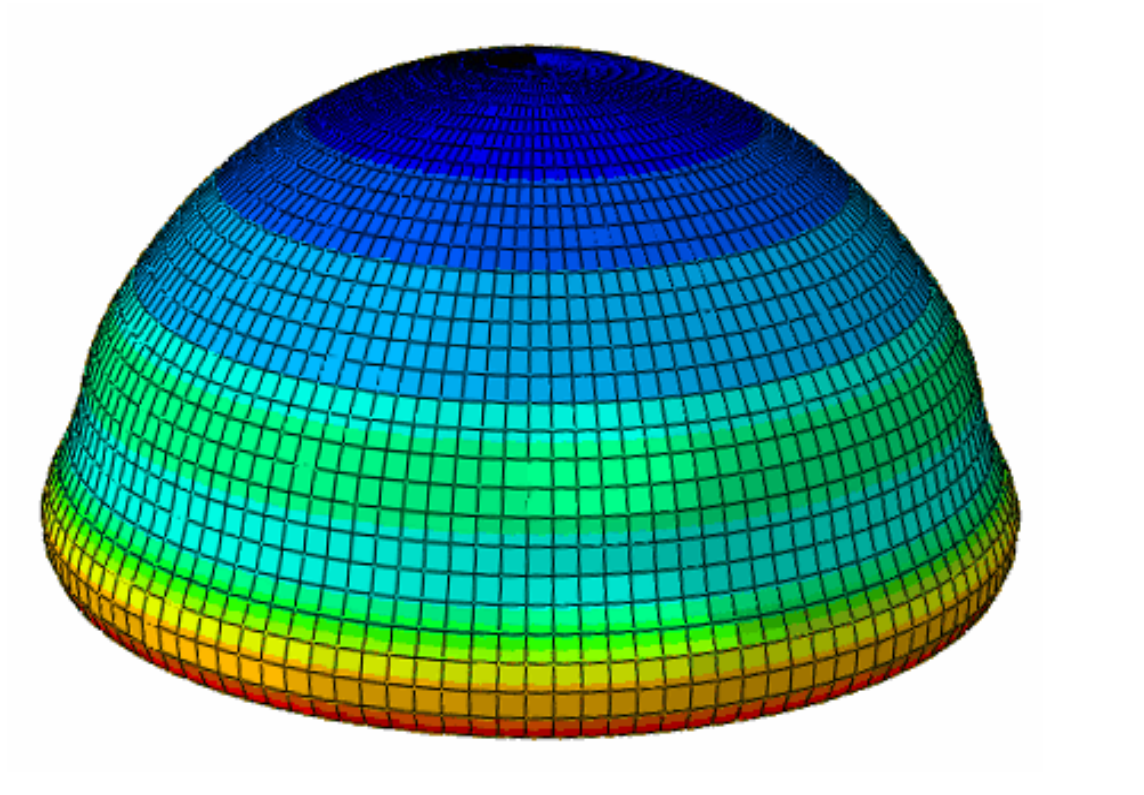
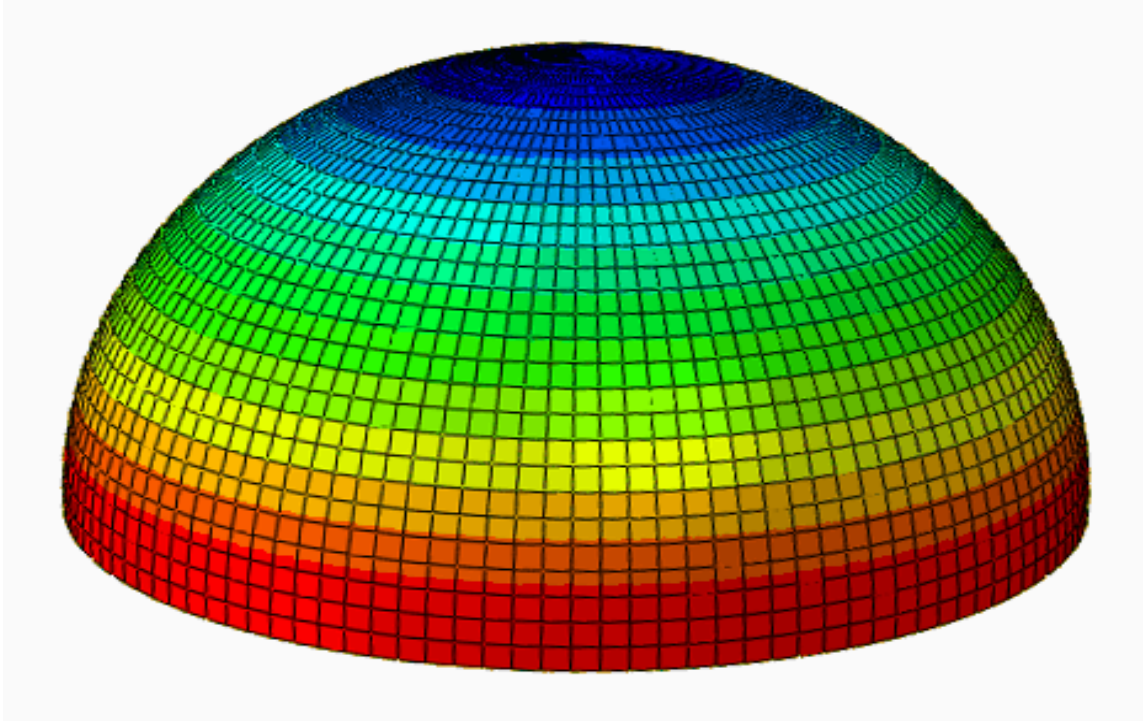


Figure 2. 24: Buckling initiations of the hemispherical shell with hinge support under gravity loading

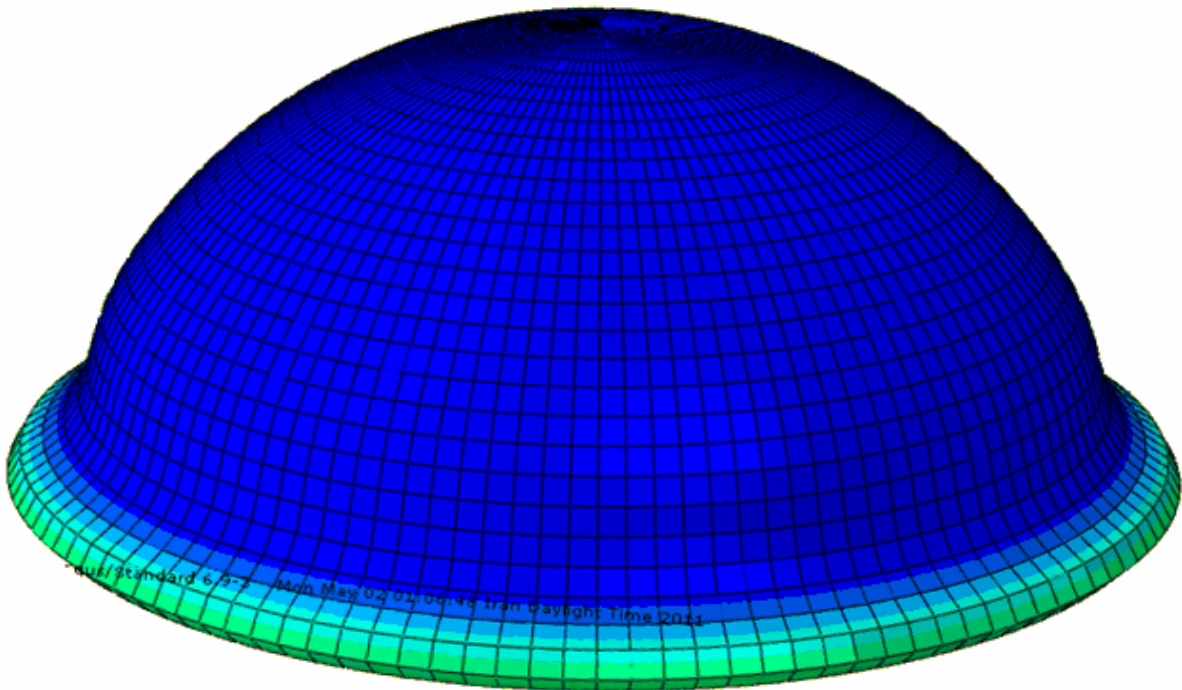
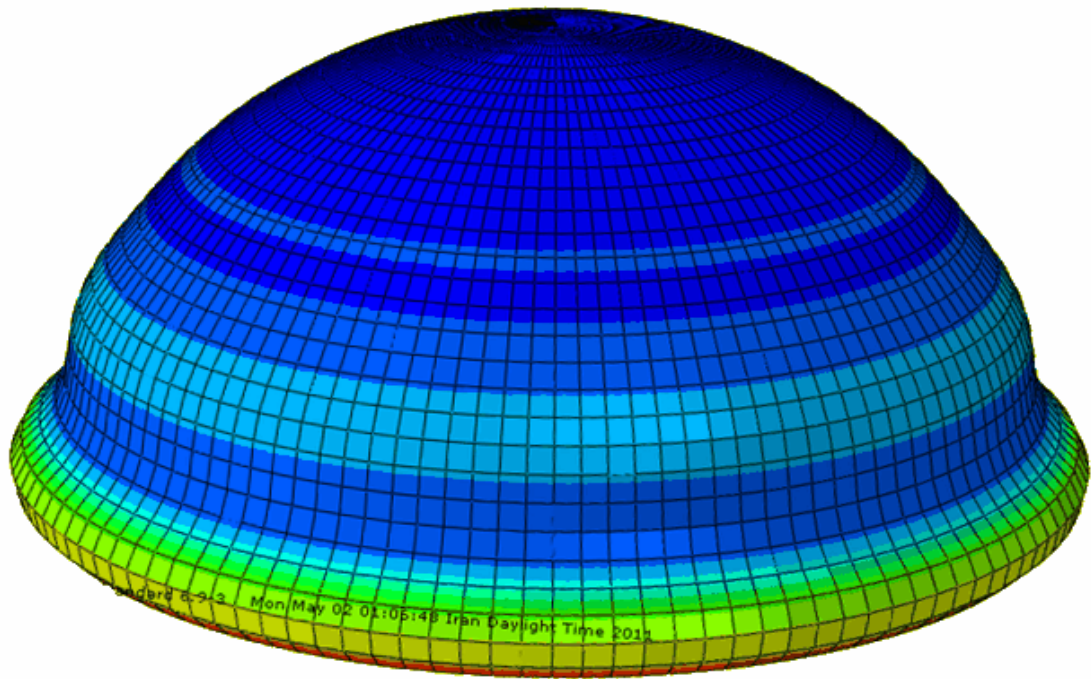


Figure 2. 25: Subsequent deformation of the hemispherical shell with hinge support under gravity loading

2.7. Experimental Program

In this part, an attempt is made to find the critical load for hemispherical shells pinned at the base and subject to uniform pressure in a purely experimental way. It is intended to show that the formulation which has been derived in this study give correct results for shells of revolution under various axisymmetric loading conditions.

A total of six thin walled polyethylene hemispherical shells were constructed and tested under uniform suction pressure. The base diameters of these shells were 15 cm and 10 cm and their wall thickness were 0.05 cm yielding R/t ratios of 150 and 100 respectively. It is evident that the construction of these shells through machining would have been difficult and for the following reasons, the shells were made of solid polyethylene plastic which posses good tensile, flexural, and impact strengths and its flexural modulus is proportional to the stiffness of the material. Its creep resistance is excellent and is substantially superior to most plastics. Its mechanical properties are as follows:

Flexural modulus: 650 MPa

Poisson's ratio: 0.4

Density: 1150 kg/m³

Poisson's ratio: 0.4

A complete family of hemispherical shells is shown in Fig 2.26.

The manufacturing of these shells was carried out with the aid of machined male and female molds made from cast aluminum alloy. The aluminum alloy molds were machined with considerable precision and then the spherical shells were cast by "puddling" technique. Each shell was inspected by a polariscope to ensure that no air bubbles were trapped in the shell wall.



Figure 2. 26: Hemispherical shells samples made of polyethylene



Figure 2. 27: A test made of $R=75$ mm shell using suction pressure and three displacement gages at various points.

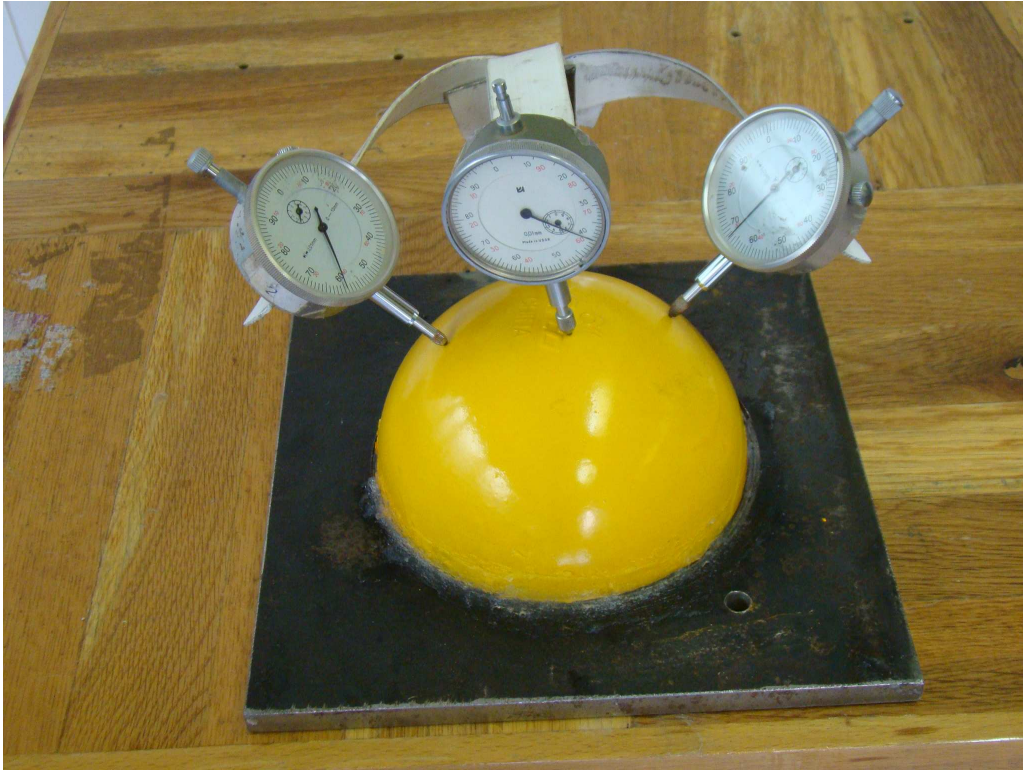


Figure 2. 28: Deformation measurement with three gauges at different locations in hemispherical shells under uniform suction pressure ($R= 75\text{mm}$).

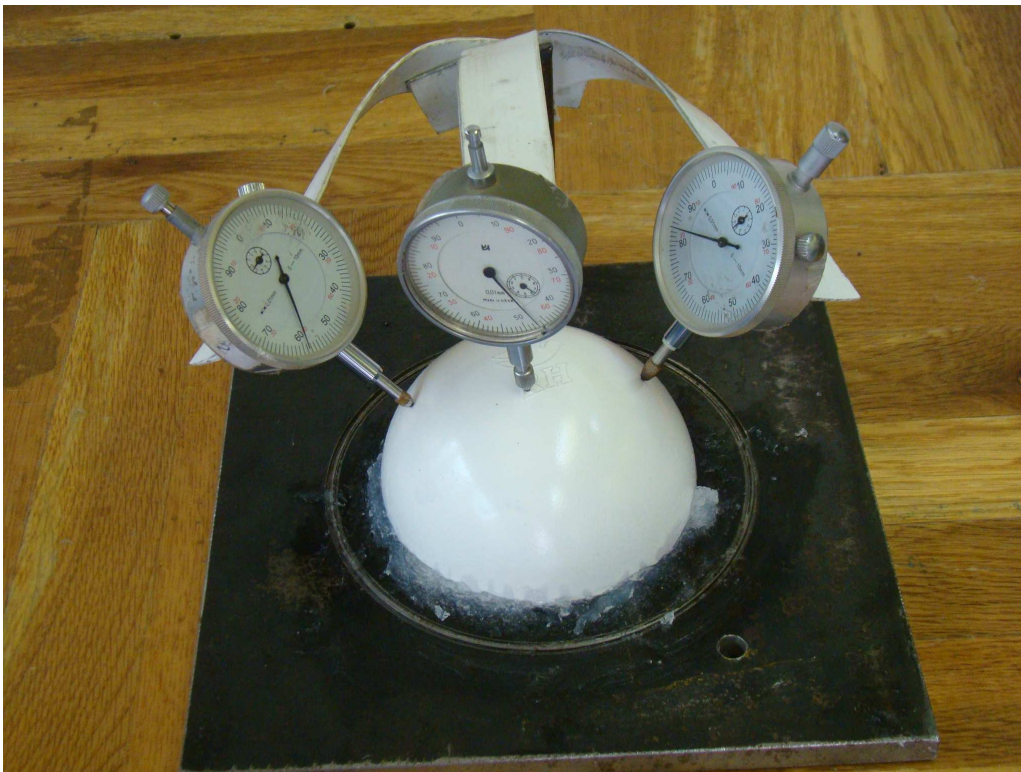
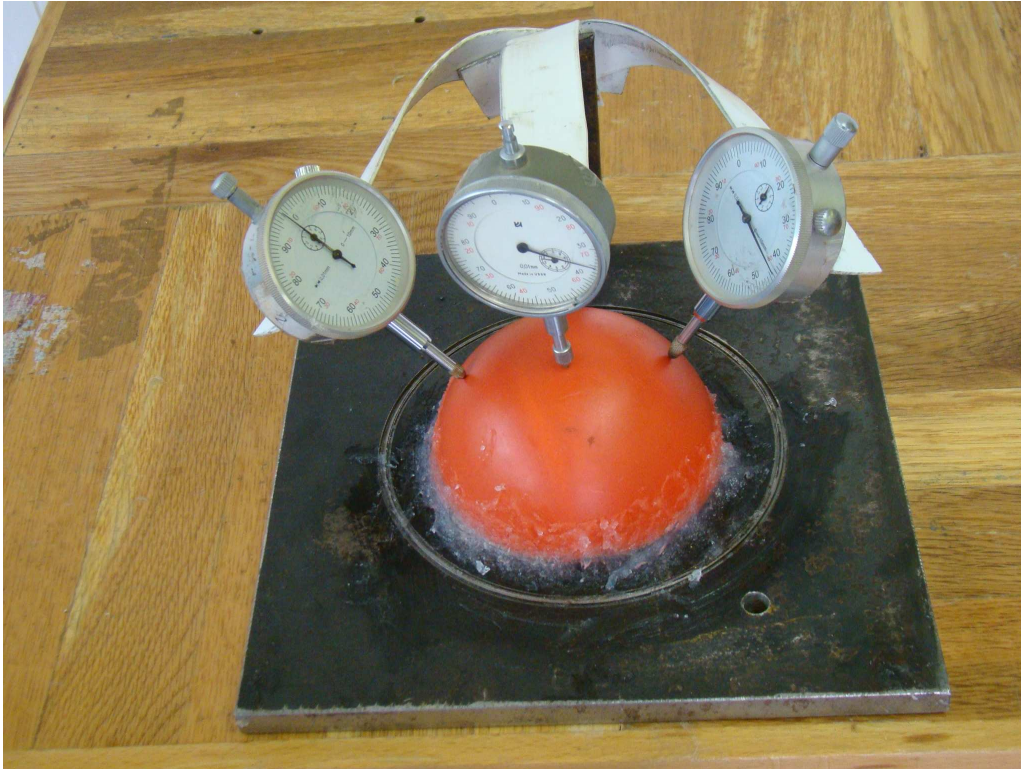


Figure 2. 29: Tests made of $R=50$ mm shells with suction pressure and three displacement gages at different locations hemispherical shells under uniform suction pressure ($R= 50$ mm).

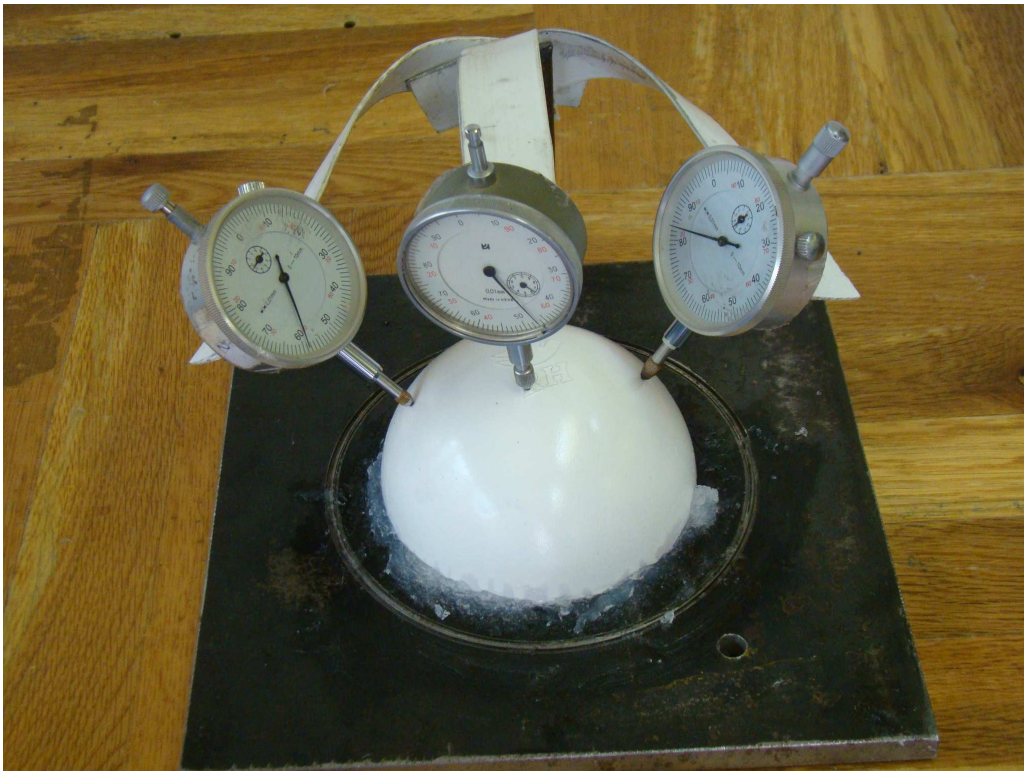
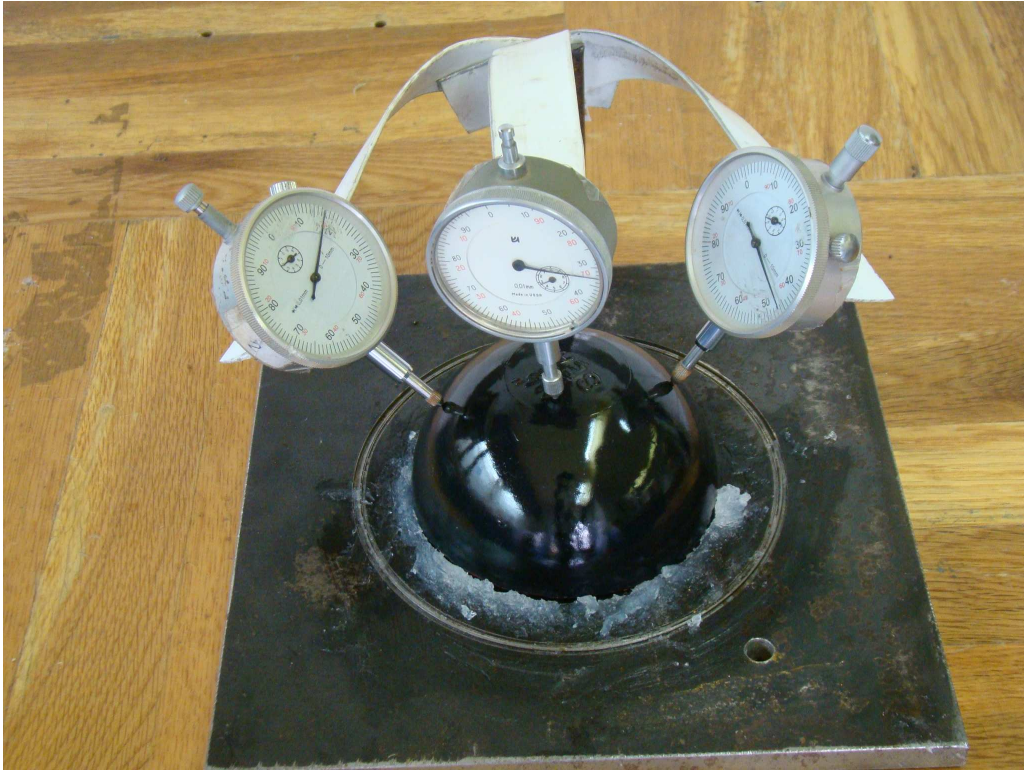


Figure 2. 30: Deformation measurement with three gages in different locations at hemispherical shells under uniform suction pressure ($R= 50$ mm).



Figure 2. 31: Initial buckling of hemispherical shells under uniform suction pressure ($R= 50$ mm).



Figure 2. 32: Initial buckling of hemispherical shells under uniform suction pressure ($R= 50$ mm).



Figure 2. 33: Initial buckling of hemispherical shells under uniform suction pressure ($R= 75$ mm).



Figure 2. 34: Several tests made on different samples using suction pressure with three and five gages at different locations.

2.8. Results and Discussion

In this study, the Southwell predictions are compared with experimentally, and numerically obtained values. The results of the investigation are summarized in Figs 2.35 to 2.45 which the predictions of the Southwell method are compared with measured buckling loads in experimental study and numerical simulations. Scatter in the experimentally obtained buckling pressures is probably due to variations that existed occurred in the specimens because of the fact that each one was cast separately. The manufacturers did, however, take considerable care during the manufacturing process, and especially with the mix, and for this reason the scatter is very small. Thus, it is likely that the main source of error compared to theory is because of measurement reading errors, and imperfections in material properties. However, the agreement between measured buckling load and Southwell prediction is remarkable. Mostly, the Southwell method tended to yield buckling loads which are slightly higher than those measured and the disparity of buckling load is somewhat difficult to detect. Nevertheless, the predicted loads are reliable to be slightly higher (up to about 17%) than the actual load encountered. Therefore, a reasonable degree of caution is recommended to be exercised. Scatter in the numerically obtained buckling pressures for axisymmetrical buckling cases are very small and it is most likely due to the assumptions of the finite element solution. For the case of buckling of spherical shell with roller support under uniform pressure, the buckled shape is not axisymmetric anymore (Fig 2.15). So, once data are collected from the principle axes locations, the answer is acceptable and there is only 13% error otherwise, the deviation from the correct values is considerable.

Briefly, the method provides valuable technique for estimating the buckling load of spherical shells without having to conduct a destructive test. The results obtained have logical accuracy and the method does not suffer from the any major issues. Any boundary condition at

the edge may be taken into account and as long as the loading is axisymmetric, this procedure can be used with reasonable accuracy.

2.8.1 Experimental work findings

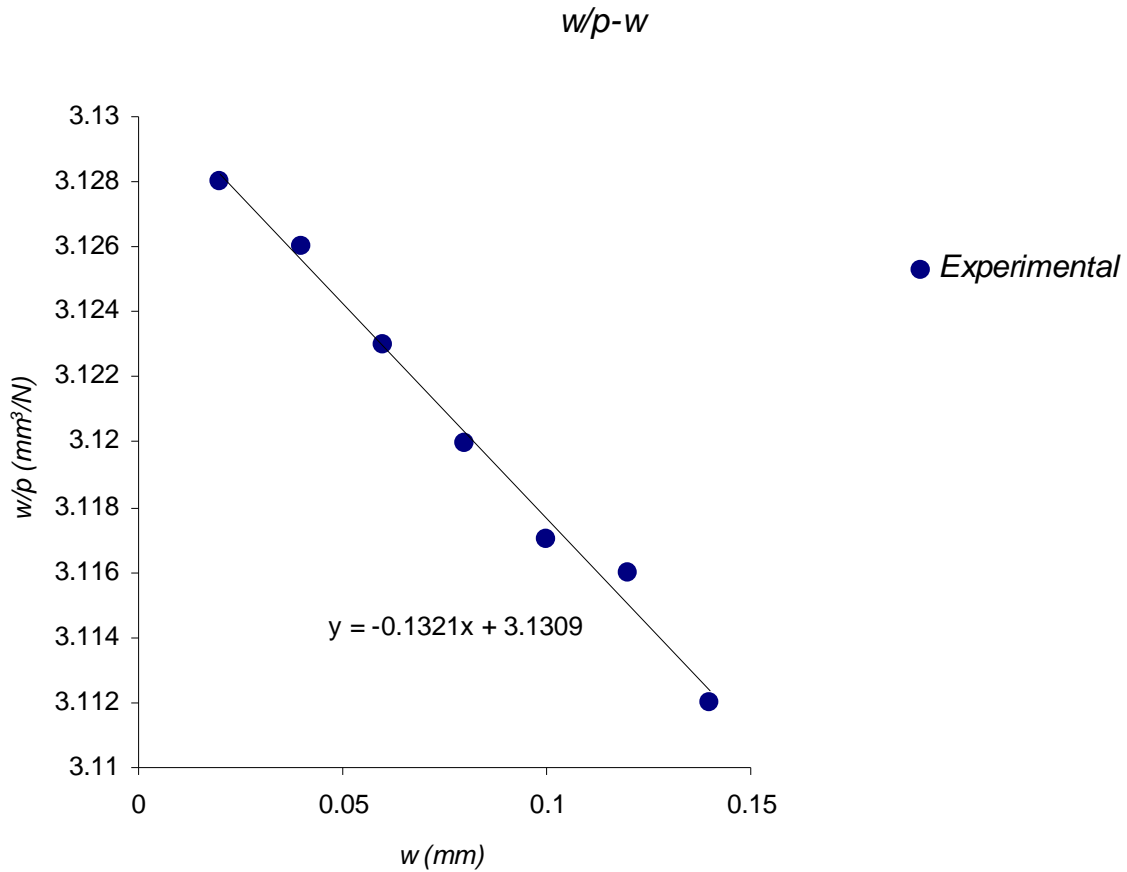


Figure 2. 35: Plot of $\frac{w}{p}$ against w ($R = 50mm, t_0 = 0.5mm$)

$$S = -0.1321$$

$$p_{cr}^2 = \frac{-4Em^3}{3(1-\nu^2)S} \rightarrow p_{cr} = 0.088MPa$$

$$\text{From test } \bar{p} = 0.078MPa$$

$$\text{Error for this case: } \frac{0.088 - 0.078}{0.078} \times 100 = 12.8\%$$

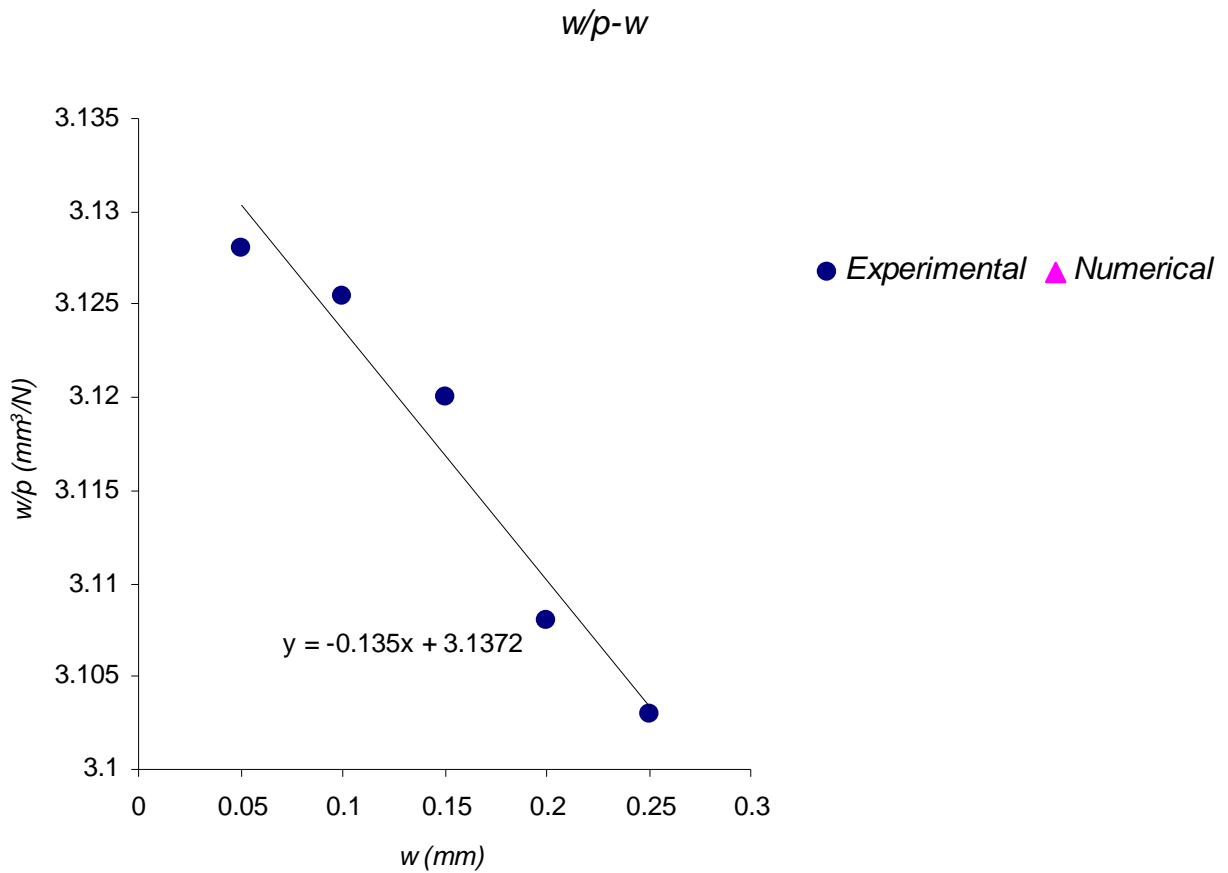


Figure 2. 36: Plot of w/p against w ($R = 50mm, t_0 = 0.5mm$)

$$S = -0.135$$

$$p_{cr}^2 = \frac{-4Em^3}{3(1-\nu^2)S} \rightarrow p_{cr} = 0.087MPa$$

From test $\bar{p} = 0.078MPa$

Error for this case: $\frac{0.087 - 0.078}{0.078} \times 100 = 10.15\%$

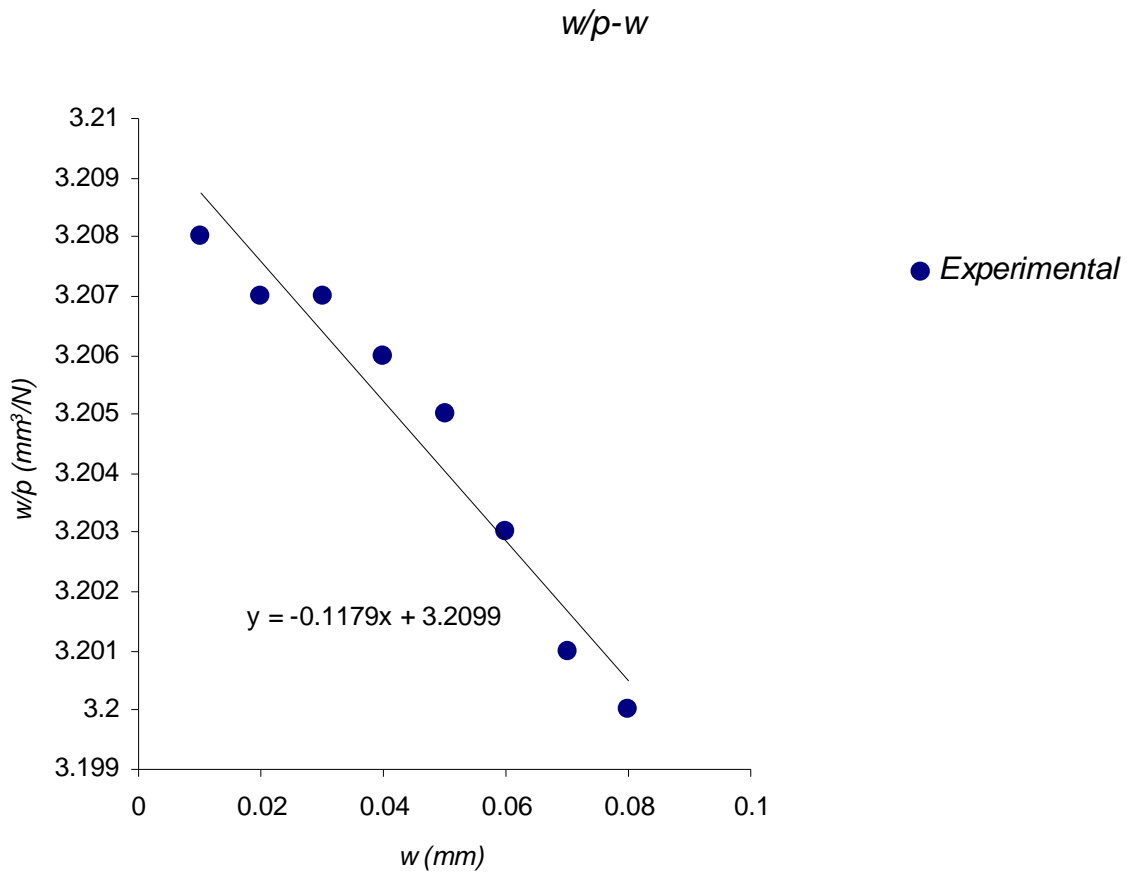


Figure 2.37: Plot of $\frac{w}{p}$ against w ($R = 50mm, t_0 = 0.5mm$)

$$S = -0.1179$$

$$p_{cr}^2 = \frac{-4Em^3}{3(1-\nu^2)S} \rightarrow p_{cr} = 0.0935MPa$$

From test $\bar{p} = 0.08MPa$

Error for this case: $\frac{0.0935 - 0.08}{0.08} \times 100 = 16.8\%$

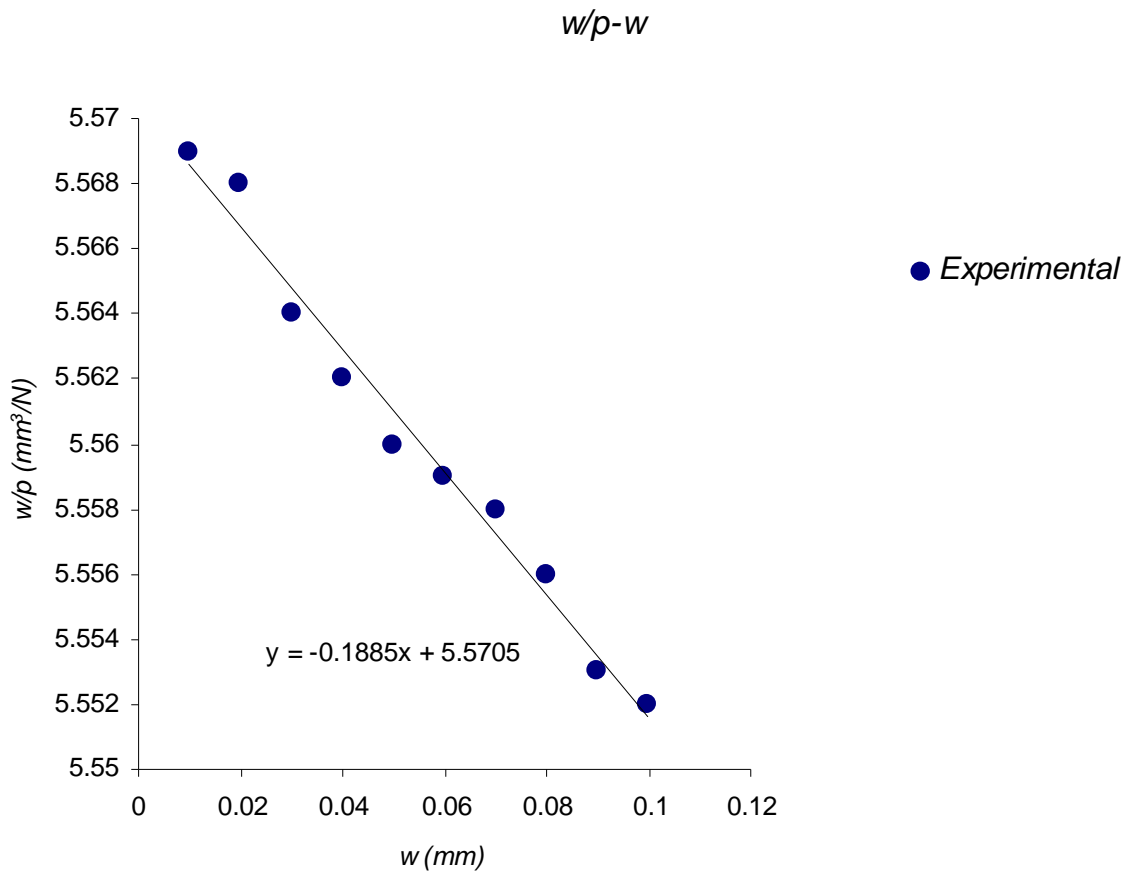


Figure 2. 38: Plot of w/p against w ($R = 75mm, t_0 = 0.5mm$)

$$S = -0.1885$$

$$p_{cr}^2 = \frac{-4Em^3}{3(1-\nu^2)S} \rightarrow p_{cr} = 0.040MPa$$

From test $\bar{p} = 0.035MPa$

Error for this case: $\frac{0.040 - 0.035}{0.035} \times 100 = 14.28\%$

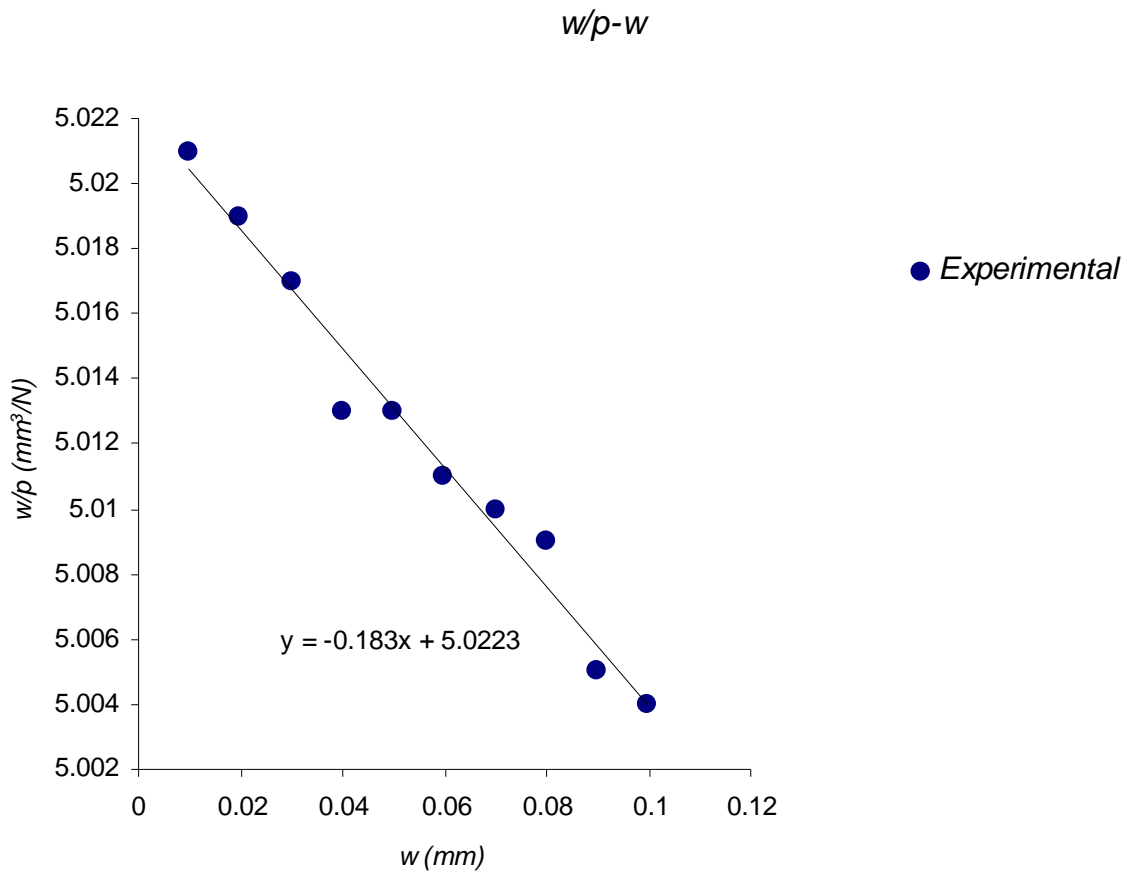


Figure 2.39 : Plot of $\frac{w}{p}$ against w ($R = 75mm, t_0 = 0.5mm$)

$$S = -0.183$$

$$p_{cr}^2 = \frac{-4Em^3}{3(1-\nu^2)S} \rightarrow p_{cr} = 0.0408MPa$$

From test $\bar{p} = 0.035MPa$

Error for this case: $\frac{0.0408 - 0.035}{0.035} \times 100 = 16.5\%$

2.8.2 Numerical Study results

2.8.2.1. For uniform radial pressure case with hinge support:

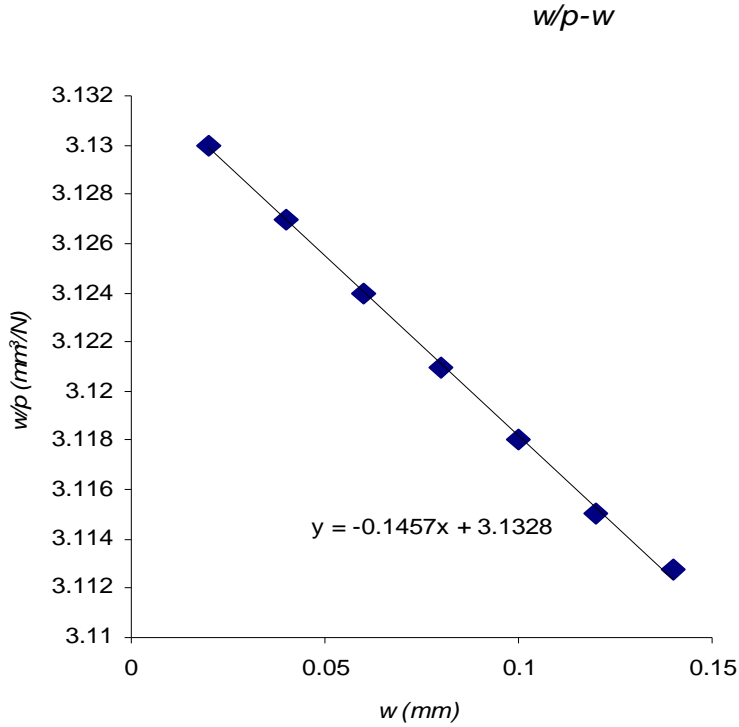


Figure 2. 40: Plot of w/p against w ($R = 50mm, t_0 = 0.5mm$)

$$S = -0.1457$$

$$p_{cr}^2 = \frac{-4Em^3}{3(1-\nu^2)S} \rightarrow p_{cr} = 0.084MPa$$

From test $\bar{p} = 0.081MPa$

Error for this case: $\frac{0.084 - 0.081}{0.081} \times 100 = 3.7\%$

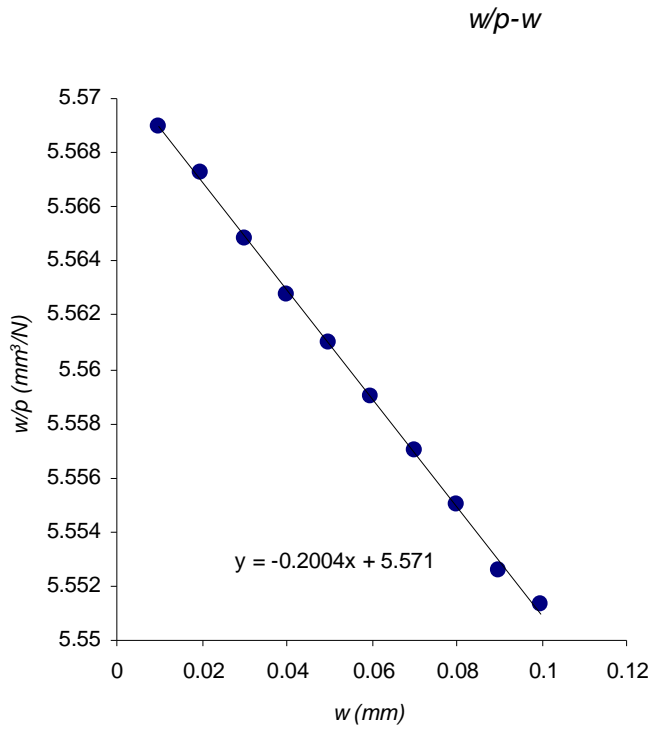


Figure 2. 41: Plot of p against w ($R = 75mm, t_0 = 0.5mm$)

$$S = -0.2$$

$$p_{cr}^2 = \frac{-4Em^3}{3(1-\nu^2)S} \rightarrow p_{cr} = 0.039MPa$$

From test $\bar{p} = 0.037MPa$

Error for this case: $\frac{0.039 - 0.037}{0.037} \times 100 = 5.4\%$

2.8.2.2. For uniform downward pressure case with hinge support:

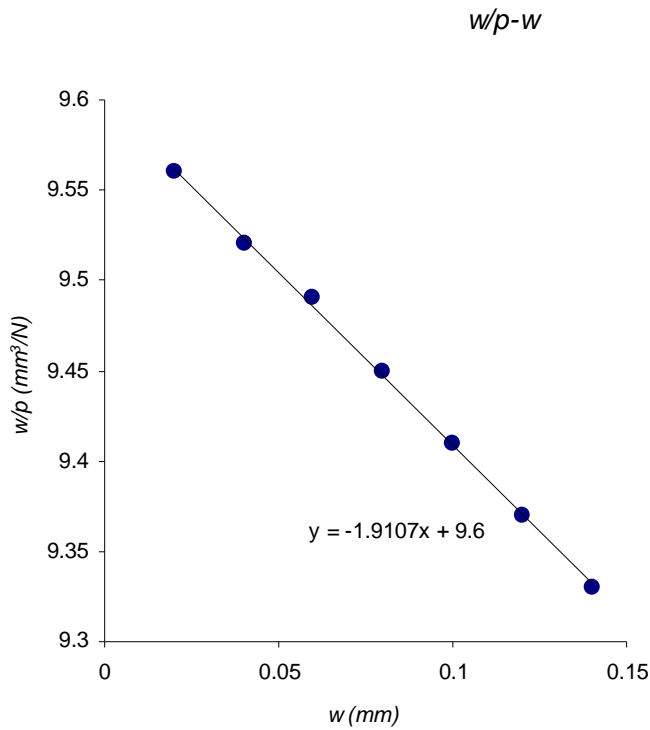


Figure 2. 42: Plot of w/p against w ($R = 50mm, t_0 = 0.5mm$)

$$S = -1.9107$$

$$\text{Buckling pressure using Southwell method } p_{cr}^2 = \frac{-4Em^3}{3(1-\nu^2)S} \rightarrow p_{cr} = 0.023MPa$$

$$\text{Buckling pressure } \bar{p} = 0.022MPa$$

$$\text{Error for this case: } \frac{0.023 - 0.022}{0.022} \times 100 = 4.5\%$$

2.8.2.3. For uniform radial pressure case with roller support :

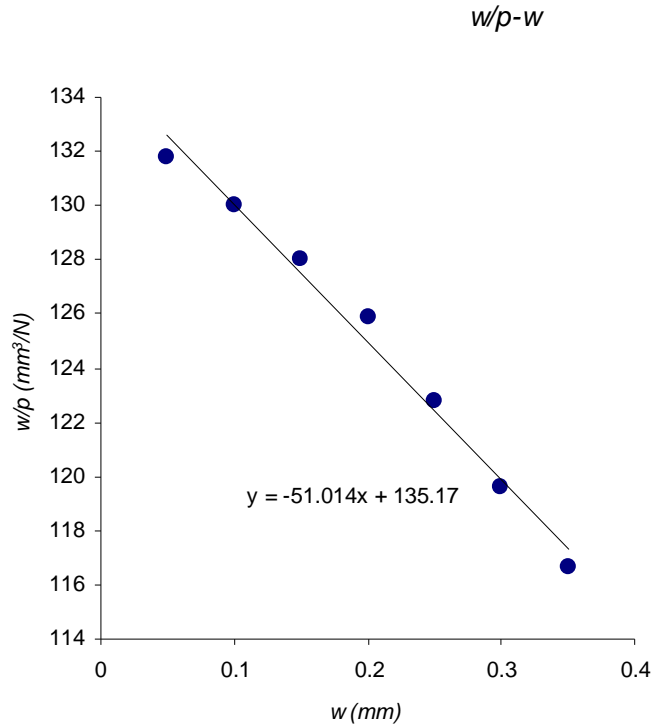


Figure 2. 43: Plot of $\frac{w}{p}$ against w ($R = 50mm, t_0 = 0.5mm$)

$$S = -51.014$$

$$\text{Buckling pressure using Southwell method } p_{cr}^2 = \frac{-4Em^3}{3(1-\nu^2)S} \rightarrow p_{cr} = 0.0039MPa$$

$$\text{Buckling pressure } \bar{p} = 0.0044MPa$$

$$\text{Error for this case: } \frac{0.0044 - 0.0039}{0.0039} \times 100 = 13.2\%$$

2.8.2.4. For Ring load case with hinge support:

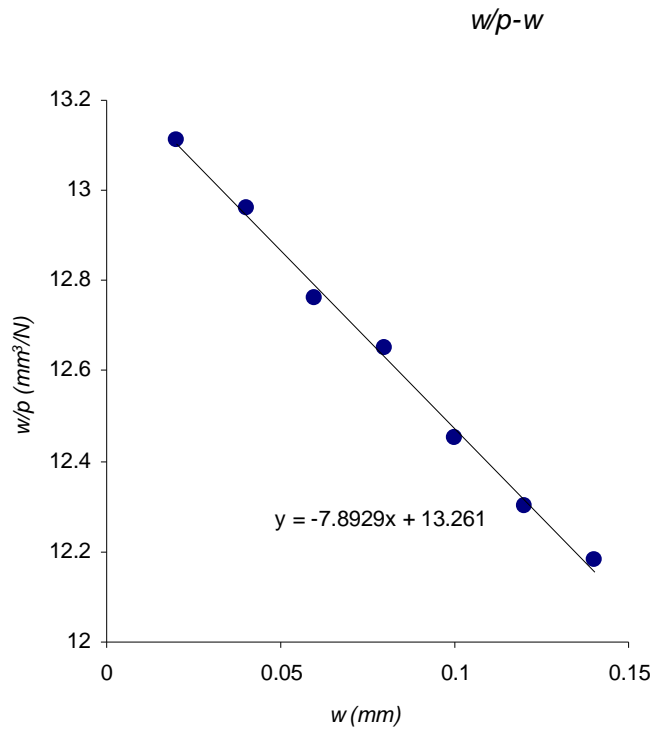


Figure 2. 44: Plot of $\frac{w}{p}$ against w ($R = 50mm, t_0 = 0.5mm$)

$$S = -7.8929$$

Buckling pressure using Southwell method

$$p_{cr}^2 = \frac{-4Em^3}{3(1-\nu^2)S} \rightarrow p_{cr} = 0.0114MPa \rightarrow q = 0.57N/mm$$

Buckling pressure $\bar{p} = 0.5MPa$

$$\text{Error for this case: } \frac{0.57 - 0.50}{0.50} \times 100 = 14\%$$

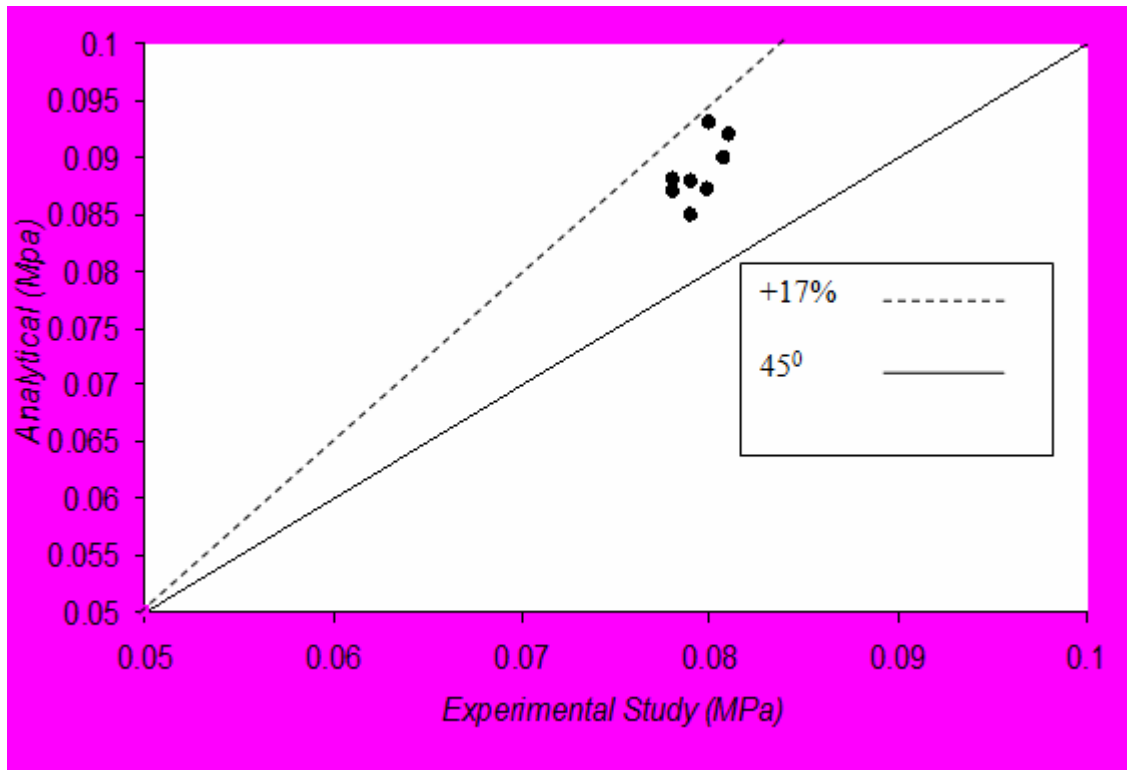


Figure 2. 45: Comparison of Southwell experimental prediction to theoretical buckling pressures.

2.9. Conclusion

The accurate prediction of buckling loads of spherical shells, based on the nondestructive buckling test data, is generally a difficult problem. Hence, this chapter presents a general methodology for predicting the critical buckling loads of spherical shells using a nondestructive test. For this purpose, the well known graphical method of predicting buckling loads, i.e., the Southwell's nondestructive method is extended to spherical shells and a new formula is derived for the critical buckling load of uniformly compressed spherical shells. The feasibility of this technique for determining critical buckling loads of spherical shells is demonstrated provided caution is exercised in analyzing the test results. This method may be used in any kind of spherical shells with arbitrary axisymmetrical loading and it provides a valuable procedure for estimating the buckling load of a spherical shell structure without having to conduct a destructive test. In this method, the curve of displacement/load is plotted against displacement, which is a straight line, and the slope of this line when multiplied by a constant value presents the critical buckling load with sufficient accuracy. The expediency of the method lies in its simplicity, and in the fact that it is nondestructive. This technique does not need any assumption as to the number of buckling waves or the exact locality of buckling so long as the loading remains axisymmetric. During experimental study, the test can be terminated if enough data points have formed a straight line. In this procedure, error may be introduced as a result of the accuracy of instruments, skill of the examiner and also approximation in determining Poisson's ratio value. Moreover, the accuracy of this method depends on the test cut off point and the mathematical function which is used for curve fitting. In the least squares fitting technique, the slope of the

fitted line is affected by the accuracy of the different displacement data points. Small inaccuracies in the measured data points cause the slope of line to be changed noticeably and may cause over prediction of the buckling load. So, with increasing the number of data points plotted together one can get more precise and realistic buckling load. The data points in the lower region are less important than the data points in the higher load region. In addition, increasing the number of gages may tremendously improve the accuracy. Even though the numerical solution can make the buckling load easily available to the user, it is here as an additional tool to verify the accuracy of the Southwell technique compared with the actual numerical and analytical buckling loads. Excellent correlation is observed.

Notation that used in this chapter

S Slope of w verses w/p line

u Displacement of the shell element in x direction

v Displacement of the shell element in y direction

w Displacement of the shell element in z direction

U_0 Effect of initial imperfections

V Shearing force in straight members

y Deflection of straight member

α Buckling coefficient to be determined experimentally

ε_x The unit elongation or strain in x - direction

ε_y The unit elongation or strain in y -direction

ε_1 The unit elongation of middle surface in x -direction

ε_2 The unit elongation of middle surface in y -direction

ν Poisson's ratio

χ_x Change of curvature in x -direction

χ_y Change of curvature in y -direction

t_0 Thickness of shell

p_{cr} Classical buckling pressure

$H()$ A mathematical operator

References

- Abramovich, H., Weller, T. and Yaffe, R. (1990). "Application of a Modified Southwell technique for the determination of critical loads of imperfect plates", *Computers and Structures*, Volume 37, Issue 4, pp.463-469.
- Archer, R.R. and Lange, C.G. (1965). "On the Nonlinear Dynamic Behavior of Shallow Spherical Shells", *AIAA Journal*. Vol.3. pp. 2313-2317.
- Archer, R.R. and Famili, J., (1965). "On the Vibrations and Stability of Finitely Deformed Shallow Spherical Shells", *J. App. Mech.* Vol. 32. pp.116-120.
- Beyer, K. (1933-1934). "Die Statik im Eisenbetonbau : ein Lehr-und Handbuch der Baustatik", vol.2 Berlin: Julius Springer.
- Bhimaraddi A., Carr J., and Moss P.J., (1989). "A Shear Deformable Finite Element for the Analysis of General Shells of Revolution", *Computer and Structures*, Vol.31, (3), pp.299-308.
- Bleich, F., (1952). "Buckling Strength of Metal Structures", McGraw-Hill, 256p.
- Bowles, R. E., and Merchant, W., (1956). "Critical Loads of Tall Building Frames" *The Structural Engineer*, Vol 36, Pp. 324-329.
- Brush, D. O., Almroth, B. O., (1975). "Buckling of bars, plates and shells", New York: McGraw-Hill Books Company, 325p.
- Budiansky, B. and Hutchinson, J. W. (1964). "Dynamic Buckling of Imperfection Sensitive Structures", *Proceeding of the XI International Congress of Applied Mechanics*, edited by Gortler, H., Springer-Verlag, Berlin, pp.639-651.

Budiansky, B., (1959). "Buckling of Clamped Shallow Spherical Shells" Proceeding of the symposium on the Theory of thin Elastic Shells, Delft, North Holland Publishing Company, Amsterdam, pp.64-94.

Budiansky, B., (1966). "Dynamic Buckling of Elastic Structures: Criteria and Estimate." Proceedings, International Conference on Dynamic Stability of Structures. Pergamon, New York, pp.83-106.

Budiansky, B., and Roth, R., (1962). "Axisymmetric Dynamic Buckling of Clamped Shallow Spherical Shells". NASA TN D-1510, pp.597-609.

Chan H.C., (1989). "Geometrically Nonlinear Analysis of Shallow Shells using Higher Order Finite Elements", *Compure Structure*, Vol. 31, No.3, pp.329-338.

Choi C., Yoo S., (1991). "Geometrically Nonlinear Behavior of an Improved Degenerated Shell Element", *Compure Structure* Vol.40, No.3, pp.785-794.

Cohen, G. A. (1968). "Effect of a Nonlinear Prebuckling State on the Postbuckling Behavior and Imperfection Sensitivity of Elastic Structures", *AIAA Journal*, Vol.6. No.8. pp.1616-1619.

Del Pozo, F, (1973). "La cúpula del Palau Blau-Grana", *Hormigón y Acero*, 107-108, pp.

Delpak R., and Peshkam V., (1991). "A Variational Approach to Geometrically Nonlinear Analysis of Asymmetrically Loaded Rotational Shells: Theory and Formulation", *Computer Structure*, Vol.39, No.34, pp.317-326.

Drucker, D. C., Greemberg, W., and Prager, W. (1951). 'The safety factor of an elastic plastic body in plane strain', *Trans. A.S.M.E., Journal of Appied Mechanic*, Vol. 173, No.1 p.371.

Drucker, D.C., and Shield, R.T., (1959). "Limit Analysis of Symmetrically Loaded Thin Shells of Revolution" Journal of Applied Mechanics, Vol. 26, pp 61-68.

Dumir, P. C. , Gandhi, M. L., and Nath, Y., (1984). "Axisymmetric static and dynamic buckling of orthotropic shallow spherical cap with circular hole " Computers and Structures, Volume 19, No.5, Pages 725-736.

Dumir, P. C., Dube, G. P., and Mallick, A., (2005). "Axisymmetric buckling of laminated thick annular spherical cap " Communications in Nonlinear Science and Numerical Simulation, Vol. 10, Issue 2, pp191-204.

Eller C., (1990) "Finite Element Procedures for the Stability Analysis of Nonlinear Parametric Excited Shell Structures", Computer and Structure Vol.35, No.3, pp.259-265.

Euler, Leonhard, (1744). "De Curvis Elasticis" Lausanne-Genf, Switerland, pp.72-160.

Famili, J. and Archer, R. R. (1965). "Finite Asymmetric Deformation of Shallow Spherical Shells", AIAA Journal, Vol.3, pp. 506-510.

Famili, J. (1965) "Asymmetric Buckling of Finitely Deformed Conical Shells", AIAA Journal, Vol.3, No.8, pp.1456-1461.

Fauconnier, (1934). "Essai de rupture d' una voûte mince conoïde en béton armé", Proceedings IABSE, Vol. II, pp. 167-192.

Fitch, J.R., and Budiansky, B., (1970). "Buckling and Postbuckling Behavior of Spherical Caps under Axisymmetric Load", AIAA Journal. Vol.8, No.4, pp.686-693.

Flügge, W, (1934). "*Statik und dynamik der schalen*", Berlin: Julius Springer, 118p.

Flügge, W, (1960). "Statique et dynamique des coques", Paris: éditions eyrolles.

Flügge, W, (1960). "Stresses in Shells", Springer-Verlag, Berlin.

Föppl, A, (1930). “Résistance des matériaux et éléments de la théorie mathématique de l'élasticité”, Paris, Gauthier-Villars et Cie.

Foster, G.C, Tennyson, R.C. (1983). “Use of the Southwell Method to Predict Buckling Strengths of Stringer Stiffened Cylindrical Shells”, An International Journal for Experimental Mechanics, Volume 19, Issue 2, pp.63-67.

Fung, Y. C. (1974). “Thin Shell Structures: Theory, Experiment and Design”, Prentice Hall, USA, pp. 247-259.

Gill S.S., and Leckie F.A., (1968).“The Effect of Geometry Change on The Application of Limit Analysis to the Design of Pressure Vessel Nozzles” International Journal of Mechcal Science, Vol 10, pp.989-993.

Goncalves, P. B. and Croll, J. G. S. A. (1992). “ Axisymmetric Buckling of Pressure Loaded Spherical Caps”, Journal of Structural Engineering, Vol. 118, No.4, pp. 970-985.

Grafton P.E., Strome D.R., (1963). “Analysis of axisymmetric Shells by the Direct Stiffness Method”, AIAA Journal, Vol.2, No.3, pp 304-332.

Gregory, M.S., (1968). “Elastic Instability”, Spon Ltd.

Grünitz, L., (2003).“The effect of welding on the buckling behavior of a spherical cap” International Journal of Pressure Vessels and Piping, Vol. 80, Issue 4, pp. 237-241.

Gupta P.K., Gupta N.K., (2009). “A Study of Axial Compression of Metallic Hemispherical Domes” Journal of Materials Processing Technology, Vol. 209, Issue 4, pp.2175-2179.

Hetenyi. M, (1950). “Handbook of Experimental Stress Analysis” John Wiley and Sons.

Hodge, P. G., (1965). “Limit Analysis of Rotationally Symmetric Plates and Shells” Prentice-Hall Inc., Englewood Cliffs, N.J.

Hsiao K., Chen Y., (1989).“Nonlinear Analysis of Shell Structures by Degenerated Isoparametric Shell Element”, Computer and Structure Vol.31, No.3, pp.427-438.

Huang N.C., (1964). “Unsymmetric Buckling of Thin Shallow Spherical Shells”, Transaction of ASME, Journal of Applied Mechanics, Vol.32, pp.447-457.

Huang N. C., (1969). “Axisymmetric Dynamic Snap-through of Elastic Clamped Shallow Spherical Shells”, AIAA Journal Vol.7, No.2, pp215-220.

Humphreys, J. S. and Bodner, S. R., (1962). “Dynamic Buckling of Shallow Shells under Impulsive Loading”, Journal of Engineering Mechanics,ASCE, Proceedings of the American Society of Civil Engineers Journal of the Engineering Mechanics Division 88 (1962), pp. 17–36.

Hutchinson, J. W. (1967). “Imperfection Sensitivity of Externally Pressurized Spherical Shells”, Transaction of ASME, Journal of Applied Mechanics, Vol. 34, No 49, pp.49-55.

Ingerslev A., (1923). “The Strength of Rectangular Slabs”, The Institution of Structural Engineers Journal. Vol.1, No.1, pp.3-14.

Jones L.L., (1962). “ Ultimate Load Analysis of Reinforced and Prestressed Concrete Structures”, Chatto and Windus, London, 248p.

Jones L.L., and Wood R.H., (1967). “Yield Line Analysis of Slabs”, Thames and Hudson, London, 405p.

Jones, G. W. and Chapman, S. J. and Allwright, D. J. (2008). “Axisymmetric buckling of a spherical shell embedded in an elastic medium under uniaxial stress at infinity,” The Quarterly Journal of Mechanics and Applied Mathematics, Vol. 61, No.4, pp. 475-495.

Kaplan, A. and Fung, Y. C. (1954). “A Nonlinear Theory of Bending and Buckling of Thin Elastic Shallow Spherical Shells” NACA TN 3212, 17p.

Koiter, W. T. (1945).“On the Stability of Elastic Equilibrium”, Thesis, Delft, H.J. Paris Amsterdam.

Koiter, W.T. (1963). “Elastic Stability and Post Buckling behavior”, Proceedings of Symposium on Nonlinear Problems, edited by Langer R. E., University of Wisconsin Press, p.257.

Liang C.C., Liao C.C. and Ma Y.C., (1991). “A large Deformation Elastic Plastic Dynamic Analysis of Square Plate and Spherical Shell Subjected to Shock Loading” Computer and Structure, Vol.39, No.6, pp 653-661.

Luo, P., Luo, H., Tong, F., (1991). “The Influence of Pre buckling Deformations and Stresses on the Buckling of the Spherical Shell”, International Journal of Offshore and Polar Engineering, Vol.1, No.4, pp 25-37.

American Institute of Steel Construction (AISC), (2008). “Manual of Steel Construction”.

Nagtegaal, J.C., Parks, D.M., and Rice, J.R. (1974). “On Numerically Accurate Finite Element Solutions in the Fully Plastic Range” Computers Methods in Applied Mechanics and Engineering, Vol. 4, No., pp 153-177.

Nie, G. H., Chan, C. K., Yao, J. C., and He, X. Q. (2009).“Asymptotic Solution for Nonlinear Buckling of Orthotropic Shells on Elastic Foundation,” AIAA Journal, vol. 47, No.7, pp. 1772-1783.

Palassopoulos, G. V. (1992). “Response Variability of Structures Subjected to Bifurcation Buckling”, Journal of Engineering Mechanics, ASCE, Vol.118, EM6 proceedings, pp. 1164-1183.

Roorda, J.,(1967). “Some Thoughts on the Southwell Plot” Journal of Engineering Mechanics Division, ASCE, Vol 93, (EM6) proceedings, Paper 5634, pp.37-48.

Seide, P. (1975). "Small Elastic Deformations of Thin Shells", Noordhoff International Publishing Leyden, California, USA, pp.227-229.

Seide, P., (1962). "On the Stability of Internally Pressurized Conical Shells under Axial Compression", Proceedings of the Fourth U.S. National Congress of Applied Mechanics, Vol.2 pp.761-773.

Singer, J. (1961). "Buckling of Conical Shells under Axisymmetrical External Pressure", Journal of Mechanical Engineering Science, Vol.3. No.4. p.330.

Singer, J., Eckstein A., Baruch. M, (1962). "Buckling of Conical Shells under External Pressure, Torsion and Axial Compression", TAE Report No.19. Technion Research and Development Foundation, pp.97-122.

Southwell, R. V., (1932). "On the Analysis of Experimental Observations in Problems of Elastic Stability" Proceedings of Royal Society of London (A), Vol.135, pp.601-616.

Stephens, W. B., and Fulton, R. E. (1969). "Axisymmetric Static and Dynamic Buckling of Spherical Caps due to Centrally Distributed Pressures", AIAA Journal, Vol.7, No.11, p.2120.

Stricklin, J.A., Martinez, J.R., Tillerson, J.R., Hong, J. H., and Haisler, W.E., (1971). "Nonlinear Dynamic Analysis of Shells of Revolution by Matrix Displacement Method", AIAA Journal Vol.9, No.4, pp629-636.

Stricklin, J.A., and Martinez, J.E., (1969). "Dynamic Buckling of Clamped Spherical Caps under Step Pressure Loading", AIAA Journal Vol.7 No.6, pp.1212-1213.

Teng J.G., and Rotter J.M., (1989). "Elastic-Plastic large Deflection Analysis of Axisymmetric Shells", Computer and Structure, Vol.31, No.2, pp.211-233.

Terndrup, P., Jensen, J., (1995). "Buckling Behavior of Imperfect Spherical Shells Subjected to Different Load Conditions", Thin-Walled Structures, Vol.23, No.4, pp.41-45.

Thurston, G. A. (1961) “A numerical Solution of The Nonlinear Equations for Axisymmetric Bending of Shallow Spherical Shells”, Transactions of ASME, Journal of Applied Mechanics, pp. 557-562.

Thurston, G. A. ,Penning, F. A. (1966). “Effect of Axisymmetric Imperfections on the Buckling of Spherical Caps under Uniform Pressure”, AIAA Journal, Vol.4, No.2, pp.319-327.

Tillman, S. C. (1970). “On the Buckling Behavior of Shallow Spherical Caps under Unifor Pressure Load”, International Journal of Solids Structures, Vol.6, pp.37-52.

Timoshenko, S., (1953). “History of Strength of Materials” Mc-Graw-Hill.

Timoshenko, S., and Gere (1961). “Theory of elastic Stability” Mc-Graw-Hill Second Ed.

Timoshenko, S., and Krieger (1959). “Theory of Plate and Shells” Mc-Graw-Hill Second Ed.

To C.W., and Wang B., (1991).“An Axisymmetric Thin Shell Finite Element for Vibration Analysis”, Computers and Structures, Vol.40, No.3, pp.555-568.

Torroja, E., (1934). “*Cubiertas laminares de hormigón armado*”, Madrid: Instituto Técnico de la Construcción u Edificación, 315p.

Uchiyama, M. and Yamada, S. (2003). “Nonlinear Buckling Simulations of Imperfect Shell Domes by Mixed Finite Elements” Journal of Engineering Mechanics,ASCE, Vol. 129,No.7, pp. 707-714.

Von Karman, T. (1909). “Untersuchungen uber Knickfestigkeit” Ver, Deust, Ing, Berlin.

Von Karman, T., and Tsien, H. S., (1939). “The Buckling of Spherical Shells by External Pressure” Journal of Aerospace Science, Vol.7, No.2, p.43.

Weinitschke, H. (1960) “On the Stability Problem for Shallow Spherical Shells”, Journal of Mathematics and Physics. Vol.38, No.4, p. 209.

Winter, G., Hsu, P.T., Koo, B., and Loh, M.H. (1948).“Buckling of Trusses and Rigid Frames”, Cornell University, Engineering Experiment Station Bulletin, No. 36.

Xie C.R., and Ho D., (1990). “Axisymmetric Buckling of Truncated Shallow Spherical Shells”, Computers and Structures, Vol.34, No.2, pp.297-301.

Xu C.S., (1991). “Buckling and Post-Buckling of symmetrically laminated moderately-thick spherical caps” International Journal of Solids and Structures, Vol. 28, No. pp1171-1184.

Yiniyi, Z. (1999). “Torsional Buckling of Spherical Shells under Circumferential Shear Loads”, Applied Mathematics and Mechanics, Vol.20, No.4.

Yuan K.Y. and Liang C.C.,(1989). “Nonlinear Analysis of an Axisymmetric Shell using Three Noded Degenerated Isoparametric Shell Element”, Computers and Structures, Vol.32, No.6, pp.1225-1239.

Zheng X., and Zhou Y., (1989). “Analytical Computerization Method for Solving a Kind of Nonlinear Equation of Plate and Shells”, Computers and Structures Vol.32, No.1, pp.185-194.

Zweig, A., (1968).“Buckling Analysis of One Story Frames”, Journal of the Structural Division, ASCE 94, ST9 , pp. 2107–2134

Appendix A - Collapse load of circular plate

A plate is supposed to yield in bending at point (x_1, x_2) if the stress tensor there obeys the yield criterion at every x_3 except $x_3 = 0$; points in the middle plane are observed as remnants of the elastic core. If the stresses σ_{i3} are assumed negligible in magnitude next to the $\sigma_{\alpha\beta}$ (this does not mean that they can be neglected in the equilibrium equations, because derivatives occur there), then a plane-stress yield criterion may apply:

$$f\left(\frac{\sigma_{\alpha\beta}}{\sigma_y}\right) = 0,$$

In every plane $x_3 \neq 0$. Equilibrium is satisfied if

$$\sigma_{\alpha\beta} = -\frac{4}{h^2} M_{\alpha\beta} \operatorname{sgn} x_3$$

If the ultimate moment is defined as $M_0 = \frac{\sigma_y t_0^2}{4}$, then the plate yield criterion is given

by $f(m_{\alpha\beta}) = 0$,

where $m_{\alpha\beta} = \frac{M_{\alpha\beta}}{M_0}$; the Mises and Tresca criteria become, respectively,

$$m_{11}^2 - m_{11}m_{22} + m_{22}^2 + 3m_{12}^2 = 1 \quad (\text{Mises}),$$

$$\max(|m_1|, |m_2|, |m_1 - m_2|) = 1 \quad (\text{Tresca}),$$

If the loading and support are axisymmetric, then the only nonvanishing moments are M_r, M_θ and the equilibrium equation is,

$$(rM_r)' - M_\theta = \int_0^r q r dr \quad (\text{A.1})$$

This equation and the yield condition constitute two equations for M_r and M_θ . Equivalently, if the yield condition is solved for M_θ in terms of M_r and the resulting expression for M_θ is substituted in (A.1), the result is a nonlinear first order differential equation for M_r . At the center of the plate, $M_r = M_\theta$ and thus, if the curvature there is positive (concave upward), $M_r(0) = M_0$ constitutes an initial condition with which the differential equation may be solved. In addition, a boundary condition at the edge $r = a$ must be satisfied; this yields the ultimate load. Let us recall that for a simply supported plate, the edge conditions are $w = M_r = 0$ thus $M_r = 0$ is a boundary condition with which the differential equation may be solved. For a clamped plate, the edge must form a hinge circle, that is, a locus of slope discontinuity. As we shall see, the edge condition there becomes $M_r(a) = M_0$ or $M_r(a) = -2M_0/\sqrt{3}$ for the Tresca or Mises material, respectively. Fig A.1 shows the Mises and Tresca yield criteria for axisymmetrically loaded circular plates. It follows from the preceding discussion that the center of the plate is in the moment state corresponding to point B, and that a simply supported edge corresponds to point C. A simply supported plate may thus be assumed to be entirely in the regime BC. For the the Tresca material, this means that $M_\theta = M_0$ everywhere, and the problem to be solved is therefore linear.

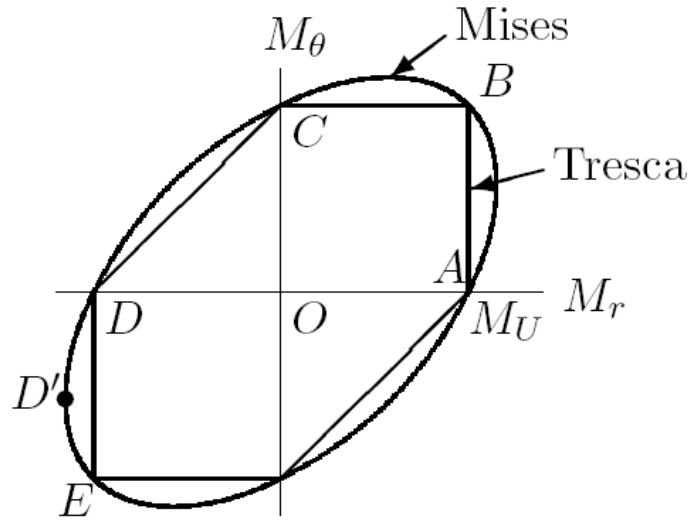


Figure A. 1: Mises and Tresca yield criteria for axisymmetrically loaded circular plates

Solution for Tresca Plate

Let us consider, for example, a downward load P_0 uniformly distributed over a circle of radius b , the plate being unloaded outside this circle. The equilibrium equation is then

$$(rM_r)' - M_\theta = \begin{cases} -\frac{P_0 r^2}{2\pi b^2} & r < b \\ -\frac{P_0}{2\pi} & r > b \end{cases}$$

The solution for $r < b$ satisfying the condition at $r = 0$ is

$$M_r = M_0 - \frac{P_0 r^2}{6\pi b^2}$$

while the solution for $r > b$ satisfying the condition at $r = a$ is

$$M_r = \left(\frac{P_0}{2\pi} - M_0 \right) \left(\frac{a}{r} - 1 \right)$$

Continuity at $r = b$ requires that

$$P_0 = \frac{2\pi M_0}{1 - \frac{2b}{3a}}$$

This result includes the extreme cases $P_0 = 6\pi M_0$ for the uniformly loaded plate $b = a$ and $P_0 = 2\pi M_0$ for a plate with concentrated load. This last case could not have been treated directly because the moments would have to go to infinity at the center which is a condition incompatible with plasticity.

Note: For this part I used from Prof. Jacon Farzan lecture notes. He is emeritus professor from Tabriz University and I passed theory of plate and shell course with him. He has taught Theory of plate and shell course for more than forty years in Tabriz University.

Appendix B - Axisymmetrically Loaded Circular Plates

Given a circular plate of radius a , the solution for a concentrated load acting at the center of the plate can be obtained by assuming that the radius of the circle b which the load is distributed becomes infinitely small, whereas the total load P remains finite. Using this assumption, we find that the maximum deflection at the center of a simply supported plate is:

$$w_{\max} = \frac{(3 + \nu)Pa^2}{16\pi(1 + \nu)D} \quad (\text{B.1})$$

The deflection and moments at any point of the circular simply supported plate at a distance r from the center are:

$$w = \frac{P}{16\pi D} \left[\frac{3 + \nu}{1 + \nu} (a^2 - r^2) + 2r^2 \text{Ln}\left(\frac{r}{a}\right) \right] \quad (\text{B.2})$$

$$M_r = \frac{(1 + \nu)P}{4\pi} \text{Ln}\left(\frac{a}{r}\right) + \frac{(1 - \nu)Pb^2}{16\pi} \left(\frac{1}{r^2} - \frac{1}{a^2} \right) \quad (\text{B.3})$$

$$M_t = \frac{P}{4\pi} \left[(1 + \nu) \text{Ln}\left(\frac{a}{r}\right) + 1 - \nu \right] - \frac{(1 - \nu)Pb^2}{16\pi} \left(\frac{1}{r^2} + \frac{1}{a^2} \right) \quad (\text{B.4})$$

The bending moment for points with $r > b$ may be found by omitting the terms in the equations (B.3) and (B.4) which contain b^2 . This gives

$$M_r = \frac{(1 + \nu)P}{4\pi} \text{Ln}\left(\frac{a}{r}\right) \quad (\text{B.5})$$

$$M_r = \frac{P}{4\pi} \left[(1+\nu) \ln\left(\frac{a}{r}\right) + 1 - \nu \right] \quad (\text{B.6})$$

To obtain formulas for a circular plate with clamped edges we differentiate equation (B.2) and find for the slope at the boundary of a simply supported plate.

$$-\left(\frac{dw}{dr}\right)_{r=a} = \frac{Pa}{4(1+\nu)\pi D} \quad (\text{B.7})$$

The bending moments $M_{r=a}$ uniformly distributed along the clamped edge produce a bending of the plate to spherical surface the radius of which is given by $\frac{1}{r_x} = \frac{1}{r_y} = \frac{M}{D(1+\nu)}$, and

the corresponding slope at the boundary is

$$\left(\frac{dw}{dr}\right)_{r=a} = -\frac{M_r a}{(1+\nu)D} \quad (\text{B.8})$$

Using (B.7) and (B.8), the condition that the built in edge does not rotate gives:

$$M_{r=a} = -\frac{P}{4\pi} \quad (\text{B.9})$$

Deflections produced by moments $M_{r=a} = -\frac{P}{4\pi}$ for one circular plate are $\frac{P(r^2 - a^2)}{8\pi D(1+\nu)}$.

Superposing these deflections on the deflections of a simply supported plate in equation (B.2), we obtain the following expression for the deflections of a clamped plate loaded at the center:

$$w = \frac{Pr^2}{8\pi D} \ln\left(\frac{r}{a}\right) + \frac{P}{16\pi D} (a^2 - r^2) \quad (\text{B.10})$$

Adding equations (B.9) to equations (B.5) and (B.6) for a simply supported plate, we obtain the following equations for the bending moment of circular clamped plate at any point not very close to the load:

$$M_r = \frac{P}{4\pi} \left[(1 + \nu) \operatorname{Ln} \left(\frac{a}{r} \right) - 1 \right] \quad (\text{B.11})$$

$$M_t = \frac{P}{4\pi} \left[(1 + \nu) \operatorname{Ln} \left(\frac{a}{r} \right) - \nu \right] \quad (\text{B.12})$$

When r approaches zero, expressions (B.5), (B.6), (B.11), and (B.12) approach infinity and hence are not suitable for calculating the bending moments. Moreover, the assumptions that serve as the basis for the theory of bending of circular plates do not hold near the point of application of a concentrated load.

Note: This part is from Timoshenko and Woinowsky-Krieger (1959) book.

Appendix C - Effect of Axial Force on the Stiffness of the Frame Member

Assume a member with one end clamped and the other end is free to rotate.

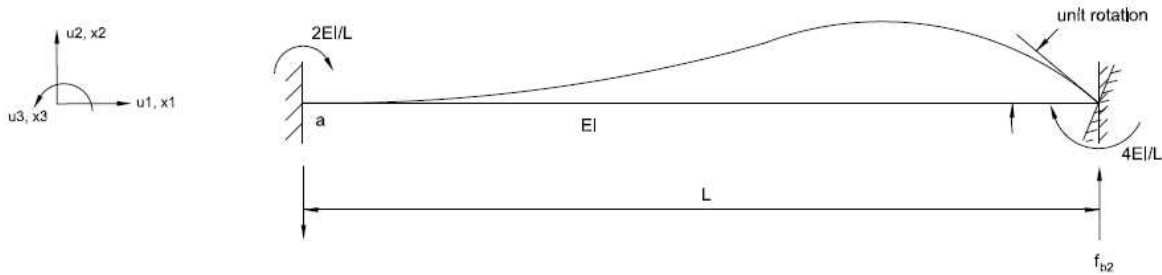


Figure C. 1

Without any axial force, a moment $\frac{4EI}{L}$ is necessary to create a unit rotation at the end b . This

moment produces $\frac{2EI}{L}$ internal moment at the point of a . When there is axial force, the

magnitude of the moment to create unit rotation will alter. Compression force will make this

moment smaller and tension force will make it bigger. Assume $K = \frac{EI}{L}$, and the moment for unit

rotation at the end of the member let be SK . Then, for any rotation u_{b3} the moment is

$$f_{b3} = SKu_{b3}, \text{ and at point } a \text{ the moment } f_{a3} = SCKu_{b3},$$

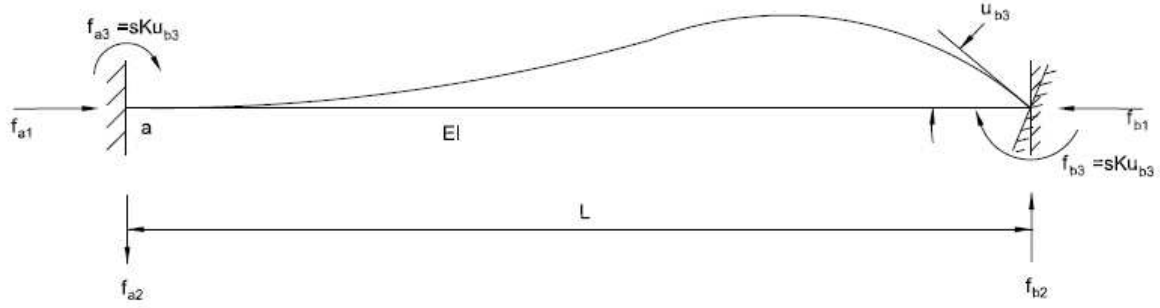


Figure C. 2

It is evident that S and C reduce to 4 and 0.5 correspondingly when $f_{a1} = 0$

$$\text{Let } P_E = \frac{\pi^2 EI}{L^2}, \quad \rho = P/P_E, \quad K = \frac{EI}{L}, \quad \text{and } \alpha = \frac{\pi}{2} \sqrt{\rho}$$

$$P_E = \text{Euler load, and } P = f_{a1} = -f_{b1}$$

$$\text{Then, } 2\alpha/L = \sqrt{\frac{f_{a1}}{EI}} \quad (\text{C.1})$$

Applying small deflection theory:

$$EI \frac{d^2 u_2}{dx_1^2} + f_{a1} u_2 = f_{a3} - f_{a2} x_1 \quad (\text{C.2})$$

$$f_{a3} = SCKu_{b3} \quad (\text{C.3})$$

$$f_{a2} = \frac{f_{a3} + f_{b3}}{L} = \frac{(S + SC)Ku_{b3}}{L} = \frac{S(1 + C)K}{L} u_{b3} \quad (\text{C.4})$$

By substituting equations (C.3) and (C.4) into (C.2) the following equation is obtained:

$$\frac{d^2 u_2}{dx_1^2} + \frac{f_{a1}}{EI} u_2 = \frac{SCK}{EI} u_{b3} - \frac{S(1+C)Ku_{b3}}{(EI)L} x_1 \quad (C.5)$$

$$\frac{d^2 u_2}{dx_1^2} + \frac{4\alpha^2}{L^2} u_2 = \frac{SCK}{EI} u_{b3} - \frac{S(1+C)Ku_{b3}}{(EI)L} x_1 \quad (C.6)$$

Solution of (C.6) is:

$$u_2 = A \cos \frac{2\alpha}{L} x_1 + B \sin \frac{2\alpha}{L} x_1 + \frac{SKu_{b3}}{f_{a1}L} CL - (1+C)x_1 \quad (A.7)$$

Boundary conditions:

$$\text{At } x_1 = 0, u_2 = 0 \quad 0 = \frac{SCK}{f_{a1}} u_{b3} + A, \quad A = -\frac{SCK}{f_{a1}} u_{b3}$$

$$\frac{du_2}{dx_1} = 0, \quad 0 = \frac{-S(1+C)K}{f_{a1}L} u_{b3} + \frac{2\alpha}{L} B$$

$$B = \frac{S(1+C)K}{2\alpha f_{a1}} u_{b3}$$

$$u_2 = \frac{SKu_{b3}}{f_{a1}L} [CL - (1+C)x_1] - \frac{SCKu_{b3}}{f_{a1}} \cos \frac{2\alpha}{L} x_1 + \frac{S(1+C)Ku_{b3}}{2\alpha f_{a1}} \sin \frac{2\alpha}{L} x_1 \quad (C.8)$$

Rearrangement,

$$u_2 = \frac{SKu_{b3}}{f_{a1}L} \left[C \left(1 - \cos \frac{2\alpha}{L} x_1 \right) + (1+C) \left(-\frac{x_1}{L} + \frac{1}{2\alpha} \sin \frac{2\alpha}{L} x_1 \right) \right] \quad (C.9)$$

To find C

$$\text{At } x_1 = L, \quad EI \frac{d^2 u_2}{dx_1^2} = -f_{a3} = -SKu_{b3}$$

$$-\frac{SKu_{b3}}{EI} = \frac{SKu_{b3}}{f_{a1}} \left(\frac{4\alpha^2}{L^2} \right) \left[(C) \cos 2\alpha - (1+C) \frac{1}{2\alpha} \sin 2\alpha \right]$$

$$-\frac{f_{a1}L^2}{EI} = -2\alpha(-2C\alpha \cos 2\alpha + C \sin 2\alpha + \sin 2\alpha) = -4\alpha^2$$

$$C = \frac{2\alpha - \sin 2\alpha}{\sin 2\alpha - 2\alpha \cos 2\alpha} \quad (C.10)$$

To find S

$$\text{At } x_1 = L, \quad \frac{du_2}{dx_1} = -u_{b3}$$

$$-u_{b3} = \frac{SKu_{b3}}{f_{a1}} \left[C \frac{2\alpha}{L} \sin 2\alpha + \frac{(1+C)}{L} (\cos 2\alpha - 1) \right]$$

$$\frac{f_{a1}L}{K} = -4\alpha^2 = S[2\alpha C \sin 2\alpha - 2(1+C) \sin^2 \alpha]$$

$$-2\alpha^2 = S[C(\alpha \sin 2\alpha - \sin^2 \alpha) - \sin^2 \alpha]$$

First solve for S and then substitute C

$$\begin{aligned}
S &= \frac{-2\alpha^2}{C(\alpha\sin 2\alpha - \sin^2 \alpha) - \sin^2 \alpha} \\
&= \frac{-2\alpha^2(\sin 2\alpha - 2\alpha\cos 2\alpha)}{(\alpha\sin 2\alpha - \sin^2 \alpha)(2\alpha - \sin 2\alpha) - \sin^2 \alpha(\sin 2\alpha - 2\alpha\cos 2\alpha)} \\
&= \frac{-2\alpha^2(\sin 2\alpha - 2\alpha\cos 2\alpha)}{2\alpha^2 \sin 2\alpha - 2\alpha\sin^2 \alpha - \alpha\sin^2 2\alpha + \sin^2 \alpha\sin 2\alpha - \sin^2 \alpha\sin 2\alpha + 2\alpha\sin^2 \alpha\cos 2\alpha} \\
&= \frac{-2\alpha^2(\sin 2\alpha - 2\alpha\cos 2\alpha)}{\alpha[\sin 2\alpha(2\alpha - \sin 2\alpha) + 2\sin^2 \alpha(\cos 2\alpha - 1)]} \\
&= \frac{-2\alpha(1 - 2\alpha\cot 2\alpha)}{2\alpha - \sin 2\alpha - 4\sin^4 \alpha / \sin 2\alpha} = \frac{-2\alpha(1 - 2\alpha\cot 2\alpha)}{2\alpha - 2\cos \alpha \sin \alpha - 2\sin^2 \alpha \tan \alpha} \\
&= \frac{-\alpha(1 - 2\alpha\cot 2\alpha)}{\alpha - \sin \alpha(\cos \alpha + \sin \alpha \tan \alpha)}
\end{aligned}$$

Finally,

$$S = \frac{\alpha(1 - 2\alpha \cot 2\alpha)}{\tan \alpha - \alpha} \quad (\text{C.11})$$

Now, the slope deflection equations (for no translation) can be written as:

$$f_{iz} = S_{ij} u_{jz} \quad (\text{C.12})$$

Where,

$$S_{ij} = K \begin{vmatrix} S & SC \\ SC & S \end{vmatrix} \quad \text{and} \quad \left. \begin{matrix} i \\ j \end{matrix} \right\} = a \& b \quad (\text{C.13})$$

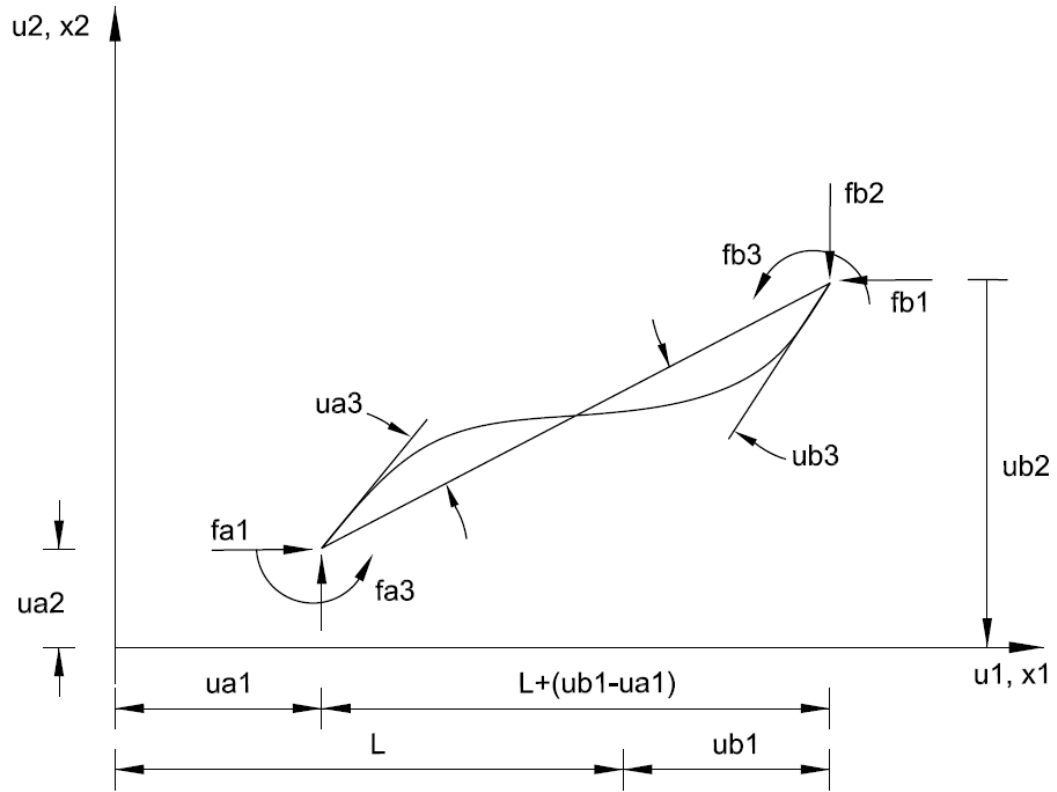


Figure C. 3

For jointed member with rotation and translation can be written:

$$EI \frac{d^2 u_2}{dx_1^2} + f_{a1} u_2 = f_{a2} x_1 - f_{a3} + f_{a1} (u_{b2} - u_{a2}) \quad (C.14)$$

The solution is:

$$u_2 = A \cos \frac{2\alpha}{L} x_1 + B \sin \frac{2\alpha}{L} x_1 + \frac{f_{a2}}{f_{a1}} x_1 - \frac{f_{a3}}{f_{a1}} + u_{a2}$$

Boundary conditions:

$$x_1 = 0, u_2 = u_{a2} = A - \frac{f_{a3}}{f_{a1}} + u_{a2}, \quad A = \frac{f_{a3}}{f_{a1}}$$

$$\frac{du_2}{dx_1} = u_{a3} = \frac{2\alpha}{L}B + \frac{f_{a2}}{f_{a1}}, B = \left(u_{a3} - \frac{f_{a2}}{f_{a1}}\right) \frac{L}{2\alpha}$$

The shear force,

$$f_{a2} = \frac{f_{a3} + f_{b3}}{L} + \frac{f_{a1}(u_{b2} - u_{a2})}{L}$$

$$u_2 = \frac{f_{a3}}{f_{a1}} \cos \frac{2\alpha}{L} x_1 + \frac{L}{2\alpha} \left[u_{a3} - \frac{f_{a3} + f_{b3}}{f_{a1}L} - \frac{u_{b2} - u_{a2}}{L} \right] \sin \frac{2\alpha}{L} x_1 + \left[\frac{f_{a3} + f_{b3}}{f_{a1}L} + \frac{u_{b2} - u_{a2}}{L} \right] x_1 - \frac{f_{a3}}{f_{a1}} + u_{a2}$$

Let $r = \sin 2\alpha, t = \cos 2\alpha$

At $x_1 = L, u_2 = u_{b2}$ and $\frac{du_2}{dx_1} = u_{b3}$

$$u_{b2} = \frac{f_{a3}}{f_{a1}} t + \frac{Lr}{2\alpha} \left[u_{a3} - \frac{f_{a3} + f_{b3}}{f_{a1}L} - \frac{u_{b2} - u_{a2}}{L} \right] + \frac{f_{a3} + f_{b3}}{f_{a1}} + (u_{b2} - u_{a2}) - \frac{f_{a3}}{f_{a1}} + u_{a2}$$

$$0 = \frac{f_{a3}}{f_{a1}} \left(t - \frac{r}{2\alpha} \right) + \frac{f_{b3}}{f_{a1}} \left(1 - \frac{r}{2\alpha} \right) + \frac{r}{2\alpha} [u_{a3}L - (u_{b2} - u_{a2})] \quad (C.15)$$

$$u_{b3} = -\frac{2\alpha r}{L} \times \frac{f_{a3}}{f_{a1}} + t \left[u_{a3} - \frac{f_{a3} + f_{b3}}{f_{a1}L} - \frac{(u_{b2} - u_{a2})}{L} \right] + \frac{f_{a3}}{f_{a1}L} + \frac{f_{b3}}{f_{a1}L} + \frac{(u_{b2} - u_{a2})}{L}$$

$$u_{b3} = \frac{f_{a3}}{f_{a1}L} (1 - 2\alpha r - t) + \frac{f_{b3}}{f_{a1}L} (1 - t) + \frac{(u_{b2} - u_{a2})}{L} (1 - t) + t u_{a3}$$

$$0 = f_{a3}(1 - 2\alpha r - t) + f_{b3}(1 - t) + f_{a1}(u_{b2} - u_{a2})(1 - t) + f_{a1}L t u_{a3} - f_{a1}L u_{b3} \quad (C.16)$$

To solve equations (C.15) and (C.16), multiply by $(1 - t)$ and $-(2\alpha - r)$ respectively.

$$0 = f_{a_3}(2\alpha - r)(1-t) + f_{b_3}(2\alpha - r)(1-t) - f_{a_1}(u_{b_2} - u_{a_2})(1-t)(r) + f_{a_1}Lr(1-t)u_{a_3}$$

$$0 = -f_{a_3}(1-2\alpha r-t)(2\alpha - r) - f_{b_3}(2\alpha - r)(1-t) - f_{a_1}(u_{b_2} - u_{a_2})(1-t)(2\alpha - r) - f_{a_1}Lt(2\alpha - r)u_{a_3} \\ + f_{a_1}L(2\alpha - r)u_{b_3}$$

$$f_{a_3}[(2\alpha - r)(1-t) - (1-2\alpha r-t)(2\alpha - r)] + f_{a_1}Lu_{a_3}r(1-t) - t(2\alpha - r) + f_{a_1}Lu_{b_3}(2\alpha - r) + f_{a_1}(u_{b_2} - u_{a_2}) \\ \times [r(t-1) + (t-1)(2\alpha - r)] = 0$$

This can be written as:

$$A_1f_{a_3} + A_2f_{a_1}Lu_{a_3} + A_3f_{a_1}Lu_{b_3} + A_4f_{a_1}(u_{b_2} - u_{a_2}) = 0 \quad (\text{C.17})$$

$$A_1 = (2\alpha - r)(1-t) - (1-2\alpha r-t)(2\alpha - r) = 2\alpha - 2\alpha^2 - r + rt - 2\alpha + 4\alpha^2r + 2\alpha + r - 2\alpha r^2 - rt \\ = 2\alpha - 2\alpha(t^2 + r^2) - 2\alpha + 4\alpha^2r + 2\alpha = 4\alpha(t-1 + \alpha r)$$

$$A_2 = r(1-t) - t(2\alpha - r) = r - rt - 2\alpha t + rt = (r - 2\alpha t)$$

$$A_3 = 2\alpha - r$$

$$A_4 = r(t-1) + (t-1)(2\alpha - r) = rt - r + 2\alpha t - rt - 2\alpha + r = 2\alpha(t-1)$$

Substituting these coefficients into equation (C.17) and solving for f_{a_3}

$$f_{a_3} = \frac{f_{a_1}(r - 2\alpha t)L}{4\alpha(1-t - \alpha r)}u_{a_3} + \frac{(2\alpha - r)f_{a_1}L}{4\alpha(1-t - \alpha r)}u_{b_3} + \frac{(t-1)f_{a_1}}{2(1-t - \alpha r)}(u_{b_2} - u_{a_2}) \quad (\text{C.18})$$

To get f_{b_3} , substitute equation (C.18) into equation (C.15),

$$0 = \frac{(2\alpha - r)(r - 2\alpha t)f_{a_1}L}{4\alpha(1-t - \alpha r)}u_{a_3} + \frac{(2\alpha - r)(2\alpha - r)f_{a_1}L}{4\alpha(1-t - \alpha r)} + \frac{(2\alpha - r)(t-1)}{2(1-t - \alpha r)}(u_{b_2} - u_{a_2}) + f_{b_3}(2\alpha - r) \\ f_{a_1}Lru_{a_3} - f_{a_1}r(u_{b_2} - u_{a_2})$$

$$(r - 2\alpha)f_{b_3} = f_{a_1}Lu_{a_3} \left[\frac{(2\alpha - r)(r - 2\alpha t)}{4\alpha(1-t - \alpha r)} + r \right] + f_{a_1}Lu_{b_3} \left[\frac{(2\alpha - r)(2\alpha - r)}{4\alpha(1-t - \alpha r)} \right] + f_{a_1}(u_{b_2} - u_{a_2}) \times \\ \left[\frac{(2\alpha - r)(t-1)}{2(1-t - \alpha r)} - r \right]$$

$$(r - 2\alpha)f_{b_3} = f_{a_1}Lu_{a_3}(B_1) + f_{a_1}Lu_{b_3}(B_2) + f_{a_1}(u_{b_2} - u_{a_2})(B_3) \quad (\text{C.19})$$

$$B_1 = \frac{2\alpha r - 4\alpha^2 t^2 - r^2 + 2\alpha r + 4\alpha r - 4\alpha^2 r^2}{4\alpha(1-t-\alpha r)}$$

$$B_1 = \frac{-4\alpha^2(t^2 + r^2) - r^2 + 4\alpha r}{4\alpha(1-t-\alpha r)} = \frac{-(2\alpha - r)^2}{4\alpha(1-t-\alpha r)}$$

$$B_2 = \frac{(2\alpha t - r)(2\alpha - r)}{4\alpha(1-t-\alpha r)}$$

$$B_3 = \frac{(2\alpha t - r)(t-1)}{2(1-t-\alpha r)} - r = \frac{2\alpha t^2 - 2\alpha t - rt + r - 2r + 2rt + 2\alpha r^2}{2(1-t-\alpha r)} = \frac{(1-t)(2\alpha - r)}{2(1-t-\alpha r)}$$

$$f_{b3} = \frac{(2\alpha - r)f_{a1}L}{4\alpha(1-t-\alpha r)}u_{a3} + \frac{(r - 2\alpha)f_{a1}L}{4\alpha(1-t-\alpha r)}u_{b3} + \frac{(t-1)f_{a1}}{2(1-t-\alpha r)}(u_{b2} - u_{a2}) \quad (C.20)$$

It is observable that (C.18) and (C.20) are slope deflection equations. The next step is to express the coefficients of the displacements in terms of the coefficients of slope deflection equations without any axial load but modified by β_i .

Let,

$$f_{a3} = \left(\frac{4EI}{L}\beta_1\right)u_{a3} + \left(\frac{2EI}{L}\beta_2\right)u_{b3} - \left(\frac{6EI}{L^2}\beta_3\right)(u_{b2} - u_{a2}) \quad (C.21)$$

$$f_{b3} = \left(\frac{2EI}{L}\beta_2\right)u_{a3} + \left(\frac{4EI}{L}\beta_1\right)u_{b3} - \left(\frac{6EI}{L^2}\beta_3\right)(u_{b2} - u_{a2}) \quad (C.22)$$

Therefore,

$$\left(\frac{4EI}{L}\beta_1\right) = \frac{(r-2\alpha)f_{a1}L}{4\alpha(1-t-\alpha r)}$$

$$\left(\frac{2EI}{L}\beta_2\right) = \frac{(2\alpha-r)f_{a1}L}{4\alpha(1-t-\alpha r)}$$

$$\left(\frac{6EI}{L^2}\beta_3\right) = \frac{(t-1)f_{a1}}{2(1-t-\alpha r)}$$

Solving for β_i , the following is obtained:

$$\beta_1 = \frac{(r-2\alpha)f_{a1}L^2}{(4EI)4\alpha(1-t-\alpha r)}$$

$$\beta_1 = \frac{(\sin 2\alpha - 2\alpha \cos 2\alpha)4\alpha^2}{16\alpha(1 - \cos 2\alpha - \alpha \sin 2\alpha)} = \left(\frac{\alpha}{4}\right) \left(\frac{\sin 2\alpha - 2\alpha \cos 2\alpha}{2\sin^2 \alpha - \alpha \sin 2\alpha}\right) = \left(\frac{\alpha}{4}\right) \frac{1 - 2\alpha \cot 2\alpha}{\tan \alpha - \alpha} = \frac{S}{4} \quad (\text{C.23})$$

$$\beta_2 = \frac{(2\alpha-r)f_{a1}L^2}{(8EI)\alpha(1-t-\alpha r)} = \frac{(2\alpha - \sin 2\alpha)4\alpha^2}{8\alpha(1 - \cos 2\alpha - \sin 2\alpha)} = \frac{(2\alpha - \sin 2\alpha)}{2\sin^2 \alpha - \alpha \sin 2\alpha} \times \frac{(1 - 2\alpha \cot 2\alpha)}{(1 - 2\alpha \cot 2\alpha)} \times \frac{(\sin 2\alpha)}{(\sin 2\alpha)} \times \left(\frac{\alpha}{2}\right)$$

$$= \left(\frac{\alpha}{2}\right) \left[\frac{(2\alpha - \sin 2\alpha)}{\left(\frac{2\sin^2 \alpha}{\sin 2\alpha}\right) - \alpha} \right] \frac{(1 - 2\alpha \cot 2\alpha)}{(\sin 2\alpha - 2\alpha \cos 2\alpha)} = \frac{SC}{2} \quad (\text{C.24})$$

$$\beta_3 = \frac{-(t-1)f_{a1}L^2}{12EI(1-t-\alpha r)} = \left(\frac{\alpha^2}{3}\right) \frac{-(\cos 2\alpha - 1)}{(1 - \cos 2\alpha - \alpha \sin 2\alpha)} = \frac{\left(\frac{1}{3}\right)\alpha^2}{(1 - \alpha \cot \alpha)} \quad (\text{C.25})$$

Define $\beta_5 = \alpha \cot \alpha$

$$\beta_1 = \frac{S}{4} = \frac{\alpha}{4} \times \frac{1-2\alpha \cot 2\alpha}{\tan \alpha - \alpha} = \frac{\beta_5}{4} \times \frac{1-2\alpha \cot 2\alpha}{1-\beta_5} = \frac{\beta_5}{4} \times \frac{\left(1-2\alpha \left(\frac{\cot^2 \alpha - 1}{2 \cot \alpha}\right)\right)}{1-\beta_5} = \frac{1}{4}[\beta_5 + 3\beta_3] \quad (\text{C.27})$$

Similarly,

$$\beta_2 = \frac{1}{2}[3\beta_3 - \beta_5] \quad (\text{C.28})$$

Therefore, β_3 can be expressed in terms of S and C

$$4\beta_1 + 2\beta_2 = \beta_5 + 3\beta_3 + 3\beta_3 - \beta_5 = 6\beta_3$$

$$\beta_3 = \frac{1}{6}[4\beta_1 + 2\beta_2] = \frac{S(1+C)}{6} \quad (\text{C.29})$$

The equilibrium condition for the member is:

$$f_{a2}L = f_{a3} + f_{b3} + f_{a1}(u_{b2} - u_{a2}) \quad (\text{C.30})$$

or

$$f_{a2} = \left[-\frac{12EI}{L^3}\beta_3 + \frac{f_{a1}}{L}\right](u_{b2} - u_{a2}) + \left[\frac{4EI}{L^2}\beta_1 + \frac{2EI}{L^2}\beta_2\right]u_{a3} + \left[\frac{2EI}{L^2}\beta_2 + \frac{4EI}{L^2}\beta_1\right]u_{b3}$$

This can be written as:

$$f_{a2} = \left[-\frac{12EI}{L^3}\beta_4\right](u_{b2} - u_{a2}) + \left(\frac{6EI}{L^2}\beta_7\right)u_{a3} + \left(\frac{6EI}{L^2}\beta_7\right)u_{b3} - \frac{12EI}{L^3}\beta_4 = -\frac{12EI}{L^3}\beta_3 + \frac{f_{a1}}{L}$$

$$\beta_4 = \beta_3 - \frac{f_{a1}L^2}{12EI} \frac{\pi^2}{\pi^2} = \beta_3 - \frac{\alpha^2}{3} = \left(\frac{\alpha^2}{3}\right)\left(\frac{1}{1-\alpha \cot \alpha} - 1\right)$$

$$\beta_4 = \left(\frac{\alpha^2}{3}\right)\left(\frac{\alpha \cot \alpha}{1-\alpha \cot \alpha}\right) = \beta_5 \times \beta_3 \quad (\text{C.31})$$

$$\text{And } 6\beta_7 = 4\beta_1 + 2\beta_2 = 6\beta_3$$

$$\beta_7 = \beta_3 \tag{C.32}$$

These derivations are based on the assumption that the axial force f_{a1} on the member is compressive. If the axial force is tensile, then the trigonometric functions in the stability functions S and C and β_i all become hyperbolic functions.